UPPSALA
UNIVERSITET

Digital Comprehensive Summaries of Uppsala Dissertations from the Faculty of Science and Technology 1707

Sputtering of Precursors for Cu_2ZnSnS_4 Solar Cells and Application of Cadmium Free Buffer Layers

TOVE ERICSON

ACTA
UNIVERSITATIS
UPSALIENSIS
UPPSALA
2018

ISSN 1651-6214
ISBN 978-91-513-0414-4
urn:nbn:se:uu:diva-357354

Dissertation presented at Uppsala University to be publicly examined in Häggsalen, Ångströmlaboratoriet, Lägerhyddsvägen 1, Uppsala, Friday, 5 October 2018 at 13:15 for the degree of Doctor of Philosophy. The examination will be conducted in English. Faculty examiner: Dr. Yaroslav Romanyuk (EMPA).

Abstract

Ericson, T. 2018. Sputtering of Precursors for Cu_2ZnSnS_4 Solar Cells and Application of Cadmium Free Buffer Layers. *Digital Comprehensive Summaries of Uppsala Dissertations from the Faculty of Science and Technology* 1707. 102 pp. Uppsala: Acta Universitatis Upsaliensis. ISBN 978-91-513-0414-4.

The aim of this thesis is to understand the influence of the deposition process and resulting film properties on Cu_2ZnSnS_4 (CZTS) thin film solar cells. Two main aspects are studied, namely formation of absorber precursors by sputtering, and alternative Cd-free buffer materials with improved band alignment.

Reactive sputtering is used to grow dense and homogeneous precursor films containing all elements needed for CZTS absorbers. The addition of H_2S gas to the inert Ar sputter atmosphere leads to a drastic decrease of Zn-deposition rate due to the sulfurization of the target. Sulfurization also leads to instabilities for targets made of CuSn, Cu and Cu_2S, while sputtering from CuS gave acceptable process stability.

The H_2S/Ar-ratio also affects film morphology and composition. Precursors with sulfur content close to stoichiometric CZTS have a columnar, crystalline structure. Materials analysis suggests a non-equilibrium phase with a cubic structure, where each S atom is randomly surrounded by 2:1:1 Cu:Zn:Sn-atoms, respectively. Substrate heating during sputtering is shown to be important to avoid cracks in the annealed films while stress in the precursor films is not observed to affect the absorber or solar cell quality.

Sputtering from compound targets in Ar-atmosphere yields precursor properties similar to those from reactive sputtering at high H_2S/Ar-ratios and both types can be processed into well-performing solar cells.

Additionally, a low temperature treatment of CZTS absorbers in inert atmosphere prior to buffer layer growth is shown to affect the device properties, which indicates that the thermal history of the CZTS absorber is important.

The alternative buffer system $ZnO_{1-x}S_x$ is found to yield lower efficiencies than expected, possibly due to inferior interface or buffer quality. The $Zn_{1-x}Sn_xO_y$ (ZTO) buffers instead give better performance than their CdS references. For optimized parameters, the activation energy for recombination coincides with the energy of the photoluminescence peak of the absorber. This can be interpreted as a shift of dominant recombination path from the interface to the CZTS bulk. A well-performing CZTS-ZTO device with antireflective coating yielded an efficiency of 9.0 %, which at the time of publication was the highest value published for a Cd-free pure-sulfide CZTS solar cell.

Keywords: solar cells, thin film, buffer layer, sputtering, reactive sputtering, CZTS, kesterite, zinc tin oxide

Tove Ericson, Department of Engineering Sciences, Solid State Electronics, Box 534, Uppsala University, SE-75121 Uppsala, Sweden.

ISSN 1651-6214
ISBN 978-91-513-0414-4
urn:nbn:se:uu:diva-357354 (http://urn.kb.se/resolve?urn=urn:nbn:se:uu:diva-357354)

To the sun and for the snow.

List of Papers

This thesis is based on the following papers, which are referred to in the text by their Roman numerals.

I T. Ericson, T. Kubart, J. J. Scragg and C. Platzer-Björkman, *"Reactive sputtering of precursors for Cu_2ZnSnS_4 thin film solar cells",* Thin Solid Films, 520: 7093-7099, 2012.

II T. Ericson, J. J. Scragg, T. Kubart, T. Törndahl and C. Platzer-Björkman, *"Annealing behavior of reactively sputtered precursor films for Cu_2ZnSnS_4 solar cells"*, Thin Solid Films, 535: 22-26, 2013.

III J. T. Wätjen, J. J. Scragg, T. Ericson, M. Edoff and C. Platzer-Björkman, *"Secondary compound formation revealed by transmission electron microscopy at the Cu_2ZnSnS_4/Mo interface"*, Thin Solid Films, 535: 31-34, 2013.

IV J. J. Scragg, T. Ericson, X. Fontané, V. Izquirdo-Roca, A. Pérez-Rodríguez, T. Kubart, M. Edoff and C. Platzer-Björkman, *"Rapid annealing of reactively sputtered precursors for Cu_2ZnSnS_4 solar cells"*, Progress in Photovoltaics Research and Applications, 22: 10-17, 2014.

V T. Kubart, T. Ericson, J. J. Scragg, M. Edoff and C. Platzer-Björkman, *"Reactive sputtering of Cu_2ZnSnS_4 thin films - Target effects on the deposition process stability"*, Surface and Coatings Technology, 240: 281-285, 2014.

VI T. Ericson, J. J. Scragg, A. Hultqvist, J. T. Wätjen, P. Szaniawski, T. Törndahl and C. Platzer-Björkman, *"Zn(O,S) Buffer Layers and Thickness Variations of CdS Buffer for Cu_2ZnSnS_4 Solar Cells",* IEEE Journal of Photovoltaics, 4: 465-469, 2014.

VII C. Platzer-Björkman, C. Frisk, J. K. Larsen, T. Ericson, S.-Y. Li, J. J. S. Scragg, J. Keller, F. Larsson and T. Törndahl, *"Reduced interface recombination in Cu_2ZnSnS_4 solar cells with atomic layer deposition $Zn_{1-x}Sn_xO_y$ buffer layers"*, Applied Physics Letters, 107:243904, 2015.

VIII T. Ericson, F. Larsson, T. Törndahl, C. Frisk, J. Larsen, V. Kosyak, C. Hägglund, S. Li and C. Platzer-Björkman, *"Zinc-Tin-Oxide Buffer Layer and Low Temperature Post Annealing Resulting in a 9.0 % Efficient Cd-free Cu_2ZnSnS_4 Solar Cell",* Solar RRL, 1(5): 1700001, 2017.

Reprints were made with permission from the respective publishers.

Personal contributions to the papers

I Materials synthesis, characterization and writing with input from co-authors.

II Materials synthesis, device fabrication, characterization and writing with input from co-authors.

III Calibration of composition measurement, part in developing the fabrication method for the absorber, discussions.

IV Calibration of composition measurement, part in developing the fabrication method for the absorber, discussions.

V Part of the experimental work and discussions.

VI Most of the materials synthesis, device fabrication and characterization. Writing with input from co-authors.

VII Part of discussions and manuscript revision.

VIII Most of the materials synthesis, device fabrication and characterization. Writing with input from co-authors.

Related work

The following papers contain work contributed to during the PhD project but not explicitly included in this thesis.

1. J. J. Scragg, T. Ericson, T. Kubart, M. Edoff and C. Platzer-Björkman, *"Chemical Insights into the Instability of Cu_2ZnSnS_4 Films during Annealing",* Chemistry of Materials, 23(20): 4625-4633, 2011.

2. J. J. Scragg, J. T. Wätjen, M. Edoff, T. Ericson, T. Kubart and C. Platzer-Björkman, *"A Detrimental Reaction at the Molybdenum Back Contact in $Cu_2ZnSn(S,Se)_4$ Thin-Film Solar Cells",* Journal of American Chemical Society, 134(47): 19330-19333, 2012.

3. J. J. Scragg, T. Kubart, J. T. Wätjen, T. Ericson, M. K. Linnarsson and C. Platzer-Björkman, *"Effect of back contact instability on Cu_2ZnSnS_4 devices and processes",* Chemistry of Materials, 25(15): 3162-3171, 2013.

4. J. Lindahl, J. T. Wätjen, A. Hultqvist, T. Ericson, M. Edoff and T. Törndahl, *"The effect of $Zn_{1-x}Sn_xO_y$ buffer layer thickness in 18.0 % effcient Cd free $Cu(In,Ga)Se_2$ solar cells",* Progress in Photovoltaics: Research and Applications, 21(8): 1588-1597, 2013.

5. J. J. S. Scragg, L. Choubrac, A. Lafond, T. Ericson and C. Platzer-Björkman, *"A low-temperature order-disorder transition in Cu_2ZnSnS_4 thin films",* Applied Physics Letters, 104: 041911, 2014.

6. Y. Ren, J. J. Scragg, T. Ericson, T. Kubart and C. Platzer-Björkman, *"Reactively sputtered films in the $Cu_xS–ZnS–SnS_y$ system: From metastability to equilibrium",* Thin Solid Films, 582: 208-214, 2015.

7. L. Van Puyvelde, J. Lauwaert, P.F. Smet, S. Khelifi, T. Ericson, J.J. Scragg, D. Poelman, R. Van Deun, C. Platzer-Björkman and H. Vrielinck, *"Photoluminescence investigation of Cu_2ZnSnS_4 thin film solar cells"*, Thin Solid Films, 582: 146-150, 2015.

8. C. Frisk, T. Ericson, S.-Y. Li, P. Szaniawski, J. Olsson and C. Platzer-Björkman, *"Combining strong interface recombination with bandgap narrowing and short diffusion length in Cu_2ZnSnS_4 device modeling",* Solar Energy Materials and Solar Cells, 144: 364-370, 2016.

9. O. V. Bilousov, Y. Ren, T. Törndahl, O. Donzel-Gargand, T. Ericson, C. Platzer-Björkman, M. Edoff, and C. Hägglund, *"Atomic Layer Deposition of Cubic and Orthorhombic Phase Tin Monosulfide",* Chemistry of Materials, 29(7): 2969-2978, 2017.

Contents

Abbreviations

ALD	Atomic layer deposition
AM1.5	Air mass 1.5 (solar spectrum)
AR	Antireflective
CBD	Chemical bath deposition
CBM	Conduction band minimum
CIGS	$Cu(In,Ga)Se_2$
CTS	Cu_2SnS_3
CZTS	Cu_2ZnSnS_4
CZTSe	$Cu_2ZnSnSe_4$
CZTSSe	$Cu_2ZnSn(S,Se)_4$
DC	Direct current
EDS / EDX	Energy dispersive x-ray spectroscopy
ERDA	Elastic recoil detection analysis
FF	Fill factor
IV	Current-voltage
IVT	Temperature dependent current-voltage
i-ZnO	Intrinsic ZnO
J_{sc}	Short-circuit current
PL	Photoluminescence
QE	Quantum efficiency
RBS	Rutherford backscattering spectrometry
RF	Radio frequency
SEM	Scanning electron microscopy
SLG	Soda lime glass
SZM	Structure zone model
TEM	Transmission electron microscopy
UV	Ultraviolet
VBM	Valence band maximum
V_{oc}	Open-circuit voltage
WDX	Wavelength dispersive x-ray spectroscopy
XRD	X-ray diffraction
XRF	X-ray fluorescence
Zn(O,S)	$ZnO_{1-x}S_x$
ZTO	$Zn_{1-x}Sn_xO_y$

1. Introduction

The transition into a more sustainable energy system is hopefully already under way. However, due to the long history of using non-renewable resources to sustain our way of life, the journey is not expected to be without problems. In a fully sustainable system, both the source of the energy and the device used to harvest it need to be either renewable or recyclable. To ensure this, devices for harvesting and storing energy should preferably contain abundant and non-toxic materials, to enable production of large quantities and facilitate the recycle process.

In the case of thin film solar cells many currently used types contain either scarce or toxic elements, such as In in $Cu(In,Ga)Se_2$ (CIGS) and Cd in CdTe, respectively [1]. New thin film solar cell materials are therefore being developed. Among them, $Cu_2ZnSn(S,Se)_4$ (CZTSSe) has been intensively studied during the last ten years, due to promising properties and similarities to the commercially available CIGS. The chalcogen ratio Se/S can be used to tune the band gap of the material but a pure sulfide might be preferable from an abundance perspective and in this thesis we limit the scope to Cu_2ZnSnS_4 (CZTS) [2, 3].

Additionally to the main solar cell absorber, also other layers in the solar cell stack may contain undesirable materials. For CIGS and CZTS, CdS is commonly used to complete the active part of the solar cell. Due to the toxicity of cadmium, alternative material systems are considered. Part of this thesis is focused on the use of cadmium free alternatives for CZTS.

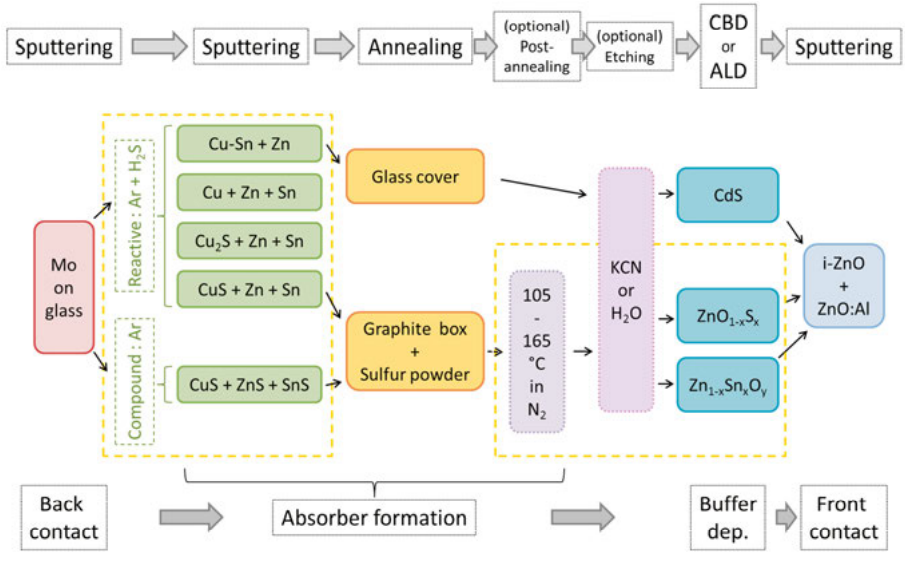

Figure 1. Overview of the production steps for the solar cells investigated in this thesis. The top row shows the different process types used. The bottom row indicates which layer that is concerned. The focus areas of this thesis, namely sputtering of precursors for the absorber, post-annealing and application of Cd-free buffer layers, are encircled in yellow.

The production steps for the solar cells investigated in this thesis are shown in Figure 1, with the main aspects studied encircled in yellow. The aim is to understand the influence of deposition processes and film properties on the formation of the CZTS absorber, and thus to be able to improve its performance. This is studied in Paper I-V and described and discussed in Chapter 4. Furthermore, the change to a cadmium free complementary material may also, if correctly understood and chosen, improve the solar cells, due to better transparency and a better match with the CZTS material. This is studied in Paper VI-VIII and described and discussed in Chapter 5. Chapter 2 is intended to give a background of the concepts and materials concerned and Chapter 3 describes some of the measurement techniques used, with possible implications of applying them in the case of CZTS. In Chapter 6 a conclusion and outlook is presented.

In short the goal is to create a solar cell that contains only abundant and non-toxic materials but nonetheless has high performance.

2. Background

2.1 Basic solar cell principles

The purpose of a solar cell is to convert sunlight into electricity. The first step in this process is the energy transfer from the light into a material. On an atomic scale, the incoming photons excite electrons from a lower energy state to a higher, as exemplified by A in Figure 2. There are several ways of extracting these electrons as a current. The most common is to use an inorganic semiconductor solid state junction. There are also other types of solar cells, such as dye-sensitized solar cells and organic solar cells which have shown promising efficiencies in recent years, however, the long term stability remains an uncertainty [4].

2.1.1 Semiconductors

Semiconductors are materials with conductivities in-between those of conductors and insulators. Additionally, the conductivity can often be altered by external means, such as temperature, light or small amount of impurity atoms. This is caused by the crystal structure of the semiconductor material which leads to that certain electron energies, or states, are forbidden. In a semiconductor these states are placed so that there is a small gap, a band gap, between the highest states which contain electrons (VBM for valence band maximum), and the lowest unoccupied allowed states (CBM for conduction band minimum), see Figure 2. Absorption of photons with sufficient energy will enable electrons to be excited from the valence band to the conduction band, where they can move and thus be collected, i.e. a current can flow. To ensure the collection of the electrons, two different semiconductors, with a surplus (n-doped) and lack of free electrons (p-doped), respectively, are put together to form a junction (pn-junction).

The most common semiconductor used for solar cells is doped Si but also semiconductors comprised of two (GaAs, CdTe) or more (CIGS, CZTS) elements are used. In a solar cell these materials are called absorbers, due to their function of absorbing photons. For the common Si solar cell the pn-junction consists of Si doped with B or Ga for the p-side and Si doped with P for the n-side. When the pn-junction consists of one semiconductor material, as in the case of differently doped Si, it is called a homojunction. For other solar cell materials it is common to complete the pn-junction with a second

semiconductor. For CIGS and CZTS, which are intrinsic (not intentionally doped) p-type materials, a buffer layer and a window layer are making up the n-side of the junction. Such a junction, comprised of two, or more, different semiconductor materials, is called a heterojunction.

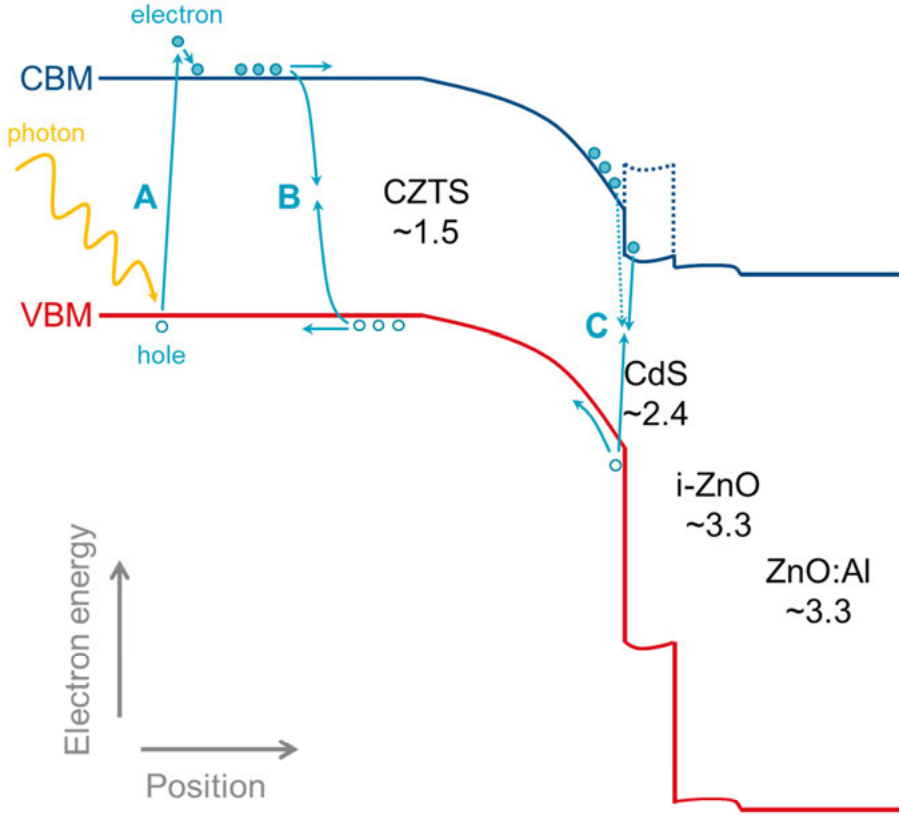

Figure 2. Schematic band diagram for a CZTS solar cell. Approximate band gap values are given in eV under each material. A) shows an electron being excited from the valence band to the conduction band. B) represents bulk recombination while C) indicates interface recombination close to the pn-junction. Two different band alignments between the CZTS absorber and the buffer are presented, a cliff in solid lines, expected for the CdS buffer, and a small spike in dashed lines, which is preferable. An even higher spike could however block the current flow and thus give deteriorated solar cells.

2.1.2 Choosing band gap

For solar cells to work as efficiently as possible, the energy difference between the conduction band and the valence band, the band gap, has to be just below the energy of the incoming photons, since lower energy photons will not be able to excite electrons over the band gap, and the extra energy for

higher energy photons will be lost as heat. Sunlight consists of a spectrum of photon energies, where the exact distribution depends on the temperature of the sun, the composition of the atmosphere and the distance the photons have travelled through the atmosphere.

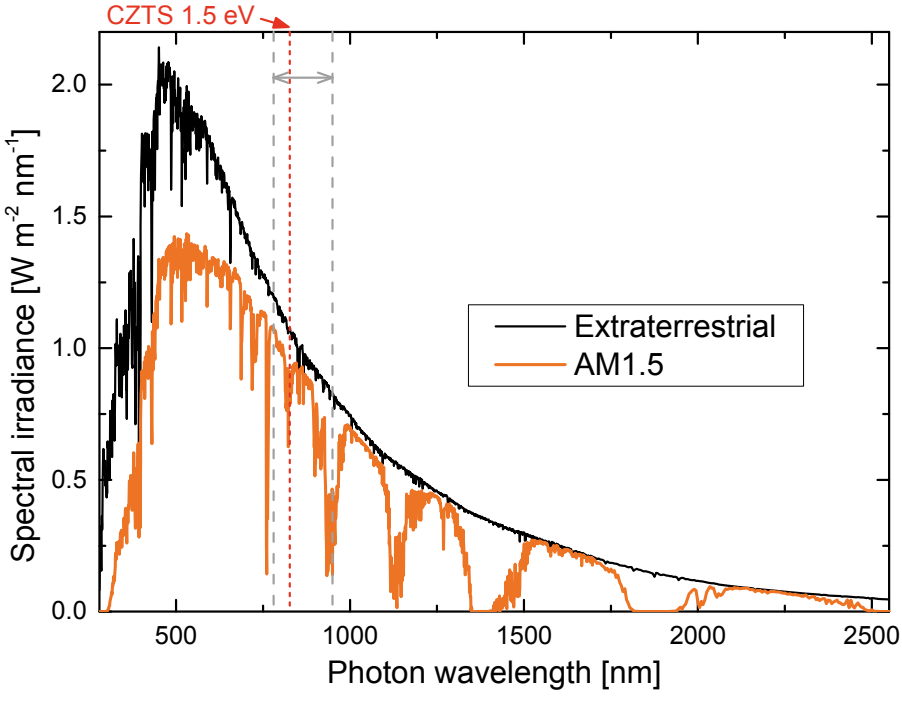

Figure 3. Solar irradiance spectra, extraterrestrial and the standard spectra used for solar cell measurements (AM 1.5). The expected optimal range for single junction solar cells is 1.3-1.6 eV which is marked in grey. The CZTS band gap is indicated in red.

The standard spectrum used for characterizing solar cells is shown in Figure 3. It represents photons that have travelled through 1.5 times the thickness of the atmosphere and this spectrum is therefore denoted air mass 1.5 (AM1.5). To utilize the complete spectrum, several different materials with a range of band gaps would have to be used. This is applied in multi-junction solar cells, which consist of several semiconductor junctions stacked on top of each other. These kinds of solar cells give the highest efficiencies but are complex and expensive to produce. The more widely used solar cells therefore contain only one absorber material. It has been calculated that, when using only one material, the optimal band gap for the solar cell is in the range of 1.3-1.6 eV [5]. The sulfide CZTS has a suitable band gap of 1.5 eV, see also Figure 3.

The band gap of a material can be either direct or indirect. This affects how efficiently photons can be absorbed in the material. Crystalline Si has

an indirect band gap and therefore requires hundreds of micrometers to absorb the sunlight. For materials with direct band gaps, such as CZTS, a much thinner film, around one micrometer, can be used to achieve the same absorption. This means that less raw material is needed which is good both from cost and environmental perspectives. Additionally, it enables the use of flexible substrates since the thin film is bendable, unlike conventional Si solar cells which are too thick to be flexible. This creates possibilities for new application niches and lighter solar cell modules. Another advantage of using thin films is that they can be grown on large areas by common high-throughput production techniques and that the cells can be connected monolithically, in contrast to crystalline Si where commonly smaller individual solar cells are made and then separately connected into modules.

2.1.3 Band alignment

The electrons excited to the conduction band are only possible to collect for a certain time, before they relax down to the valence band again, a process called recombination. Recombination is facilitated by defect states within the band gap. These defect states could have several origins, such as poor crystal quality, grain boundaries or impurity atoms. Recombination that takes place in the main part of the absorber is generally grouped together as bulk recombination, indicated by B in Figure 2.

In a heterojunction an important part is the interface between the two semiconductors, where interface recombination can occur, indicated by C in Figure 2. This can be caused by inferior material quality at the interface, either due to impurities or lack of lattice matching between the two crystals. Another property which has a major impact on the electronic properties of the heterojunction solar cell is how well the energy bands of the different materials align, both in terms of offsets and band bending. The choice of buffer and window material for CIGS and CZTS is therefore crucial for a well-functioning solar cell.

In the case of pure sulfide CZTS, the conduction band alignment with the standard CdS-buffer has been shown to be negative, forming a so-called cliff, depicted with the solid line in Figure 2. This band alignment leads to a lower open-circuit voltage (V_{oc}) than optimal [6, 7]. However, if the conduction band offset is too positive there will instead be a barrier for the electrons at the buffer-absorber interface and the fill factor (FF) will drop. An optimal conduction band line up (for CIGS) is predicted for a small positive spike of 0-0.4 eV at the buffer-absorber interface, as shown by the dotted line in Figure 2 [7]. The alternative buffers investigated in this thesis, $ZnO_{1-x}S_x$ (Zn(O,S)) and $Zn_{1-x}Sn_xO_y$ (ZTO), have tunable conduction band positions, including the range where an optimal fit together with CZTS is expected.

2.2 The CZTS solar cell stack

A thin film semiconductor solar cell stack is usually built up of substrate, back contact, absorber, buffer layer and finally a transparent front contact (see Figure 4). On top a gridded metallic contact can be added. The layers are generally very thin with typical thicknesses around 350 nm for the back contact, 800-1500 nm for the absorber, 10-100 nm for the buffer layer and around 400 nm for the front contact.

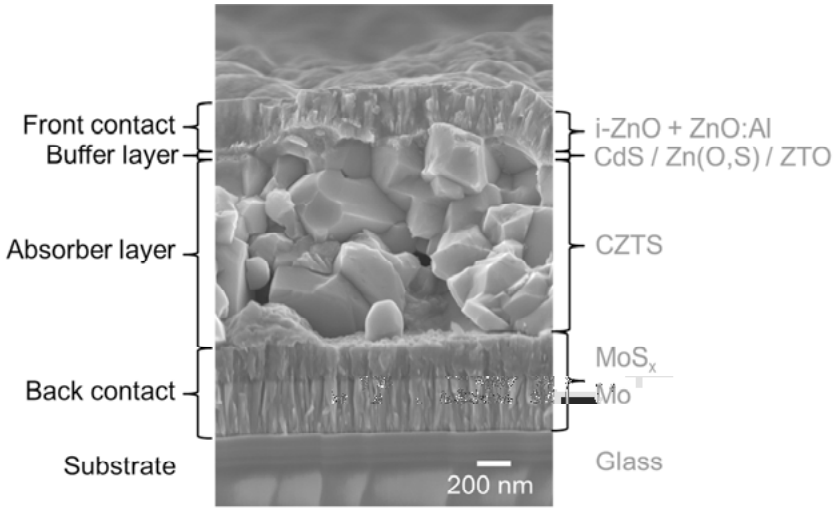

Figure 4. Typical thin film solar cell stack. Here exemplified by a scanning electron microscope image of a CZTS cross section. The materials used in this thesis are given at the right side.

The most commonly used substrate is a 1-3 mm soda lime glass (SLG). The glass consists mainly of SiO_2 but also contains plenty of additional elements at lower concentrations, for example Na, as can be seen in Table 1. For CIGS it has been shown that the Na migrating from the glass has beneficial effects on the solar cell performance [8]. This is expected also for CZTS and there are reports indicating the importance of Na for both crystal growth and optoelectronic behavior [9-11]. If a Na-free substrate is used one can instead add Na, either before, during or after absorber deposition. Examples of other substrates tested for CZTS are flexible glass [12] and stainless steel [13], as well as flexible Mo [14] and Al foils [15].

Depending on the substrate, additional adhesion layers or barrier layers to prevent diffusion of elements into the solar cell, may be needed. However, for SLG the usual approach is to deposit a back contact directly on the substrate. The standard material is Mo, deposited so that Na can diffuse through

to the absorber. This is inherited from the optimization of the CIGS solar cell structure.

Table 1. *Composition of the soda lime glass substrate used in this thesis.*

Compound	Amount [%]
SiO_2	72.2
Na_2O	14.3
CaO	6.4
MgO	4.3
K_2O	1.2
Al_2O_3	1.2
SO_3	0.3
Fe_2O_3	0.03

The part of the Mo-contact closest to the CZTS may react into MoS_2 (see Figure 4) during the high temperature annealing which is the second step of the absorber formation (see Figure 1). In the case of CIGS, the similarly formed $MoSe_2$-layer has been observed to be beneficial for the electrical properties [16]. However, the sulfur pressures during annealing required to produce high-quality CZTS may lead to a too thick MoS_2-layer, which instead could block hole transport at the back contact interface, resulting in degraded solar cell performance [17, 18]. Furthermore, a chemical instability between CZTS and Mo is predicted according to Reaction (1), which was calculated to have a large negative change in free energy, resulting in additional MoS_2 and several secondary phases [19].

$$2\ Cu_2ZnSnS_4 + Mo \rightarrow 2\ Cu_2S + 2\ ZnS + 2\ SnS + MoS_2 \quad (1)$$

These properties have instigated research for a more suitable solution, either by introducing an intermediate layer or completely exchanging the Mo. Investigated materials include TiN, TiB_2, ZnO and Al_2O_3 [20-23]. None of these modified back contacts have yet stood out as a new standard, mainly due to difficulties to form a favorable electronic contact with the absorber, but also because of the implications of Na-supply from the underlying SLG.

On top of the back contact, the absorber CZTS is deposited. This is further described in Section 2.4.

The pn-junction is formed by adding a buffer layer. Different methods can be used for depositing this layer. In this thesis, the CdS buffer is formed by chemical bath deposition (CBD). This technique uses formation of a solid compound from solution, which means that the samples are immersed into newly mixed liquid chemicals which creates an atom-by-atom growth on the surfaces as well as precipitates within the solution. The process parameters used for these depositions are described in Section 5.2. The Cd-free buffers

investigated in this thesis, Zn(O,S) and ZTO, are instead deposited by atomic layer deposition (ALD). In this method layers are created by self-terminating gas to solid-reactions. Different precursor gases are pulsed into a temperature controlled reaction chamber where the sample is placed. In an ideal process a monolayer of the gas molecules is chemisorbed to the sample in each pulse. Alternating different gases then create a slowly growing compound film, with the possibility to tune the composition by the ratio of gas pulses. In-between every precursor pulse a purge pulse of an inert gas is used to remove unreacted precursor gas and gaseous by-products. The process temperature is typically 80-350 °C. The specific process parameters used for the buffer layers in this thesis are described in Section 5.3 and 5.4. The CZTS absorber may be affected by the elevated temperatures during the ALD process. This is investigated and discussed in Section 4.3.

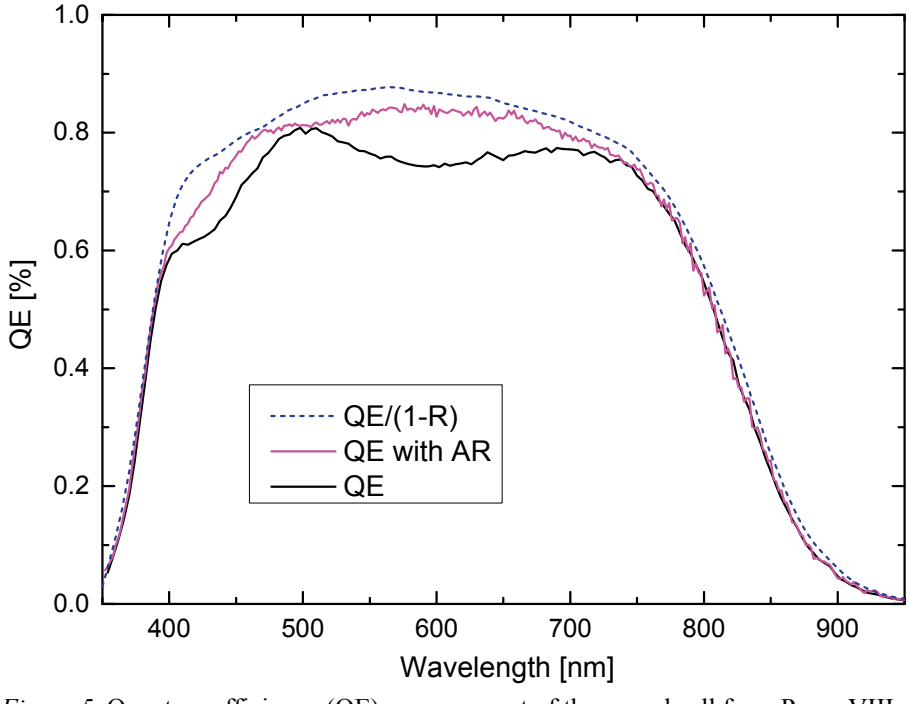

Figure 5. Quantum efficiency (QE) measurement of the record cell from Paper VIII, with and without an antireflective (AR) MgF_2-layer. Also shown is the calculated internal QE, with the full measured reflectance (R) removed.

To prevent possible shunt paths caused by defects in the CZTS absorber it is common to deposit a thin intrinsic ZnO (i-ZnO) layer before completing the solar cell with a transparent front contact. In this thesis, the front contact material used is Al-doped ZnO. The transparent contact layer is designed to have a low sheet resistance but can still not match the conductivity of a metal. A metal grid can therefore be deposited on top of the transparent front

contact. This means that part of the solar cell becomes shaded and thus the design of the grid is an optimization between shading and better conductivity. The metal layer is often Al, with a thin Ni layer below and above to decrease contact resistance otherwise caused by oxidation of Al. Commercial CIGS solar modules are generally produced without metal grid, but with a thicker transparent front contact layer.

To improve the solar cell efficiency, an antireflective (AR) coating can be added. Commonly MgF_2 is used and the thickness of the layer is adapted to the band gap, to limit the reflectance within the wavelength region where the solar cell has the highest absorption. The effect of an AR layer is illustrated in Figure 5 by a quantum efficiency (QE) measurement (see Section 3.2.2) of a sample with and without this layer, together with a calculated curve showing the potential of completely removing the reflection.

2.3 Properties of CZTS

The CZTS compound has several beneficial properties which make it suitable as an absorber material in solar cells. All its constituents are abundant and non-toxic. It has a direct band gap that ensures efficient absorption of photons, which means that only a thin layer of active material is needed. The atomic and electronic structure is similar to the commercially used CIGS absorber, which could allow for an easy exchange of absorber material in already established production processes, if CZTS proves to be the better alternative.

The band gap of CZTS is 1.5 eV which is within the optimal range for a single junction solar cell (see Section 2.1.2). The upper edge of the valence band has been calculated to consist of S *p* and Cu *d* states, while the lower part of the conduction band consists of S *s, p* and Sn *s* states [24]. By exchanging some of the S for Se it is possible to tune the band gap down to 1.0 eV for a pure selenide. Also other substitutions can be made, for example Cu to Ag, Zn to Cd and Sn to Ge. Such exchanges affect numerous parameters and have been studied both as possible new materials but also to improve CZTS solar cells [25]. Several of these substitution elements are however questionable from both availability and toxicity perspectives.

The atoms of CZTS can be ordered in several crystal structures that fulfill the octet rule. The two main structures are stannite and kesterite, which differ only in the placement of Cu and Zn, as can be seen in Figure 6. First-principles calculations show that kesterite has the lowest total energy and therefore should be the more stable form, but also that the energy difference between the structures is small [26]. Due to the similarity of Cu and Zn, both in size and charge, it is hard to distinguish between the structures in measurements, but neutron diffraction experiments have confirmed kesterite to be the dominating structure [27].

Another implication of the similarity of Cu and Zn is that it is likely that they will take each other's place, resulting in a disordered kesterite, see Figure 6. It has been shown that CZTS thin films are highly disordered, that the amount of disorder is related to the process parameters and that this also creates an apparent decrease of the band gap [28]. Neutron scattering experiments confirm the occurrence of Cu-Zn disorder [29], and nanoscale composition inhomogeneities of Cu and Zn at sizes between 1.5-5 nm were also observed with aberration corrected scanning transmission electron microscopy [30].

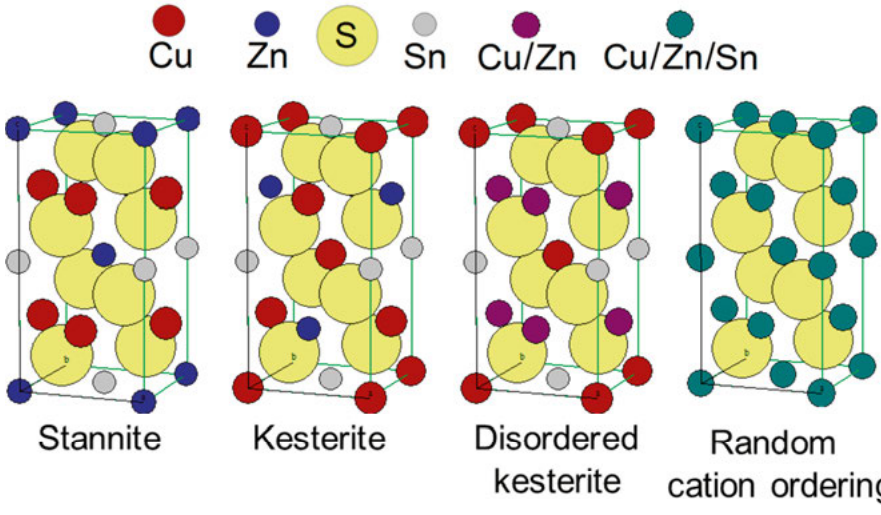

Figure 6. Examples of Cu-Zn-Sn-S crystal structures. Kesterite and stannite are the main CZTS structures and kesterite has been shown to be the dominating form. Due to the similarity between Cu and Zn there is a disorder on the Cu-Zn planes in thin film material. To the right a complete random ordering of cations is shown.

A possible disadvantage of CZTS compared to CIGS is that, while a moderate variation in In/Ga-ratio for CIGS, will not cause secondary phases, since these atoms share the same position in their crystal structure, only very small changes of the Zn/Sn ratio in CZTS are possible since these elements have specific places in the kesterite structure. This is also one of the reasons for the small single phase region for CZTS, as can be seen in the ternary phase diagram, shown in Figure 7. Controlling the composition of CZTS is therefore crucial to avoid the many secondary phases that can occur, such as the binary ZnS, SnS, SnS_2, Sn_2S_3, CuS, Cu_2S and the ternary Cu_2SnS_3, Cu_3SnS_4 compounds. Moreover, many of these phases are also hard to distinguish using common characterization methods such as X-ray diffraction (XRD) and Raman spectroscopy, due to overlap with CZTS, which further compli-

cates the pursuit for single phase material. This is also discussed in Section 2.5 and Section 3.1.

CZTS has been measured to be a p-type semiconductor [31]. Calculations indicate that the intrinsic defects mainly responsible for the doping are copper atoms on zinc sites, Cu_{Zn}^{-}, and vacancies of copper, V_{Cu}^{-} [24]. Additional to charged defects causing the doping, certain neutral defect complexes are suggested to form away from the stoichiometric point. Depending on the composition, different complexes are expected to dominate and these have been used to classify off-stoichiometric CZTS into different types, A-J, as can be seen in Figure 7.

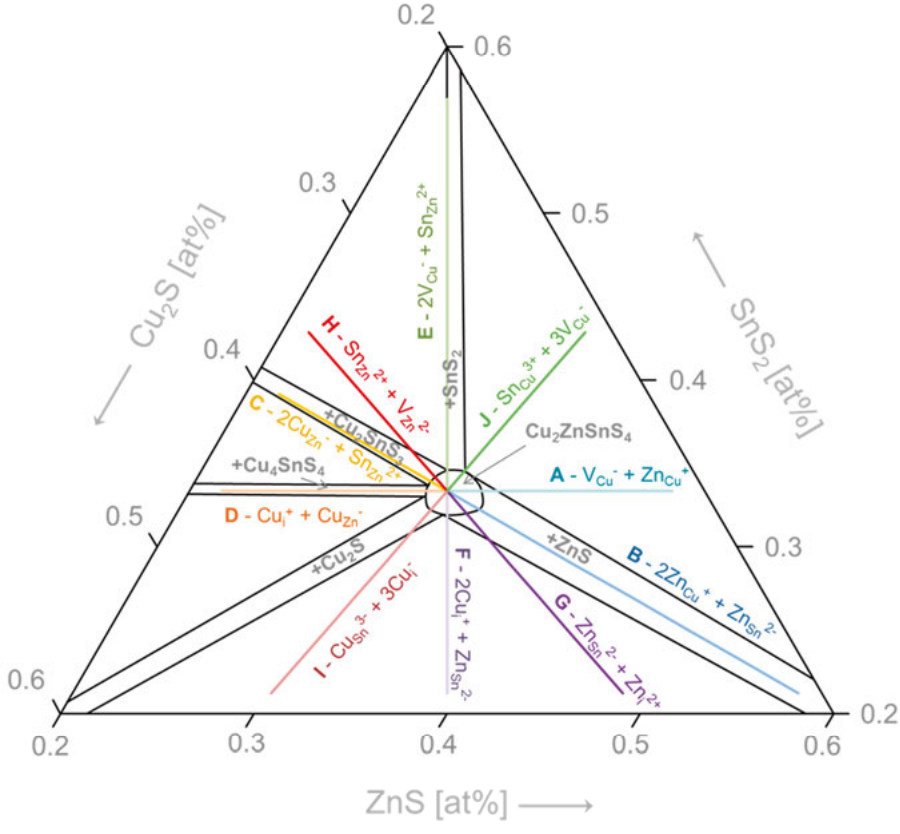

Figure 7. Part of the Cu_2S-ZnS-SnS_2 ternary phase diagram at 400 °C, adapted from [32] by J.J.S. Scragg, with the $Cu_2ZnSn_3S_8$-phase removed, following the findings in [33]. More secondary phases are found for other sulfur contents, which would be represented by a fourth axis out from the paper. Overlaid are the defect complexes expected to form in off-stoichiometric CZTS with different composition, denoted by letters according to convention in current literature.

The best CZTS solar cells are produced from Zn-rich, Cu-poor material [34], in the region between the A- and B-type lines in Figure 7. This has been

attributed to the avoidance of the Cu-S and Cu-Sn-S secondary phases (see Section 2.5). There are also indications that the CZTS material itself is superior for this composition. Cu-rich CZTS has been observed to give poor solar cell performance, tentatively attributed to high doping densities of the absorber [35]. For Cu-poor CZTS one would expect an increase in the amount of V_{Cu}^- compared to Cu_{Zn}^- which could be beneficial since V_{Cu}^- is a more shallow acceptor [24]. It has also been observed that the Cu-Zn disorder is counteracted in A-type CZTS which could be beneficial if it also affects the associated reduction of the band gap [36, 37]. Additionally, a Zn-rich composition may help to avoid the Sn_{Zn} deep defect [38, 39].

The CZTS surface has been observed to be sensitive to decomposition at low pressure and high temperature. An explanation to this was presented in [40] and arises because Sn can have several oxidation states. In CZTS, Sn has the oxidation state IV but at low S_2 pressures the II oxidation state is the stable form. The consequence is a reduction, according to Reaction (2).

$$Cu_2ZnSn^{IV}S_4\ (s) \leftrightarrow Cu_2S\ (s) + ZnS\ (s) + Sn^{II}S\ (s) + \tfrac{1}{2}\ S_2\ (g) \qquad (2)$$

Additionally, SnS has a high vapor pressure and may be lost from the CZTS surface quickly, especially at low pressures and high temperatures according to Reaction (3).

$$SnS\ (s) \leftrightarrow SnS\ (g) \qquad (3)$$

Calculations indicate the S_2 and SnS pressures needed to keep the CZTS surface stable during high temperature processing [40]. Even higher pressures are suggested to be necessary to create CZTS of A-, E, H- or J-type [36]. This limits which fabrication methods that can be used, both for the absorber itself as well as for subsequent production steps.

The properties and challenges of the CZTS material have also been described in several review articles, for example [3, 41, 42].

2.4 Deposition techniques for CZTS

Numerous techniques can be used to form the CZTS absorber. Although it is possible to grow the material into solar cell quality using a single step, most of the methods contain two or more steps, either to improve material properties or to be able to use a series of more simple methods. The deposition techniques are commonly divided into vacuum and non-vacuum methods depending on the condition of the precursor step.

A widely used vacuum technique is evaporation, where the elements are evaporated together in a chamber and then condense on the substrate to create a film. A problem with applying this technique for CZTS is the instabil-

ity of the material at high-temperature-low-pressure conditions, described in Section 2.3. This means that Sn is easily lost as SnS vapor which is then removed from the evaporation chamber through the pump system. For the selenide CZTSe it has been shown that it is possible to compensate for this behavior and produce well performing solar cells (9.2 % in efficiency) from a single-step evaporation process [43]. Also sulfide CZTS solar cells have been fabricated by this method although with lower efficiencies of 4.1 % [44]. Additionally, evaporation can be used in two-step approaches, both for depositing metal layers which are then sulfurized, for example in [45], and also for simultaneously depositing all elements and then shortly annealing it, as in for example [46].

Sputtering is another commonly used vacuum technique. Since it is the method used to produce the CZTS material in this thesis it is more thoroughly described in Section 4.1. Sputtering can be used both for depositing metal layers in two-step approaches, as for example in [47], as well as sulfur containing films, either by sputtering from targets containing sulfur [48], or by adding sulfur in the sputtering atmosphere [49]. Most of the sputtered films need a second heating or sulfurization step to crystallize into solar cell grade material but there are also attempts on single-step processes, for example in [50] yielding a solar cell efficiency of 5.5 %.

The vacuum techniques are successful for the full sulfide CZTS and most of the top performing solar cells, with just over 9 % in efficiency, are produced with two-step approaches based on evaporation or sputtering [51, 52].

For the mixed sulfo-selenide CZTSSe the vacuum-based processes have reached an efficiency of 12.3 % [53], while the top efficiencies up to 12.7 % instead are produced by non-vacuum, solution based methods [54, 55]. In these techniques all the constituents of the material are dissolved in a liquid which is then distributed on a substrate. The sample is heated to remove the solvent and crystallize the film. Several different solvents have been tried with good results, however, it is the highly toxic hydrazine which has yielded the top efficiencies.

The non-vacuum techniques are generally cheaper due to lower cost of machines, but usually results in material with more impurities. That these techniques show competitive efficiencies for CZTS could be due to the fact that the high vapor pressures of SnS, Zn and S limits the processing parameters for vacuum based methods, which causes worse material quality than expected.

Another non-vacuum method is electrodeposition. Here metal layers are created by drawing metal ions to a substrate by a voltage difference in a liquid. The plated layers can then be sulfurized in a similar way as the evaporated or sputtered films, which was done in for example [56] yielding small CZTS solar cells with an efficiency of 8.0 %.

A completely different route for creating CZTS solar cells is to synthesize small single crystal grains, monograins, in sealed ampoules and then embed

them in a thin epoxy matrix to get a thin film solar cell. This has the advantage of a wider process window during the CZTS synthesis but means that a large part of the actual solar cell area will not be active, since the grains cannot be infinitely densely packed. “Active area” efficiencies of 9.1 % [57] and actual area efficiencies of at least 5.2 % [58] have been shown for this approach.

For the two-step methods, the annealing step can be performed in a furnace or on a hot plate, with or without addition of S and Sn-S in different forms. The temperatures are usually between 500-600°C but the annealing times used vary from just a few minutes to several hours. The specific conditions used in this thesis are described and discussed in Section 4.2.

In many cases the absorber fabrication is finished by one or more etching steps to remove unwanted secondary phases. The most common etch is KCN, which effectively removes copper sulfides [44]. The etching step is usually performed just before buffer deposition to also remove possible surface compounds and avoid contaminants in the absorber-buffer interface. KCN etching was employed for most of the solar cells in this work but a comparison between untreated, KCN-etched and water-dipped absorbers can be found in Paper VII and is discussed in Section 5.5.

2.5 Secondary phases in CZTS solar cells

Since CZTS is a quaternary material with a small single phase region, as seen in Figure 7, several secondary phases are regularly found also in solar grade material. Many of these phases are hard to distinguish using common characterization methods such as XRD and Raman spectroscopy, as discussed for each method in Section 3.1. In the following section some possible implications of the sulfide secondary phases are described. A more thorough review can be found in for example [39].

ZnS is a semiconductor with a large band gap around 3.6 eV [59]. Since the best solar cell efficiencies are usually achieved for Zn-rich material, as discussed in Section 2.3, ZnS is almost always present in solar grade CZTS films. The high band gap of ZnS, together with its normally high resistivity, could cause current blocking and increase the series resistance, as exemplified in the case of ZnS as a buffer layer in Paper VI. This example also indicates that the location of the secondary phase has a large impact. A thin layer of ZnS on top of the absorber is clearly detrimental but the effect of ZnS grains within the CZTS film is more unclear. Since it exists also in high efficiency CZTS solar cells one could argue that it is benign. However, clear degradation of device performance with increasing ZnS volume fraction has also been observed [60].

There are various copper sulfides with electrical properties ranging from semiconductors, with band gaps between 1.2-2.5 eV, to electric conductors

[61]. The phases with lower band gap than the CZTS film risk to lower the V_{oc} of the solar cell [62] and phases with high conductivity risk creating shunt paths between the front and back contact. The copper sulfides are therefore generally unwanted in the CZTS film and usually etched off with KCN before buffer deposition, as discussed in Section 2.4.

Possible ternary phases include for example Cu_2SnS_3, Cu_4SnS_4 and Cu_3SnS_4, of which the first is the most commonly observed in CZTS films. The ternary phase Cu_2SnS_3 has a narrow band gap of roughly 1 eV [63] and is therefore a potential cause of low V_{oc}. Cu_2SnS_3 has similar structure and lattice parameters as CZTS and one would therefore expect that grain boundaries in-between them would be less detrimental than grain boundaries between more differently structured materials, this was also observed in [64]. However, the similarity also means that, especially for small amounts, Cu_2SnS_3 is hard to distinguish using most material characterization techniques.

Numerous tin sulfide secondary phases can be found in CZTS thin films, such as SnS, SnS_2 and Sn_2S_3. As can be seen in [65] the occurrence of different tin sulfides is mainly dependent on the sulfur partial pressure during the annealing part of the absorber formation. Several phases can also coexist in the same film. According to [65] it is mainly the SnS phase that occurs in our solar cell material. An expected narrow band gap of 1.1-1.3 eV suggests that it is detrimental for the electrical properties. However, in [66] a beneficial effect is seen from SnS at the back contact and it is hypothesized that, despite the narrow band gap, the band alignment between the two phases is spike-like (see also Section 2.1.3). But also in this case the location of the secondary phase has a large impact and SnS at the absorber-buffer interface is observed to be detrimental.

Additional secondary phases that contain more elements than the ones in CZTS can also form in, or close to, the absorber, for example MoS_2 (discussed in Section 2.2) and different Na-containing compounds (discussed in Section 5.5).

2.6 Efficiency limitations for CZTS solar cells

For the CZTS material to be of commercial interest a conversion efficiency of 15-20 % is required at research level. The pure sulfide CZTS solar cell efficiencies were initially improved rapidly, starting at 0.7 % in 1997 and continuously increasing up to 6.8 % in 2008 by the efforts of only a few research groups, see Figure 8. The increasing efficiency values attracted attention and the research intensified, both at universities and companies, which brought the record up to 9.2 % at the end of 2012 [51]. In the latest years the efficiency improvement has slowed down and the record in a published article was stagnant at 9.2 % for a several years, however over time

reached by several groups. Very recently a solar cell with 11.0 % efficiency was published [67]. The latest improvement was attributed to an optimized annealing process and a post-annealing of the heterojunction causing inter-diffusion between CZTS and CdS and thus improving the interface properties.

For the mixed sulfoselenide the record in a published article is 12.7 % since mid-2014, however, the certified value for this cell was 12.3 %, and one could therefore also argue that the certified 12.6 % solar cell published in late 2013 is the current record, see Figure 8 [54, 55].

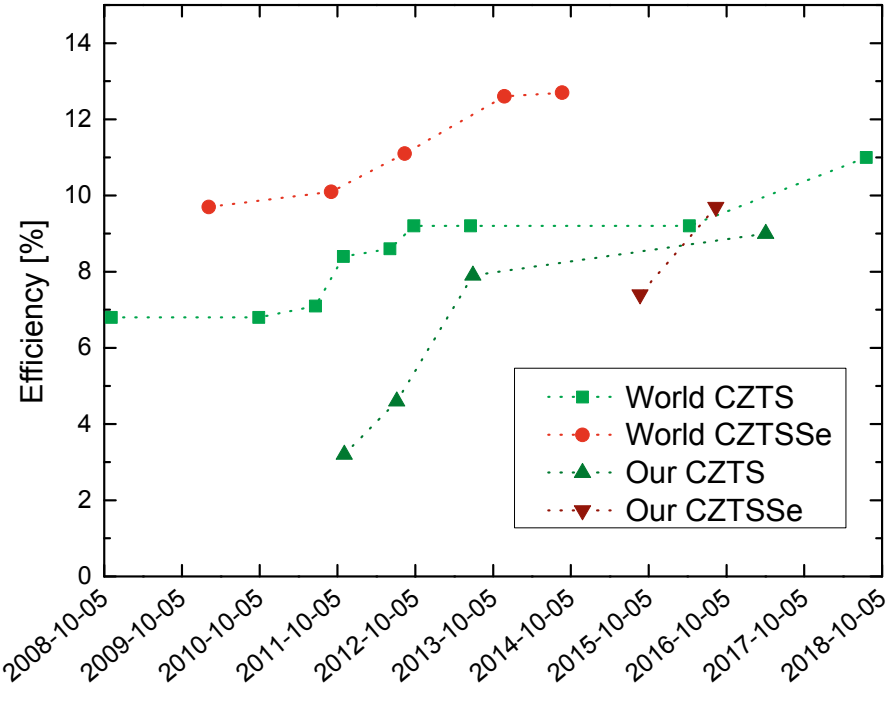

Figure 8. Top efficiencies in published articles for CZTS and CZTSSe from the last ten years, world records and group records. Data from Paper IV, Paper VIII and [17, 20, 35, 45, 46, 51, 52, 54, 55, 67-75].

The efficiency progress from our research group is also outlined in Figure 8 and shows an initial rapid improvement, both due to optimization of the absorber precursor, such as composition calibration and incorporation of sulfur, and annealing parameters, mainly the change-over to a sulfur containing atmosphere. Additionally, our latest efficiency increase comes from optimization of the buffer layer. The focus for our group was initially the pure sulfide CZTS and this has led to efficiencies close to the world records. Part of the work leading to these improvements is described in this thesis.

The main parameter limiting CZTS efficiency has for a long time been a low V_{oc}, especially compared to what is expected from a material with this

band gap. Several origins for low efficiency and low V_{oc} have been identified by the research community and some of them are presented in more detail below, together with references to the sections in this thesis where the problems have been addressed.

2.6.1 Secondary phases

The small single phase region combined with the limited fabrication methods available, due to the risk of decomposition, leads to a high probability for secondary phases in the CZTS thin films. Additionally, the surface reaction described in Section 2.3, and the suspected instability with the Mo back contact shown in Section 2.2, may result in secondary phases at the interfaces. The secondary phases can be detrimental to the solar cell efficiency in several ways depending on their location and electrical properties, as was discussed in Section 2.5.

A way to limit the amount of secondary phases is to optimize the fabrication route to ensure an even distribution of all the constituent elements before attempting a crystallization step. This is especially important for CZTS due to the absence of a suitable ternary metallic Cu-Zn-Sn compound [76]. Thus a fabrication route starting with a metallic film is expected to suffer from phase separation during processing, as also exemplified by the phase separated metallic film presented in Paper I and discussed in Section 4.1.2. Including sulfur in the precursor film ensures the possibility of a rapid formation of the CZTS phase, with less risk for secondary phase segregation and a better basis for a void-free morphology. Additionally, it limits the need for long annealing times, which would risk to cause surface decomposition or back contact reaction. A precursor film with such properties can be fabricated by reactively sputtering the appropriate metals in a H_2S-atmosphere, or by compound sputtering of sulfur-containing binaries, creating a film with all the necessary elements for CZTS homogenously mixed. Creating such films is addressed in the first part of this thesis, which focuses on the development of sulfur containing precursors for CZTS absorbers, see Chapter 4. These precursors have a similar crystal structure to CZTS and therefore only need a short annealing time to form well performing solar cell material, a 3 min annealing for reactively sputtered precursors is described in Paper IV and a 1 min annealing for compound sputtered precursors is shown in [65].

2.6.2 Band alignment at the CZTS-buffer junction

The most common buffer layer used for CIGS solar cells is CdS and this was thus the first choice also for CZTS. However, for the full sulfur CZTS it has been shown that the band alignment with CdS is cliff-like which is known to decrease V_{oc}, as also discussed in Section 2.1.3. Even for the champion CZTSSe solar cells, interface recombination is pointed out as one of the

main problems [54]. The optimization of the CZTS-buffer junction is addressed in the second part of this thesis, see Chapter 5.

2.6.3 Defects and band tailing

Recently the discussions about the low V_{oc} of CZTS focus on the electrical quality of the bulk material. Band tailing, meaning that there is a large number of defect states close to the band edges which can deteriorate the electrical properties and/or narrow the band gap, has been presented as a likely cause for the low V_{oc}. Both measurement observations by photoluminescence (PL) and QE, and calculations, suggest the presence of band tailing [28, 77]. The origin of the band tails is most often suggested to be the Cu-Zn disorder, causing either a variation of band gap [28] or electrostatic potential fluctuations [77]. Depending on the physical scale of regions with different Cu-Zn exchanges one would expect both type of fluctuations to co-exist. This is also what is described for CIGS in [78] and observed for CZTSSe in [79]. The low dielectric constant for CZTSSe is suggested to increase the materials sensitivity to potential fluctuations [77]. Remedies for these problems are suggested to be band gap grading, substituting Cu or Zn with elements that are less similar, and defect engineering, such as aiming for a CZTS material with higher amount of the more shallow acceptor V_{Cu}^{-} instead of Cu_{Zn}^{-}, for example by using of A-type CZTS (see Figure 7) [28, 79, 80].

In a recently published survey, the conclusion was that the most important limitation of the CZTS material is short carrier lifetime due to recombination via deep defects [81]. First-principles calculations have also indicated the presence of deep defects, especially for the full sulfide CZTS, where Sn_{Zn}^{2+} and V_S^{2+} have relatively low formation energies and could act as electron traps [24, 82]. However, from materials analysis, neutron scattering rather observed Zn_{Sn}-defects for device relevant compositions [29]. In [82] the calculations indicate that the cooling conditions and potential post-annealing can have a large impact on which defects and defect complexes that are present in CZTS and thus the electrical properties of the material. This is also investigated in Paper VIII and discussed in Section 4.3.

3. Characterization techniques

3.1 Materials characterization

In this section, techniques used to measure the materials properties of the thin films will be discussed. The emphasis is on the application for CZTS characterization.

3.1.1 Composition measurements

Due to the complexity of the CZTS material and the small single phase region, the desired accuracy for the metal composition is within a couple of atomic percent. A good knowledge of the composition also makes interpretation of other experimental results more reliable.

Composition is usually given in relative quantities, e.g. atomic percent (at%) or weight percent (wt%). A composition measurement can be derived by modeling of an expected signal, accounting for all the elements in the sample, or be calibrated with a known reference sample, which has been characterized by a measurement method that yields the absolute number of atoms for a sample.

An early project in this thesis work was to create a simple and reliable composition measurement procedure for the CZTS samples and precursors. This is thoroughly described in my licentiate thesis [83] and will therefore only be briefly mentioned here. The method chosen was to use two thickness series, Cu-Sn and Zn respectively, characterized with Rutherford backscattering spectrometry (RBS), to calibrate an x-ray fluorescence system (XRF). With RBS it is possible to determine an absolute areal density for thin films of heavy elements, while XRF is a quick technique, yielding a signal from a large part of the sample. RBS measurements are more time consuming and therefore generally appropriate for reference samples or limited sample series.

These two composition measurement techniques are described below, together with the frequently used energy dispersive x-ray spectroscopy (EDS) technique.

Energy dispersive x-ray spectroscopy (EDS or EDX)

The most commonly available method for composition measurements is EDS. This technique utilizes the interaction between incoming electrons and

sample atoms which causes emission of characteristic x-ray radiation. An electron beam, usually in a scanning or transmission electron microscope (SEM or TEM), is directed towards the sample surface and interacts with the material in many ways, creating secondary electrons, backscattered electrons and x-rays. The electrons can be used to create images with a secondary or backscattered electron detector. The composition is measured with an EDS-detector which analyzes the energies of the x-rays that are created when the incoming electron excites an inner shell electron in the atom and an outer shell electron takes its place. The x-ray energy is dependent on the energy difference between the shells and this is specific for different elements. It is therefore possible to decide in which element the x-ray was created and thus which elements the material consists of.

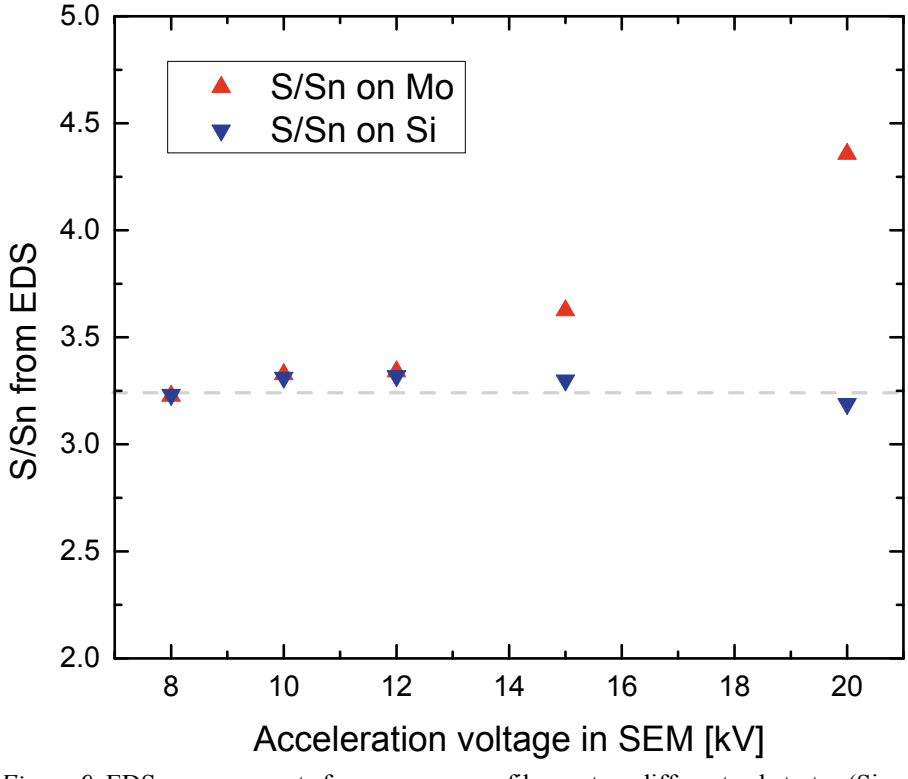

Figure 9. EDS measurements from a precursor film on two different substrates (Si and Mo-coated SLG) produced in the same sputtering run. The information depth of the measurement was investigated by decreasing the acceleration voltage in the SEM. For this sample 12 kV was low enough to avoid signal from the Mo-layer and below this voltage the sulfur content of the two films agrees well. Above this voltage, the seemingly increased sulfur content in the precursor on Mo is due to the overlap of S and Mo in the EDS technique.

The amount of characteristic x-rays coming from the sample is proportional to the amount of the specific element, but also depends on how easy it is to excite electrons in that specific atom, how likely it is that an x-ray will be formed and also on the other elements that are included in the material, since these will affect the electrons going in and the x-rays coming back to the detector. The composition data from EDS are therefore always relative and based on software calculations. To refine this, one can measure known standards, similar to the unknown sample, which helps to account for the matrix effects. In some software programs, one can also insert models of how the elements are distributed in the sample, for example that the sample consists of a thin film on top of a substrate. If this is not done, the software will assume a homogenous sample, potentially giving misleading results.

Overlap between characteristic energies of different elements can be a problem. This is the case for Mo and S, where the energy distance between the innermost shell and the next in S, is almost the same as between the second innermost and the next in Mo. Using a detector which measures the x-ray wavelength instead of energy (WDX), improves the resolution, but these detectors are generally slower and therefore less commonly used. If the overlapping elements are at different depths it may be possible to distinguish between them by reducing the incoming electron energy, limiting the penetration depth of the electrons thus ensuring that the signal only comes from a layer close to the surface, as is exemplified in Figure 9.

The EDS system mainly used in this thesis was an EDAX included in a LEO 440 SEM. The instrument had been calibrated with a range of pure elemental samples (not specifically Cu, Zn and Sn) and was run with the standard software.

Rutherford backscattering spectrometry (RBS)

In RBS the material of interest is bombarded with ions with high and well-defined energy. The ions are backscattered by the atoms in the material and their energy will then depend on the mass of the atom it interacted with and the distance through the material it travelled before it reached this atom. The intensity of backscattered ions as a function of their energy is recorded. An ion that has been backscattered by a heavy atom has a higher energy than one that has been backscattered by a light atom. Additionally, an ion that has travelled through some material and been scattered from an atom deeper in the film has lower energy than an ion that has been backscattered from an atom on the surface. The relationship between the intensities from different elements gives the composition, and the widths of peaks give the thickness of the film. The interactions can be simulated in a program and if a good fit can be obtained the measurement yields an absolute areal density of atoms.

The RBS method is most easily applied to thin films of heavy atoms on substrates made of light elements, since overlap in the signals are then avoided and the fitting is more obvious.

As for most measurement techniques, a certain amount of energy is added to the sample by the incoming species, in this case ions. It is therefore important to make sure that this does not affect the sample. The risk for damage to occur is higher for samples that have a non-equilibrium form or are easily evaporated. A way of detecting this is to monitor the measurement and make sure that the peak profile does not change over time.

Due to the similar atomic mass of Cu and Zn, their peaks overlap almost completely in RBS when using a 2 MeV He^+ ion beam, as was done in this thesis. For our composition calibration of CZTS we therefore chose to make two different thickness series, one with a Cu-Sn-alloy and one with pure Zn. The measurements were done at the Uppsala Tandem Laboratory (Ion Technology Center). To analyze the results, the simulation program SIMNRA [84] was used. Care was taken to fit the peaks both by shape and integrated peak intensity.

A complementary ion beam technique, more suitable for light elements, is elastic recoil detection analysis (ERDA) which generally uses heavier incoming ions and analyzes the recoiled sample atoms.

X-ray fluorescence (XRF)

The XRF technique utilizes characteristic x-rays, as in EDS, but instead of generating them by an electron beam, they are generated by irradiating the sample with x-rays. The fluorescence effect is largest when the incoming x-rays have an energy just above the characteristic absorption edge of the element. This means that, to get as large signal as possible, different incoming x-ray energies, for the different elements to be detected, should be used. This can be achieved by having one x-ray source but several secondary targets in the XRF-system. The penetration depth is much larger for x-rays compared to electrons which mean that the information depth generally is larger for XRF compared to EDS.

The intensity of the emitted fluorescence directly gives an indication of the amount of material, if two similar samples are compared, but to be able to get the composition in atomic percent, a calibration has to be made.

For films that are thinner than a couple of micrometers, it can be assumed that the fluorescence counts are proportional to the amount of material but to get a more exact result, especially for thicker films, the attenuation of the x-rays can be taken into account. The attenuation follows Equation 4, where A is the attenuation, I is the intensity coming from the sample, I_0 is the unattenuated intensity, x is the sample density multiplied by the thickness, and c is the mass attenuation coefficient.

$$A = 1\text{-}I/I_0 = 1 - e^{-cx} \tag{4}$$

The density multiplied with the thickness, x, is the same as areal density, which is the result that is obtained from RBS. The RBS values can therefore

directly be inserted in this equation without knowing the physical thickness of the film. The mass attenuation coefficients can be taken from [85] and are given for a certain element, but can also be calculated for compounds using the wt% of the constituents.

Assuming that characteristic x-rays are created evenly throughout the film thickness, the attenuation should be integrated, from the deepest emission point of x-rays, to the surface. This integral and its solution are shown in Equation 5, where A_{tot} is the total attenuation that the signal will suffer and u is the fraction of film between the emission point and the surface.

$$A_{tot} = \int_0^1 (1 - e^{-cxu}) du = 1 + \frac{1}{cx}(e^{-cx} - 1) \quad (5)$$

An even more exact calculation would include what happens to the attenuated x-rays since these can, for example, be re-emitted as characteristic x-rays from the atom that absorbed it. However, in our case the characteristic x-ray energy from Zn is not high enough to ionize electrons from the Cu K-shell and the x-ray energies from Sn are too high to create more than a negligible amount of fluorescence in Cu and Zn.

The XRF system used in this thesis was a PANalytical Epsilon 5. The noise and background signals were low. A Ge secondary target was chosen for the measurement of Cu and Zn and BaF_2 for Sn. The measurement live time was set to 60 s in each case. For each element an energy region was chosen in which the counts were integrated. Cu and Zn are close in energy and thus, if the count is high, the tails of their peaks could overlap slightly. The chosen energy range was therefore kept close to the middle of the peak for these elements.

3.1.2 Raman spectroscopy

Raman spectroscopy exploits the fact that atoms bonded together vibrate with certain frequencies. When laser light is shone on a sample, a fraction of it gets inelastically scattered and shifted in wavelength. The amount of the shift is connected to which atoms are involved in the vibration and how they are arranged. This means that a given material has a certain pattern of shifts, corresponding to peaks in a Raman spectrum.

This technique is usually very surface sensitive because the wavelength of the incident laser light is in the visual range and the penetration depth therefore is limited, for CZTS to around 100 nm when using a 514 nm laser [86, 87]. However, the information depth is slightly changed depending on the wavelength of the laser and this can also be utilized to distinguish materials properties that varies with depth [88].

Raman spectroscopy on CZTS gives a spectrum with specific peak positions and intensities, but several secondary phases, such as SnS_2, Sn_2S_3 and

most of the Cu-Sn-S-compounds, have peaks in the same region and can therefore seldom be easily excluded. The Raman peaks from the secondary phase ZnS also overlaps with CZTS if using an excitation wavelength of 514 nm but changing to a 325 nm laser enables separation of the signals, since this wavelength causes resonant excitation in ZnS but not in CZTS. SnS and several Cu-S-compounds can also be distinguished with Raman spectroscopy. Raman spectra of CZTS and its secondary phases have been investigated and discussed in several publications, such as [33, 89-91].

The Raman spectroscopy measurements in this thesis were mostly done with a Renishaw system, at an excitation wavelength of 514 nm.

3.1.3 X-ray diffraction

X-ray diffraction (XRD) is an analysis method that can be used to observe the structure parameters of crystalline materials. A crystalline material is arranged in a lattice where atoms have certain positions depending on the structure of the material. This ordering also creates planes of atoms and thus a distance between planes. When irradiating the crystalline material with x-rays, the light waves will interact with the electrons of the atoms in the planes and constructive interference will occur for certain conditions, depending on the wavelength and angle of the incoming x-rays, and the distance between the atomic planes. Additionally, the type of atoms in the structure will influence the intensity. A plot of intensity versus angle will thus yield a specific pattern for a certain material, called a diffractogram. Patterns can be calculated from the structure of a material but there is also a library with measured reference samples to compare with.

The reference patterns are usually recorded from powders, and applying this technique to thin films has additional challenges, such as lower intensities due to a smaller interaction volume. A thin film can also be affected by the growth method or the substrate it has been produced on, causing preferential orientation or strain in the films, which alters the diffractogram.

CZTS, ZnS and several Cu-Sn-S-compounds have similar crystal structures which mean that many of the peaks in their patterns overlap. Among them ZnS has the simplest structure and thus yields fewest peaks. The CZTS pattern contains small, additional peaks and is therefore distinguishable, but the presence of ZnS cannot easily be ruled out. Sn-S and Cu-S compounds are generally more straightforward to differentiate from CZTS by XRD.

Since the x-rays have a large penetration depth it is possible to detect secondary phases both in the bulk and at the back contact, if the amount is large enough. Specific x-ray measurements can also be performed in the diffractometer to find the thickness, texture and stress of thin films.

Most of the measurements in this thesis were performed with a Siemens D5000 system or a Phillips X'pert MRD diffractometer.

3.1.4 Stress measurements

Stress in films can cause delamination and cracks, as well as changes in crystal formation and electronic properties. It is therefore usually important to measure and control stress in thin films.

Several approaches can be used to measure the stress. One way is to look at the peak shifts in XRD, since stress will affect the distances between the atomic planes, hence shifting the peak position. However, peak shifts in XRD could also have other origins, such as off-stoichiometry or secondary phases. A more direct way of measuring the stress is to look at the difference in curvature of a sample, before and after film deposition. If the substrate is flexible enough, and the stress in the thin film is high enough, it will cause a measurable change in the curvature. This transformation can be evaluated either by a mechanical approach, for example with a profilometer, or optically, either from the side, measuring reflection, or from the top, measuring interference patterns.

In this thesis the profilometer approach was chosen and the measurements were done with a Veeco Dektak 150. The most common substrate to use for such measurements are Si-wafers, but since the growth, and therefore stress, could be different on different substrates, we chose to use Mo-coated thin glass slides (100 µm thick cover glass D 263® M from Schott). In this way we could ensure that the results were relevant for solar cell films produced on Mo.

In the case of Si-wafers, it is often assumed that the untreated wafer is flat, but the glass substrate had a curvature already before the CZTS precursor deposition due to the applied Mo film, which also contained certain stress. It was therefore important to measure the curvature both before and after the CZTS precursor deposition. The measurement was made along two directions, perpendicular to each side of the quadratic glass piece, and was individually compared to the respective values after the precursor deposition. The curvatures were fitted by a least squares method. The resulting radii were used to calculate the stress, σ, using the Stoney formula (6) found for example in [92], where r_{pre} and r_{post} are the radii before and after the precursor deposition, E is the Young modulus for the glass (72.9 kN/mm^2, given by the manufacturer), ϑ is the Poisson ratio for the glass (0.208, given by the manufacturer) and t_s and t_f are the thickness of the substrate and film respectively.

$$\sigma = \frac{1}{6}\left(\frac{1}{r_{post}} - \frac{1}{r_{pre}}\right)\frac{E}{1-\vartheta}\frac{t_s^2}{t_f} \tag{6}$$

3.2 Electrical characterization

In this section the techniques used to characterize the electrical properties of the solar cells are described.

3.2.1 Current-voltage

The most straightforward method to characterize a solar cell is to look at its current response for different voltages, a current-voltage (IV) measurement. This can be done both in dark and under illumination and it gives several important parameters such as the open-circuit voltage (V_{oc}), short-circuit current (J_{sc}), fill factor (FF) and the efficiency of the solar cell. Additionally, by fitting the curve or part of it, most often to a one-diode model, other parameters can be obtained, such as series resistance (R_s), shunt conductance (G_{sh}), ideality factor (A) and saturation current density (J_0). A commonly used procedure for extracting these parameters is described in [93]. However, to do this certain assumptions must be made and caution should therefore be taken when applying this to solar cells with low efficiency or non-ideal behavior [93].

Two different IV-setups were used to measure the solar cells in this work. For Paper II, IV and VI a tungsten halogen lamp was used as illumination. To minimize the error from mismatch between the halogen lamp and the AM1.5 spectrum, the intensity of the lamp was adjusted to yield the J_{sc} from the QE measurement (described in Section 3.2.2), after correcting this value with the expected grid shading from the metal top contact.

For Papers VII and VIII a class A solar simulator from Newport was used. In both cases the samples were placed on a temperature controlled stage kept at 25 °C.

3.2.2 Quantum efficiency

The solar cell response to photons of different wavelengths is represented by a QE measurement. Light with a known intensity and wavelength is shone on the cell and the resulting current is recorded. This is then repeated over the spectrum range of interest. The ratio of the number of charge carriers collected, to the number of incoming photons, gives the external QE. When correcting for the measured reflectance the internal QE can be obtained, see also Figure 5.

The standard QE is measured under short-circuit conditions but the measurement can also be performed with either forward or reverse bias applied. This is a way to judge if the effects observed in the QE origins from optical or electrical losses, since only the latter should be affected by the applied bias. Such measurements are usually presented as a ratio between the biased and non-biased curves.

From the cut-off at the high wavelength side the band gap of the main material can be retrieved. Several methods for extracting the band gap value are used in literature. For Paper IV the band gap was retrieved by plotting $(QE)^2$ versus photon energy and extrapolating the linear region at the low energy side of the spectrum to the x-axis, interpreting its intersection as the band gap. For Paper VIII (photon energy*(ln(1-QE)))^2 was used instead of $(QE)^2$. Both methods include questionable approximations, where the $(QE)^2$ is one step further expanded. According to an internal study by S.-Y. Li [94] the methods yield slightly different results and are more or less sensitive to solar cell thickness and band tailing. By comparing with simulations the ln-method was found to give most robust results (as an example the QE^2-method yielded 1.44-1.53 eV and ln-method 1.52-1.55 eV for a simulated variation of thickness and band tailing). A similar method, (ln(1-(internal QE))^2 vs. E, was evaluated in [95] and found to give sound results for $Cu_2ZnSnSe_4$ (CZTSe).

For the papers in this thesis the external QE was measured in a homebuilt setup, calibrated with an external Si calibration cell from Hamamatsu.

3.2.3 Temperature dependent current-voltage

By measuring the current-voltage curve at a range of temperatures (IVT), additional information can be gained. For example, when plotting V_{oc} versus T and extrapolating the linear part close to room temperature to 0 K the activation energy of the dominant recombination path is found according to Equation (7), as also described in for example [93].

$$V_{oc} = \frac{E_A}{q} - \frac{AkT}{q} ln\left(\frac{J_{00}}{J_L}\right) \quad (7)$$

Here E_A is the activation energy, q is the elemental charge, A is the diode ideality factor, k is the Boltzmann constant, T is the temperature, J_{00} is the saturation current prefactor and J_L is the photocurrent density. If the activation energy achieved is lower than the band gap of the absorber, it is typically assumed that the solar cell is limited by interface recombination (see Section 2.1.3 and Figure 2).

In this thesis, IVT measurements were performed at 100 to 330 K by placing the sample on a liquid nitrogen cryostat connected to a Lakeshore 325 auto tuning temperature controller and using a Keithley 2041 SourceMeter. White light LED was used as the light source and its intensity was calibrated to match the J_{sc} previously measured with IV. The temperature independence of the ideality factor was checked for the values included in the linear extrapolation of V_{oc} to 0 K.

4. Cu_2ZnSnS_4 absorber formation

As described in Section 2.4 there are several ways to create the absorber material CZTS. In the following chapter the methods investigated and optimized in this thesis will be discussed. Part of this is also covered in my licentiate thesis [83].

4.1 Sputtering

4.1.1 Introduction to sputtering

Sputtering is a physical vapor deposition technique where atoms are ejected from a solid surface (target) by energetic ions. Sputtering is a scalable technique and widely used for production of thin films.

The process takes place in a deposition chamber which is evacuated to low pressure by a pump system. A sketch of a sputtering system can be seen in Figure 10. The substrate to be coated is placed in the chamber together with one, or several, solid material targets containing the coating elements. When supplying a controlled amount of gas and applying a high negative potential to the target, the gas becomes ionized and a plasma is created. Since the ions are charged they are drawn towards the target, which acts as the cathode. When they hit the target, atoms from the coating material are ejected, or sputtered. The sputtered atoms will travel through the chamber and end up on all surfaces, including the substrate intended to be coated.

Also electrons are ejected when the ion hit the target. These are needed to sustain the plasma in the chamber. The average number of electrons emitted from one incident ion is denoted secondary electron yield and depends on the target material and the state of the target surface.

To increase the probability of the secondary electrons to ionize the gas one can use a magnetic field to cause the electrons to move in spirals close to the target and thus create a denser plasma at this position. The equipment used to create the magnetic field is called a magnetron and this technique is therefore known as magnetron sputtering. This method enable lower process pressures without losing the plasma and increases the sputtering rate significantly. However, most magnetron setups create an inhomogeneous erosion profile of the target due to a variation of the direction of the magnetic field

over the target area, and thus decrease the target material utilization. This can partly be solved by more advanced magnetic field designs.

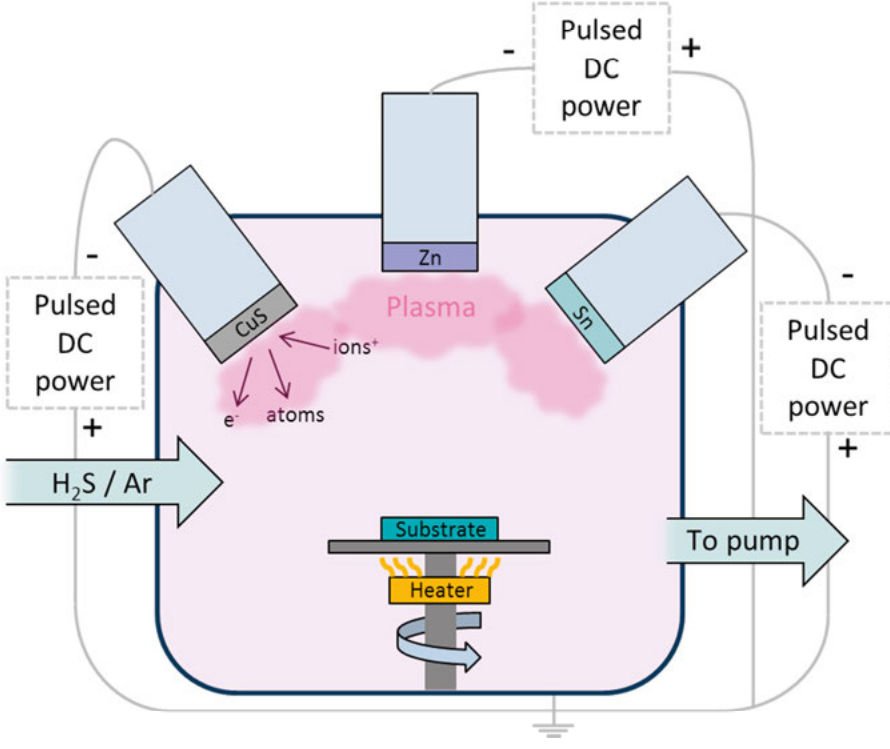

Figure 10. Sketch of a sputter setup, here exemplified by the arrangement used in Paper VII.

Several parameters can influence the properties of a sputtered film, such as pressure in the chamber, distance between the substrate and target, deposition rate and temperature of the substrate. Sputtered films generally have good quality and adhesion due to the energy the incoming atoms gain from the sputtering event. Additionally, the growing layer may be subjected to particle bombardment both from neutrals and negative ions, depending on the deposition parameters, and this may also affect the film quality.

A structure zone model for sputtering (SZM), as shown in Figure 11, can be used to classify the morphology of sputtered films. The variation of film properties with temperature arises mainly because higher substrate temperature improves the surface mobility of the sputtered atoms, which means increased probability of finding favorable positions in the growing film. At even higher temperatures also bulk diffusion and recrystallization occurs. The effect of the process pressure is caused by a higher probability of collisions between the sputtered atoms and the process gas with increasing pres-

sures. This both randomizes the direction of the arriving atoms and additionally reduces their energy which decreases the surface mobility.

Films with multiple elements can be created by using one target with several elements or several targets in the same chamber directed towards a single substrate position, the latter usually denoted co-sputtering. In such a setup it is also possible to create composition gradients within the film depth since the deposition rate from a certain target can be varied by changing the target power.

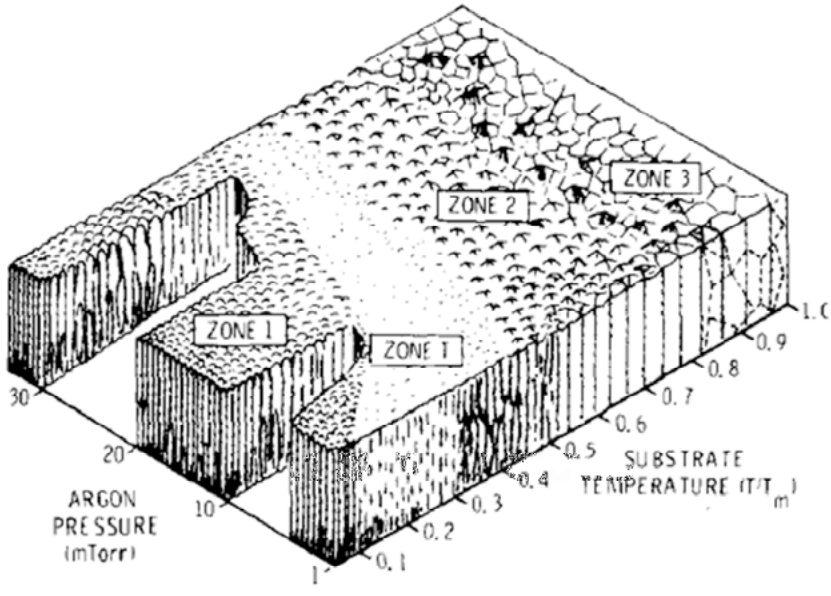

Figure 11. Structure zone model from [96] showing the characteristics of films sputtered at different conditions.

The voltage applied to the target can either be constant (DC sputtering), or applied with a frequency (pulsed DC sputtering or RF sputtering). The different types are used depending on the conductivity of the target. If the target is weakly conductive or insulating, a charge will be accumulated at the surface eventually leading to sudden electrical breakdown and an arc discharge. In pulsed DC and RF sputtering this is avoided by turning the voltage off, or reversing its direction, for short times, meaning that the surface is discharged and never reaches the point of breakdown. A disadvantage with RF sputtering is that the equipment is more complex and therefore more expensive. The deposition rate is also substantially lowered and this requires longer deposition times, which is undesirable from a production point of view. Low deposition rates also generally yield films with a higher degree of contamination because, even at the low pressures used in sputtering, there are small

amounts of oxygen and other contaminants adsorbing on the surfaces during the deposition, which are then incorporated in the film.

In reactive sputtering, an additional reactive gas is added to the sputtering atmosphere and sputtering is performed, either solely in the reactive gas, or in a mixture of the reactive gas and the inert working gas. The targets are most often metals and the target surface can thus react with the gas to form a compound. The altered target surface can in turn affect the deposition rate and secondary electron yield, and thus, if the process is run in constant power mode, also the target voltage. To describe these changes, measurements at different reactive gas flows can be made and put together in a process curve. The film composition can, as in normal co-sputtering, be changed by varying the target powers, but additionally by adjusting the fraction of reactive gas.

If only using compounds as target materials it can be referred to as compound sputtering. Compound sputtering is conceptually easier than reactive sputtering since there is no metal-compound transition of the targets. A disadvantage of insulating compounds is the need for RF sputtering. Compounds are also in general more brittle compared to metals and have a lower thermal conductivity which means that more care has to be taken when increasing and decreasing target power to avoid cracks in the targets. The price of a compound target is usually substantially higher than the price for a metal target.

4.1.2 Reactive sputtering of precursors for CZTS

An advantage with reactive sputtering of Cu-Zn-Sn-S films is the possibility to adjust the sulfur content. If separate metal targets are used also these elements can be controlled without restrictions, making it possible to produce samples over the whole composition range.

Reactive sputtering setup

The film depositions for Paper I-VI were performed in a Von Ardenne CS600 sputtering system with two magnetrons and a front side heater, all facing the substrate at an angle of 45° at 160 mm distance. The absorber in Paper VII was deposited in the same system, but it was rebuilt to comprise a heater under the substrate, enabling space for an additional magnetron. For Paper VIII another sputter system was used, this is described in Section 4.1.3.

The targets were 102 mm in diameter and 6 mm thick. The base pressure was below 10^{-4} Pa. The maximum setting for the radiative front side heater was 500°C, yielding a maximum temperature at the substrate of approximately 300 °C. The heater installed under the substrate could give a maximum substrate temperature of around 500-600 °C but the absorber depositions concerned in this thesis were mainly performed at 180 °C.

As the deposition system was initially limited to two target positions an alloy target had to be used to be able to deposit all metals needed for CZTS. Due to the low melting point of Sn and its good miscibility with Cu, a Cu-Sn-alloy target was chosen. This allowed easy control over the Zn-content in the films, but the Cu/Sn-ratio was, in theory, determined by the specific target composition. Two different Cu-Sn-alloys were used, one with 67 at% Cu and 33 at% Sn (purity 99.99 %) and one with 65 at% Cu and 35 at% Sn (purity 99.999 %). The Zn-target had a purity of 99.994-99.995 %.

When the system was rebuilt to include a back side heater, three targets could be used, enabling full control of the metal ratios. Pure metal targets were tested but instabilities in the Cu deposition rate, in combination with arc discharges and flakes from the target, were observed. This was caused by that the Cu-target surface became highly sulfurized from the background pressure in the chamber. The Cu-target was therefore replaced by a Cu_2S-target but also this process was unstable and the target exhibited cracks after usage. These issues are further discussed in the "Target stability"-section below. The Cu_2S-target was replaced with a CuS-target (purity 99.99 %) which performed stably and thus was used for sputtering the absorbers in Paper VII, together with metallic Zn (purity 99.994-99.995 %) and Sn (purity 99.998-99.999 %).

To incorporate sulfur in the precursors, H_2S (purity 99.5 %) was used as a process gas, solely or together with Ar. For Cu-Sn-, Zn- and Sn-targets the magnetrons were operated in constant power mode by pulsed DC with a frequency of 20 kHz, supplied by two Huttinger PFG 3000 DC power supplies equipped with Advanced Energy Sparc-le 20 pulsing units. The insulating ZnS surface layer on the Zn-target was sufficiently thin not to cause arcing problems at this frequency. The CuS-target was operated in constant power mode, with a pulsing frequency of 150 kHz and an off time of 2 μs by an Advanced Energy DC Pinnacle Plus.

Process curve

The process curve of the first target setup, using a Cu-Sn-alloy and a Zn-target, is included and described in Paper I. It shows that the Zn-target is affected at a lower H_2S-flow than the Cu-Sn-target, indicating that the Zn is first to be sulfurized. This agrees with ZnS having a lower free energy of formation compared to Cu-S and Sn-S compounds. The abrupt transition for the Zn-target indicates high reactivity and a large difference in sputtering yield between Zn and ZnS. The Cu-Sn-target transition from metal to compound mode is more gradual and the voltage continuously increases over a large range of H_2S-flows. Samples sputtered at four different Ar-to-H_2S-ratios show that the deposition rates decrease with increasing amount of reactive gas, both from the Zn- and the Cu-Sn-target, and that the change in Zn-rate is more abrupt, agreeing well with the metal-to-compound transition types observed by the voltage measurement.

For the CuS-Zn-Sn setup a process curve is shown in Figure 12. As expected the Zn-target shows the same behavior, with a sharp transition, however here at a higher H_2S-flow. This difference could be caused by that the Zn in this case is run at a higher power compared to the other metals. This is supported by the fact that depositions from a fully sulfurized run done at similar conditions came out Zn-poor for the "two target"- case and Zn-rich for the "three target"- setup, when compared to CZTS stoichiometry. Another difference between the two process curves is that the "three target"- case is run with new, unused, Zn- and Sn-targets, while for the "two target"- case, the setup had been used for some time before running the process curve. Even if the system was run in pure Ar-atmosphere until the voltages were stable, the results in Paper V indicate that the targets have long stabilization times and this difference may therefore still affect the resulting process curves in both cases.

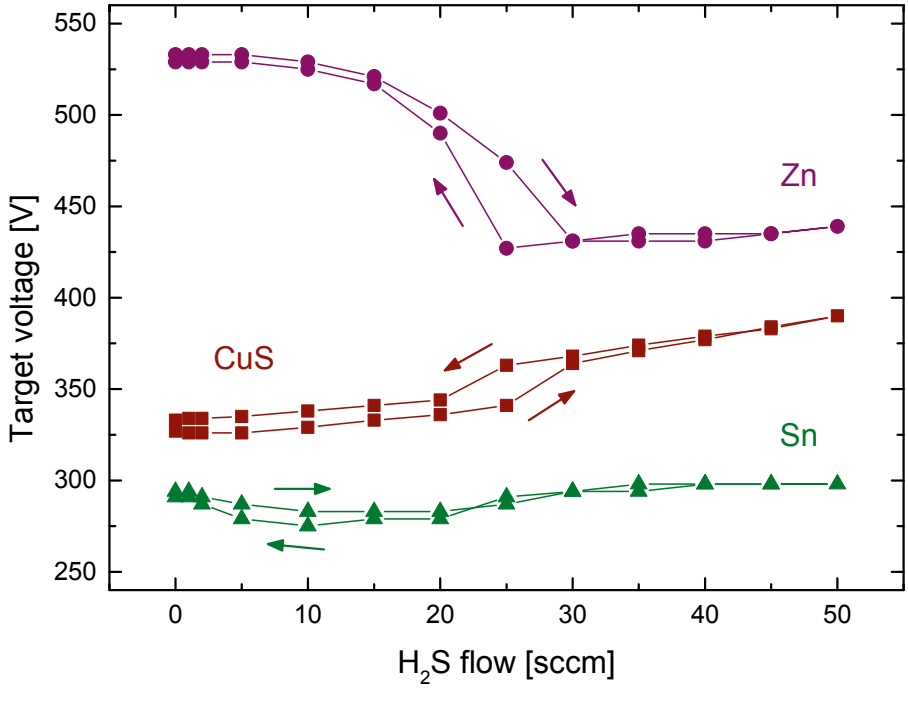

Figure 12. Process curve for the three target (CuS, Zn, Sn) setup. The process pressure was 0.67 Pa and the total flow at every point was 50 sccm (H_2S complemented by Ar). Set powers were CuS: 150 W, Zn: 400 W and Sn: 100 W.

Regarding the deposition rates for the three target setup with CuS-Zn-Sn-targets, no dedicated studies were made, but from the work with different sulfur compositions presented in Section 4.1.4, we can conclude that the Zn-target also in this setup has four to five times lower deposition rate in compound mode compared to metal mode (see Figure 13). During these experi-

ments it was also observed, as expected, that both the H_2S-flow and target power are important to keep the Zn-target in compound mode. This is exemplified in Figure 13 where decreasing the H_2S-flow from 4 to 0 sccm (run 139-141) while keeping the Zn-power constant gives a sudden increase of Zn-deposition rate for 0 sccm when the Zn-target transfers from compound to metal mode. Increasing the H_2S-flow back to 2 sccm in run 142 does not bring the deposition rate down indicating a hysteresis effect. However, the CuS-target power was slightly decreased for this and further runs, which means that less S is supplied to the system, counteracting the increase of S from the higher H_2S-flow. A lower Zn-power is used for run 143 and the deposition rate is then reduced because the target transfers back to compound mode. For run 143-147 the H_2S-flow is kept constant at 2 sccm while the Zn-power is gradually increased. Again a sudden transition occurs (run 147) when the target surface goes from compound to metal mode, this time due to the increased power.

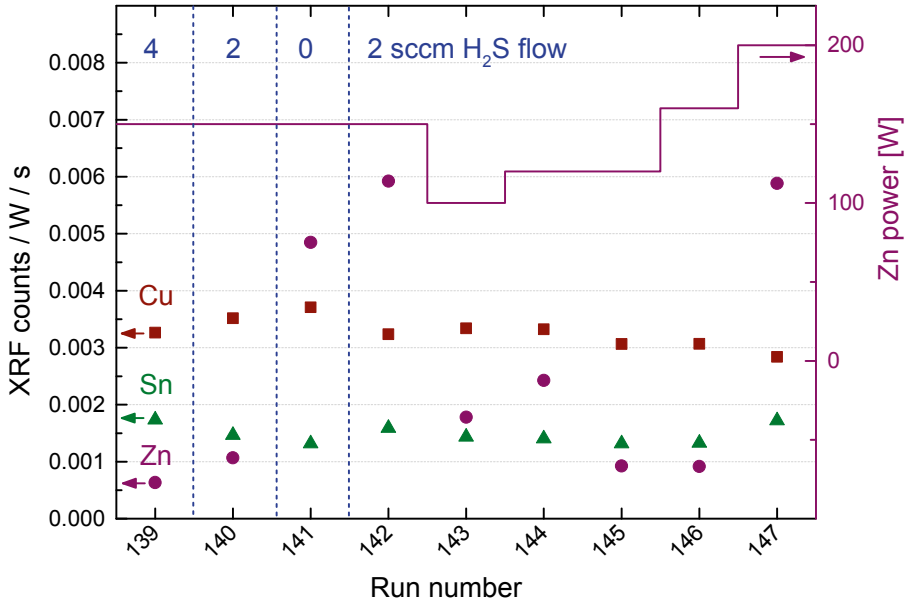

Figure 13. Example from the CuS-Zn-Sn process of metal-compound transitions of the Zn-target, causing large changes in the deposition rate. The deposition rates are here evaluated by raw XRF counts normalized by dividing with applied target power in W and deposition time in s. The first runs show that, when decreasing the H_2S-flow from run to run, the Zn deposition rate suddenly increases indicating a transition to metal mode. The second part of the graph shows that the same happens when H_2S-flow is kept constant and the power to the Zn-target is increased. The difference between run 144 and 145 is a longer deposition time for the latter which in this case gave a lower average deposition rate.

For the CuS-target no abrupt change in voltage or deposition rate is expected since this target should continuously be in compound mode. However, sputtering a sulfide target in pure Ar can cause the surface to be depleted of sulfur due to preferential sputtering and this can result in a minor change in target voltage. In our experiments higher H_2S-flows yielded a moderate increase in voltage and a slight decrease in deposition rate for the CuS-target (Figure 12 and Figure 13) which could be due to the change in the target surface condition or sputtering atmosphere.

For Sn a metal-compound transition is expected but no clear step appears in voltage nor in deposition rate (Figure 12 and Figure 13). This could either indicate that the secondary electron yield, and deposition rate, is similar for Sn and Sn-S, or that the target surface is in either metal or compound mode for the whole range of flows investigated. Since Sn-S has a less negative free energy of formation than Zn-S it is expected that the transition would occur at a higher H_2S-flow than for Zn. This would mean that Sn should not be in compound mode for the whole range, which leaves the other two explanations. For Sn in Ar/O_2 reactive sputtering only a small target voltage difference was seen between Ar-sputtering and an Ar/O_2-ratio assumed to give fully oxidized Sn-target [97].

Different ranges for the H_2S-flow are used for the two process curves since the baseline settings used at the two occasions were different. A process curve for the "two target"-setup for H_2S-flow 0-30 sccm was also performed and showed qualitatively the same behavior as the 0-20 sccm curve in Paper I, but with the addition that the Cu-Sn-target voltage leveled out at the highest H_2S-flows.

Properties of reactively sputtered films

The properties of sputtered films may vary for different sputtering powers, process pressures, substrate temperatures and amounts of reactive gas. In Paper I and Paper II, the effect of these parameters was investigated.

When sputtering from Cu-Sn- and Zn-targets in pure Ar, a grainy metallic film was obtained for which XRD measurements indicated the presence of Cu_5Zn_8 and elemental Sn. Increasing the H_2S-flow to 50 % of total flow, yielded an almost amorphous film which showed broad XRD intensities for the main peaks of ZnS and Cu-Sn-phases, indicating that the sulfur content was enough to sulfurize Zn but not to fully react the film. Further increasing the H_2S-flow to 75 % and 100 % gave a columnar film with a zinc blende XRD-pattern, with peaks common for CZTS, Cu_2SnS_3 (CTS) and sphalerite ZnS, with only small shifts. None of the weak reflections specific for CZTS or CTS were observed. This pattern is hereafter referred to as Σ, following the notation in [98]. Raman spectroscopy with a 514 nm laser showed a clear but very broad peak around 335 cm^{-1}. Peak fitting with Lorentzian curves gave good agreement for four peaks between 200 and 500 cm^{-1}, with intensities and positions best matching CZTS. However, secondary phases with

Raman intensities in the same range, such as ZnS, CTS and Cu_3SnS_4, could not be ruled out by this measurement.

Structure of the as-deposited films

Sputtering can yield non-equilibrium phases and, as discussed in Paper IV, we suggest that the films sputtered at the higher H_2S-flows have a non-equilibrium phase with S-ions in the zinc-blende configuration and the metal ions randomly ordered at the cation sites, see Figure 6. This agrees with the XRD and Raman results, where a ZnS structure is suggested from XRD but Raman spectroscopy indicates that each S atom is surrounded by 2:1:1 Cu:Zn:Sn, as in the kesterite structure. A random ordering of the cations would also mean a range of slightly different S environments causing a broadening of the Raman peak. Additionally, Raman spectra from 325 nm excitation wavelength performed in Paper IV strongly indicates the absence of ZnS in the film, which was the pattern observed in XRD. Examining the samples by TEM, as described in Paper III, revealed a homogenous film composition and no indication of more than one phase, which further supports the hypothesis of a non-equilibrium phase for the as-deposited material.

Effect of sputtering pressure

A study of the influence of process pressure was made in Paper I. Two different pressures, 0.67 and 1.33 Pa, and three different H_2S/Ar-flows were compared. The films were generally very similar at the two pressures. Differences were only seen in the transition region between metal and compound mode where the system is very sensitive to changes. For the lower pressure at this H_2S/Ar-ratio an additional peak appeared in the XRD pattern, besides the broad ones indicating Cu-Sn and ZnS. The new peak matches the close packed plane for elemental Zn, indicating that the lower pressure setting did not supply enough sulfur to completely react the Zn.

Effect of substrate temperature

The substrate temperature during deposition is predicted to affect morphology and stress of thin films due to the increased surface mobility of the arriving atoms. Two temperature series were studied in Papers I and II respectively. The substrate temperature was varied between room temperature and 300 °C. Since film composition also can affect these properties, the temperature series in Paper II was designed to give three controlled compositions at three different substrate temperatures, yielding in total nine samples. This was accomplished by using different Cu-Sn-alloy targets. Possible variations in sulfur content were however not compensated for.

In the first series (Paper I), which was done with fixed process settings besides the substrate temperature, it was clear that the resulting film composition was highly affected. Comparing the raw XRF counts, it could be seen

that the difference was mainly due to a decrease of Zn- and Sn-content with increasing temperature, probably due to the high vapor pressures of Zn and SnS. Additionally, lower sulfur content at higher temperature was seen by EDS measurements. This can also be assigned to the high vapor pressure of S_2.

Higher substrate temperatures gave slightly denser films but generally the density of the sputtered films was low compared to a CZTS powder reference. This is not surprising for films sputtered at moderate temperatures [96].

All depositions exhibited the Σ-pattern in XRD. However, the intensities of the peaks changed within the series, indicating that the film became more oriented towards the (111) (for ZnS) or (112) (for CZTS) planes with higher temperature. This kind of texture, with the closest packed plane horizontal to the substrate, is common for sputtered films and the increased orientation is expected due to the higher surface mobility with temperature. A (200) pole figure was measured with XRD, which confirmed that the film had a (111)/(112) preferred orientation but no in-plane orientation.

The internal stress of the films, measured by the deflection of thin glass substrates, as described in Section 3.1.4, was determined to be compressive for all samples, except for one with an unusual morphology. For the series with constant deposition parameters there was a weak trend showing lower stress values for higher temperature, but these were also the samples with the highest copper content. For the constant composition series there was a slight correlation between high copper content and lower stress but no trend with temperature. This indicates that the different thermal expansion coefficients of the different layers, causing a difference in shrinkage when the sample cools, is not a significantly contributing factor to the magnitude of stress. A further possible explanation for the stress variations in the constant composition series could be that the copper rich samples were made from a different sputtering target and at a higher deposition rate. A high deposition rate is expected to increase compressive stress [96], the opposite to what is seen here. However, direct comparisons of stress levels in films deposited from different targets is not straightforward, since the angular distribution of the energetic species changes overtime as the target is eroded, resulting in different growth conditions. Supplementary residual stress measurements were done with XRD. For a sample which had high stress and weak preferred orientation, good agreement with the curvature measurement was obtained. However, more textured samples were not possible to evaluate by this XRD-method.

Differences in stress also cause peak shifts in the standard XRD pattern, although several other factors, such as composition and phase mixture, influence the peak position as well. For the measured samples, all the visible Σ-peaks are slightly shifted to lower angles while the peaks from the Mo-back contact are well aligned. The (111)/(112) peak is observed to be 0.1-0.3 de-

grees lower compared to ZnS or CZTS references. Combining the results from the two substrate temperature series, we conclude that at least some of the peak shift is connected to the Cu/Sn-ratio, since the samples with more stoichiometric Cu/Sn-ratios have peaks closer to the powder reference. However, there also seems to be a contribution from stress, since the sample with unusual morphology, which showed a small positive stress, also had by far the smallest peak shift.

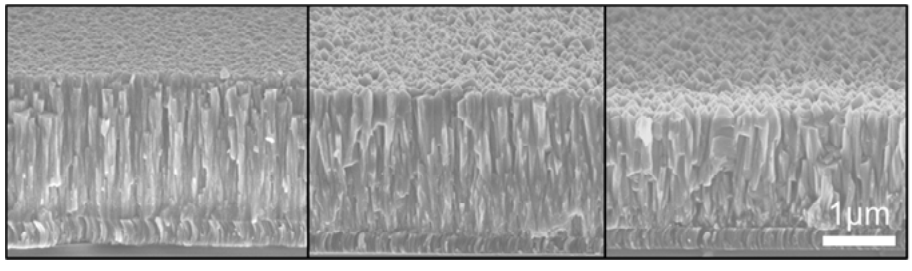

Figure 14. SEM cross sections of films sputtered at different substrate temperatures, from left: 40, 180, 300 °C. Adapted from Paper II.

Comparing SEM images of three of the samples from Paper II (Figure 14) to the standard SZM (Figure 11) shows that the low temperature depositions exhibit features of zone 1-zone T, with a columnar structure and rounded surfaces. The high temperature deposition appearance is closer to zone T-zone 2 morphology, with facetted surfaces and angled grain boundaries within the film. When calculating the approximate ratio of substrate temperature and CZTS melting temperature the resulting positions in the SZM agrees well with the observed structures.

Target stability

The reactive sputtering process can be challenging, especially due to target instabilities. These can include arc discharges, flaking, preferential sputtering and long term changes. Due to the narrow composition window for CZTS (see Figure 7) and since the films are intended for photovoltaic devices and therefore are sensitive to defects, high process stability is required.

In Paper V, some of the peculiar behaviors of the alloy Cu-Sn-target were investigated. Firstly, we showed that the deposition rate and the resulting Cu/Sn-ratio had a long stabilization time after Ar-sputtering, about 2 h. Large variations in the composition were therefore observed when applying the standard reactive sputtering approach of pre-sputtering the targets in Ar before every deposition. The procedure was changed to instead pre-sputter at the same conditions as the deposition, and this yielded more consistent compositions. Additionally, we observed a long term alteration of the Cu-Sn-target, occurring even when the system was not used. The background pressure of S was sufficient to induce severe surface sulfurization. This led to

variations of the Cu/Sn-ratio at a longer time scale. The sulfurization of the target created a layered structure, with a thick Cu_2S-layer at the top and an almost pure Sn-layer underneath. This was attributed to the high reactivity and mobility of Cu in combination with preferentially removed Sn, possibly by evaporation of SnS through the porous Cu_2S.

As mentioned, the metallic Cu-target was abandoned due to problems with the target surface. A large degree of sulfurization was observed even for the background pressure in the chamber, which resulted in unstable deposition rates, arcing and flakes. This is exemplified in Figure 15, where it can be seen that the deposition rate dropped considerably when the target had been unused for some days. After sputtering in pure Ar the rate was increased substantially, but several runs in H_2S were needed to re-stabilize the deposition rate.

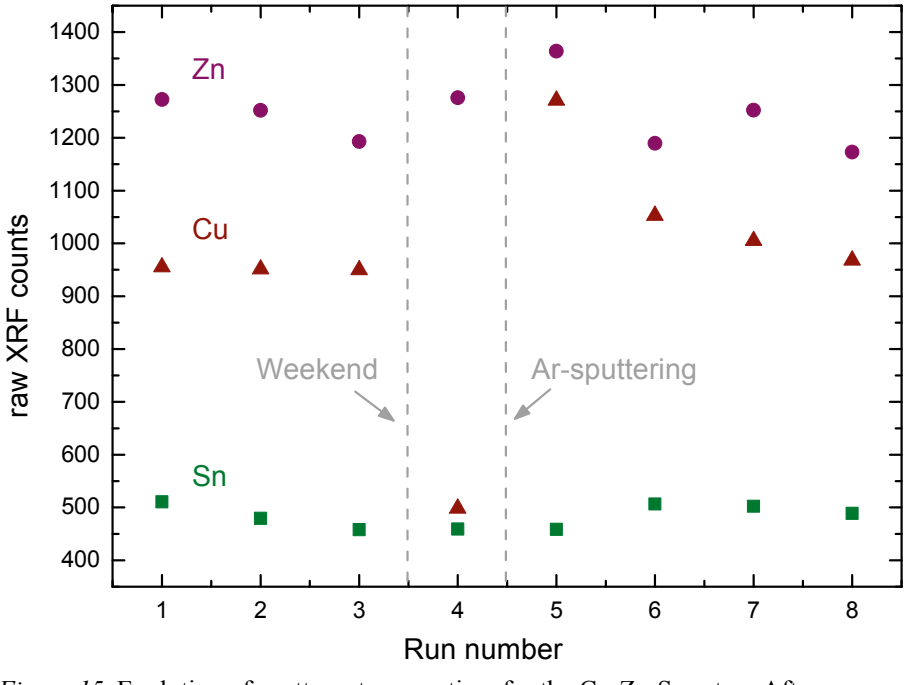

Figure 15. Evolution of sputter rates over time for the Cu-Zn-Sn setup. After a weekend a large drop in sputter rate from the Cu-target was observed (run 4). A pure Ar-sputtering increased the rate substantially and several runs in H_2S were needed to stabilize the deposition rate again.

Also for the Cu_2S-target the deposition process was unstable, with flakes and cracks appearing on the target, as can be seen in Figure 16. The reason may be a sensitivity to the sulfur atmosphere, or that the cooling of the target was insufficient, in combination with a too aggressive power increase at start-up and a high thermal expansion coefficient of the material [99].

For the Zn-target we have seen long stabilization times for the deposition rate after a metal-to-compound transition of the target surface. Additionally, the deposition rate has continued to change over time at a noticeable but manageable pace. The Zn deposition rate has also been sensitive to changes of the other process parameters, which increased the difficulty of controlling the composition of the films. Part of these problems might have arisen due to insufficient cooling of the target. Additionally, the power supply used for controlling the Zn-target had a limited resolution on power control and could only be changed in 10-20 W steps, which further complicated the control of the Zn-amount.

Figure 16. Cu_2S-target with flakes and cracks.

The Sn-target has generally showed stable operation. In this setup however the flexibility of the rate was somewhat limited by the low melting point of Sn in combination with low resolution of the power supply power setting.

The challenges encountered with reactive sputtering encouraged us to additionally work with compound sputtering, as is described in the next section.

4.1.3 Compound sputtering of precursors for CZTS

Compound sputtering of Cu-Zn-Sn-S films in Ar is more straightforward than reactive sputtering due to the absence of metal-compound transitions for the target surfaces. However, the sulfur content of the resulting film is not as readily controlled in this setup. It mostly depends on the sulfur content of the chosen targets, and can only be varied slightly by other process parameters. The sulfur content of the grown film may also be substantially lower than that of the targets, both due to the high vapor pressure of S and Sn-S and due to higher scattering of the lighter S atoms by Ar on the way from the target to the substrate. This is further discussed in Section 4.1.4.

Compound sputtering setup

The precursor films in Paper VIII were sputtered in a Lesker CMS-18 system. The system has six magnetrons, but for these depositions only three of them were used. The targets were 76 mm in diameter and 4 mm thick and made of CuS, ZnS and SnS, all with purity 99.99 %. The target to substrate distance was 163 mm with an angle of 15° and the sputtering took place in 0.67 Pa Ar-atmosphere. For CuS- and SnS-targets, pulsed DC sputtering was used, whereas RF-sputtering was employed for the insulating ZnS-target. For the precursor depositions in Paper VIII, the substrate holder heater was set to 250 °C, resulting in a substrate temperature of around 225 °C.

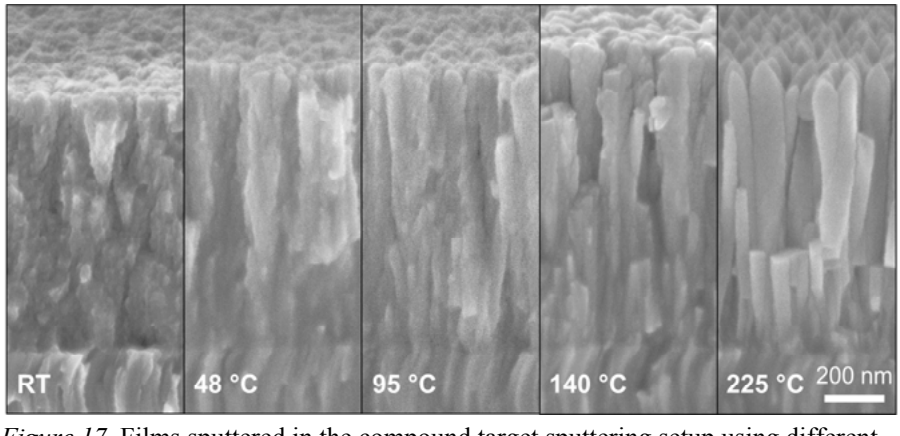

Figure 17. Films sputtered in the compound target sputtering setup using different substrate temperatures.

Properties of compound sputtered films

The properties of these films were not investigated as thoroughly as for the reactive sputtering case. There might also have been some variations of the sputtering process over time since this sputter was recently installed and one could expect a run-in phase.

A small study of the effect of substrate temperature was made and similar trends as in the reactive sputtering case were observed. SEM images show a transition from SZM Zone 1 to Zone 2 (Figure 11 and Figure 17). Comparing films sputtered at room temperature from the two systems there are indications that the film sputtered from compounds has slightly worse crystallinity. However, this film was sputtered during the first usage time of the machine and could therefore also have been affected by run-in behaviors.

Surprisingly, as can be seen in Figure 18, stress measurements with thin glass slides (as described in Section 3.1.4) show positive values, i.e. tensile stress for the compound sputtered films, opposite to what was seen for most films sputtered with the reactive process. The film sputtered at the highest temperature has the lowest tensile stress, which is expected from theory if the influence from thermal expansion coefficients of the different layers is negligible [96].

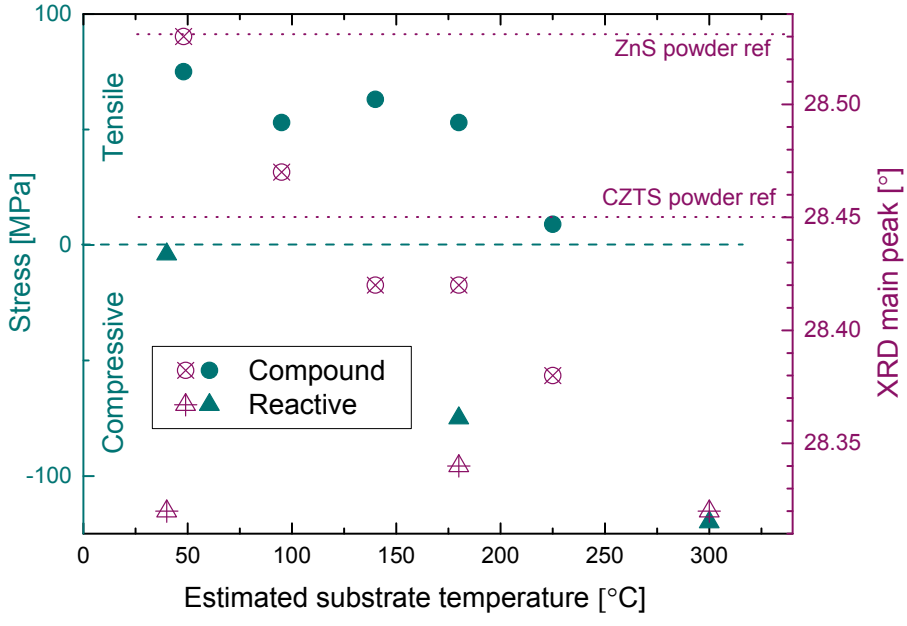

Figure 18. Stress measurements from profilometer (filled symbols-left axis) and XRD main peak positions (open symbols-right axis) for compound sputtered films compared with reactively sputtered samples (A2-C2 from Paper II was chosen because of similar composition, Cu/Sn ≈ 2.0 and Zn/(Cu+Sn) ≈ 0.4, besides the compound sputtered film from the highest temp which had Zn/(Cu+Sn) = 0.32).

The difference in stress is also seen in the position of the (111)/(112) peaks in XRD, which generally appear at higher values for these films, compared to the reactively sputtered films, see Figure 18. The film sputtered at the highest temperature has the lowest XRD peak position, closer to the values seen for the reactively sputtered film. When comparing to tabulated peak

positions for powder reference materials of ZnS and CZTS, the compound sputtered films still generally show lower values, indicating that also other properties affect the peak position. As previously discussed this could be due to differences in composition or crystal structure, which also for these films is suggested to be a non-equilibrium phase with S-ions in the zinc-blende configuration and the metal ions randomly arranged at the cation sites.

As expected, the XRD patterns (Figure 19) show an increasingly oriented film towards the (111)/(112) plane, the close-packed plane, with higher temperature. The densities calculated for these films are similar to the reactively sputtered precursors.

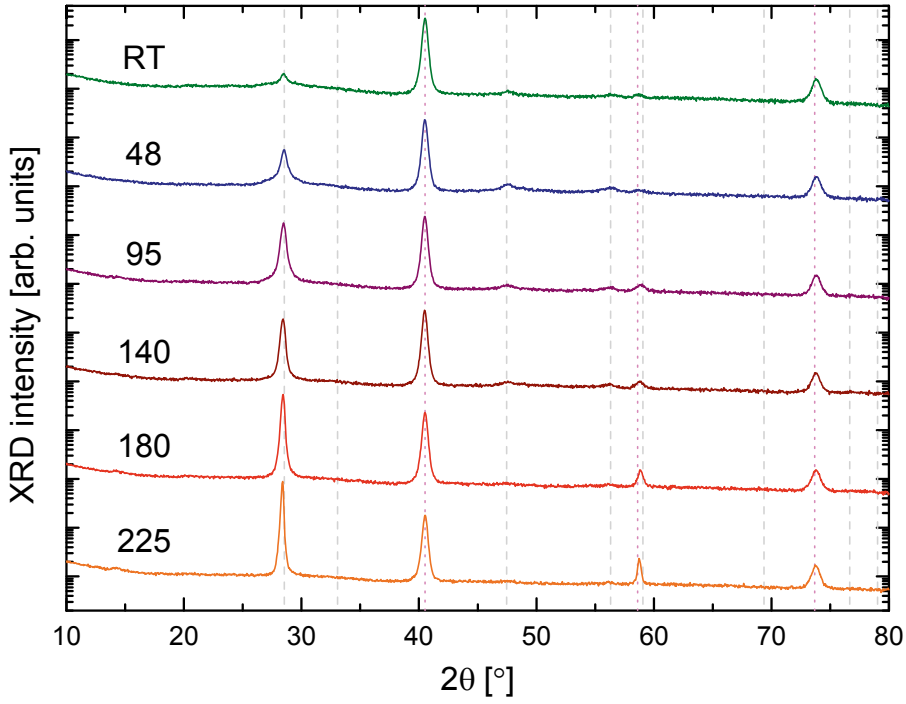

Figure 19. XRD for the compound sputtered temperature series show an increasingly oriented film with higher temperature. The estimated substrate temperature in °C is given at the left hand side. Dashed grey lines indicated the sphalerite ZnS reference pattern and dotted pink lines indicate the reference pattern of Mo (back contact).

4.1.4 Sulfur content in CZTS precursors

A possible disadvantage of compound sputtering, compared to a reactive approach, is that the resulting film might be under-stoichiometric in sulfur. This is due to the risk of loss of sulfur, or sulfur compounds, caused by lower sticking coefficients or higher vapor pressures, as well as higher scattering of S on the way from the target to the substrate, due to lower mass and thus

shorter mean free path. In a reactive setup one has the possibility to counteract such losses by increasing the H_2S-flow. When using a non-reactive setup there are fewer possibilities to vary the amount of sulfur. A higher sulfur content in the target could be used, but in general it is preferred to use stable compounds as target material, and the selection is therefore limited.

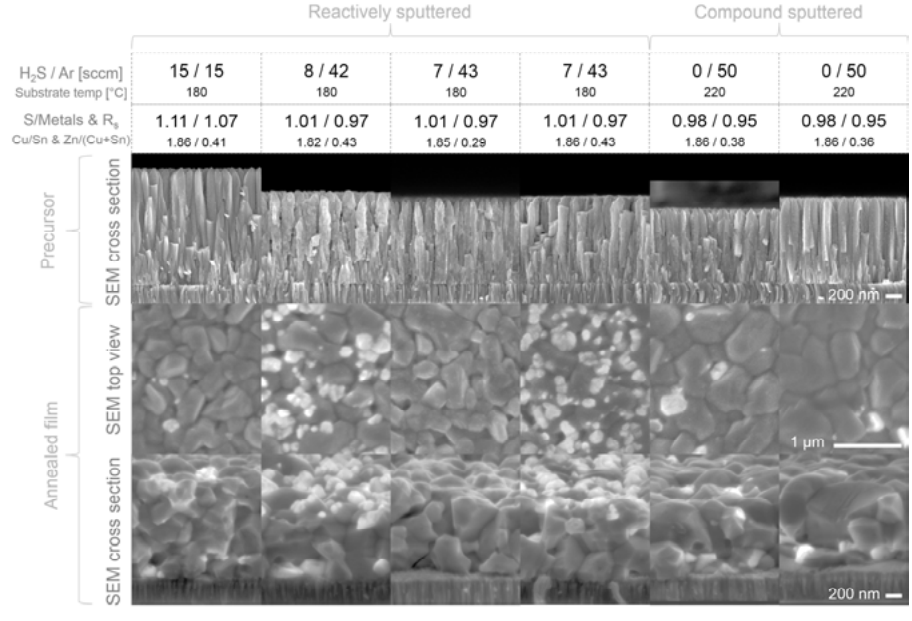

Figure 20. Comparison between reactively and compound sputtered samples, with an attempted variation in sulfur content. Process parameters, such as gas flows, are given at the top. Metal compositions are measured with XRF while S-ratios are measured with EDS. The sulfur content is given both as S/(Cu+Zn+Sn) and as R_s= 2S / (Cu + 2Zn + 4Sn), where the latter accounts for the oxidation states of the metals and thus better describe the chemical situation for a non-stoichiometric sample. The bright grains have been observed to be ZnS and can be seen in the Zn-rich films (Zn/(Cu+Sn) > 0.33).

The second step in the solar absorber processing is annealing, as seen in Figure 1. In this step it is possible to include sulfur, so a precursor understoichiometric in sulfur might not cause problems. However, if the as-sputtered precursor lacks sulfur it must diffuse into the film during annealing, which might change the needed annealing time and affect the grain size or crystal quality. Additionally, as described in Paper I and Section 4.1.2, significantly decreasing the sulfur content of the as-sputtered precursor will completely change its structure, going from a zinc-blende arrangement, to an almost amorphous material for intermediate sulfur contents and, when no sulfur is added, yielding a phase segregated metallic film.

In Paper II, there were indications that the high sulfur contents seen for room-temperature sputtered films might cause cracks in the films when an-

nealed. Additionally, we initially noticed a difference in annealing behavior between compound sputtered and reactively sputtered precursors, with compound sputtered film yielding slightly smaller grain sizes. Measurements showed lower sulfur contents in the compound sputtered films in these cases.

To investigate the influence of precursor sulfur content on absorber quality, a sample series with films sputtered at different H_2S-flows, and compound sputtered films, were annealed together and then analyzed (the annealing procedure is further described in Section 4.2, settings for this run was: 80 g S, large uncoated box, 35 kPa Ar, 560 °C, 10 min). The sulfur variation was kept small to avoid precursors with a completely different structure. Previous results from Paper I indicated that films with a S/Metal-ratio down to at least 0.73 had the metastable phase we observe in fully sulfur-stoichiometric precursors. A sulfur variation down to this value was therefore aimed for. However, the targets used for this series were CuS, Zn and Sn, as compared to the purely metallic targets used in Paper I. Sulfur was therefore also provided from the CuS-target which meant that sputtering in pure Ar yielded an XRD pattern most similar to sputtering in 50 % H_2S from metallic targets (sample B in Paper I). This, together with the metal-to-compound transition of the Zn-target which causes a large difference in deposition rate, made producing a sulfur content series from the CuS-Zn-Sn setup complicated, and a smaller variation than intended was achieved, with S/Metal-ratios ranging from 0.98 to 1.11, as can be seen in Figure 20.

The films were investigated with XRD and Raman spectroscopy but no clear correlation between sulfur content of the precursor and absorber quality was observed. SEM images of the films can be seen in Figure 20 and also do not show any significant trends with sulfur content. However, the compound sputtered films seem to have slightly larger grain sizes, opposite to what had been observed in earlier experiments.

The sulfur content was measured with EDS, using the machine calibration. This means that the values may not be very accurate, but similar films should give comparable results. However, for this series there was an unintentional trend in thickness, with thinner layers for lower sulfur contents. To investigate if this affected the EDS results, measurements were done on a previously sputtered thickness series from [100]. The results are presented in Figure 21 and show that there is either a trend of thinner films generally containing less sulfur, or a systematic measurement error yielding lower sulfur contents for thinner films. These measurements were done on films on Si-substrate, so the influence of the overlap between S and Mo discussed in Section 3.1.1 is not relevant here. There is no obvious reason for either explanation, but due to the complexity of measuring sulfur in thin films with EDS, it is not unlikely that this is a measurement problem.

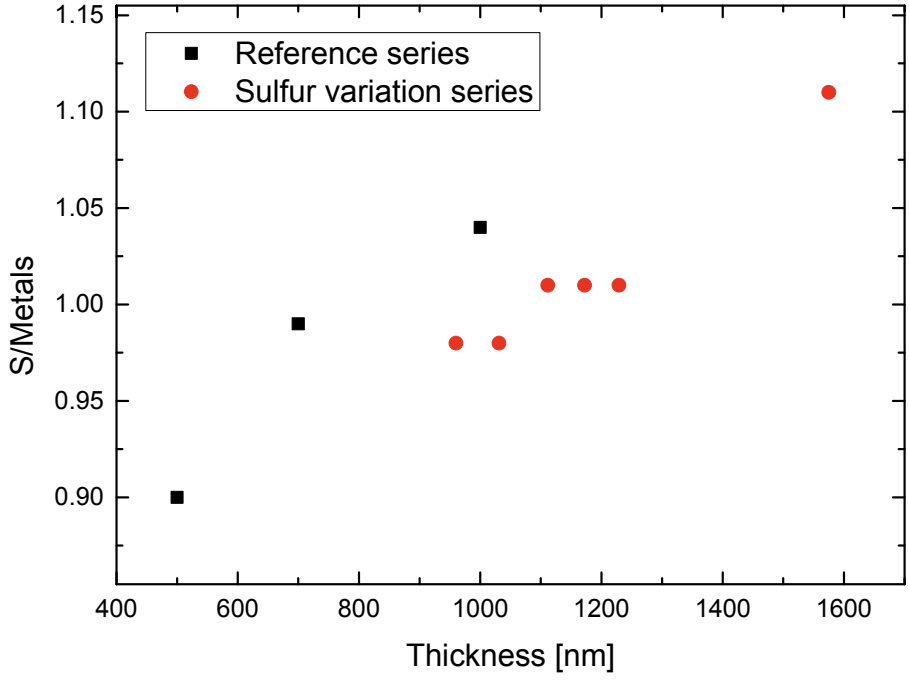

Figure 21. Measurement of sulfur content with EDS on the attempted sulfur series and a reference series with expected constant sulfur amount.

4.1.5 Discussion

Reactive and compound sputtering yield similar precursors for optimized settings. In Figure 22, XRD of precursor films from several sputtering setups are shown. Additional to the ones presented so far, there is also an example of a film sputtered from a CZTS-target in the reactive sputtering setup. All precursors show the Σ-pattern, but with small variations in peak height distribution, indicating that there might be a difference in the level of texture for the films. An additional, low intensity peak can be seen at around 14.3° for some of the films. This peak is neither associated with the substrate nor does it belongs to the ZnS pattern or any of the possible secondary phases. A hypothesis is that it is related to the close packed plane in the ZnS structure since it occurs at roughly half of the main peak value, which could mean that it represents every other close packed plane. The expected peak position for this can be calculated by Bragg's law and yields 14.1°, which is close but not perfectly matching.

From EDS measurements, slightly more O was seen for the compound sputtered precursors, possibly due to slower deposition rate. An ERDA measurement on a reactively sputtered precursor and its annealed counterpart showed very low amounts of impurities in the samples. H, C and O were detected, but well below 0.5 at% in the bulk. Comparing the two films, the

H-content was higher in the precursor, probably due to implantation of H from the H_2S-gas, which is then removed during annealing. The annealed sample instead had slightly higher O and C levels.

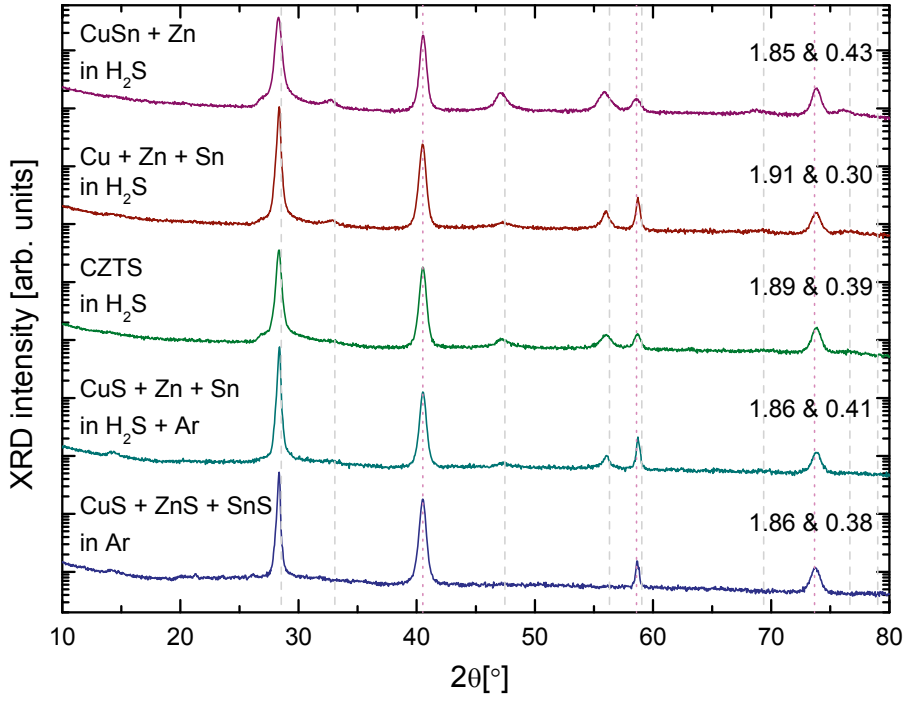

Figure 22. Examples of precursor XRD patterns from different sputtering setups. The substrate temperature was 180-220 °C and sample thickness varies. The composition for each sample is given on the right hand side by the ratios Cu/Sn & Zn/(Cu + Sn). ZnS reference pattern is shown in dashed grey and Mo (back contact) pattern is shown in dotted pink.

The difference in stress between compound sputtered, which exhibited tensile stress, and reactively sputtered films, with generally compressive stress, could have several origins. Generally the stress in the films is affected by substrate temperature, sputter pressure, target to substrate distance, angle of incidence and working gas species [96]. For the same substrate temperature and sputter pressure, the two setups yielded different types of stress so neither of these parameters should therefore be the cause. The target to substrate distance is the same in the two setups but the angle of the targets is slightly different. The general trend for angle of incidence is however that a larger angle creates more tensile tress, opposite to what is seen here [101]. The thickness of the sputtered film can also yield different stresses [102] but since the reactively sputtered films in Paper I and II include the thickness range for compound sputtered films and the differences persist, the influence of this seems negligible. The deposition rate is slightly higher for the reac-

tively sputtered films and this has been seen to give more compressive stresses, however, as discussed in Section 4.1.2, the trend with sputter rate was opposite within the reactively sputtered series, indicating that it is not significant in this case. Instead it is likely that it is the fundamental difference between reactive and compound sputtering, such as working gas and target surface state, which causes the difference in stress value. Due to the electronegativity of sulfur, negative sulfur ions are created in reactive sputtering, as shown in [103] for Cu-targets in Ar/H_2S atmosphere. For reactive sputtering in O_2 it has been observed that the negatively ionized oxygen can impact the stress levels due to high energy ion implantation [104]. In our case it is possible that negatively charged S-ions have the same effect and that more of these are created at the target in the reactive process due to the higher sulfur content in the sputter atmosphere.

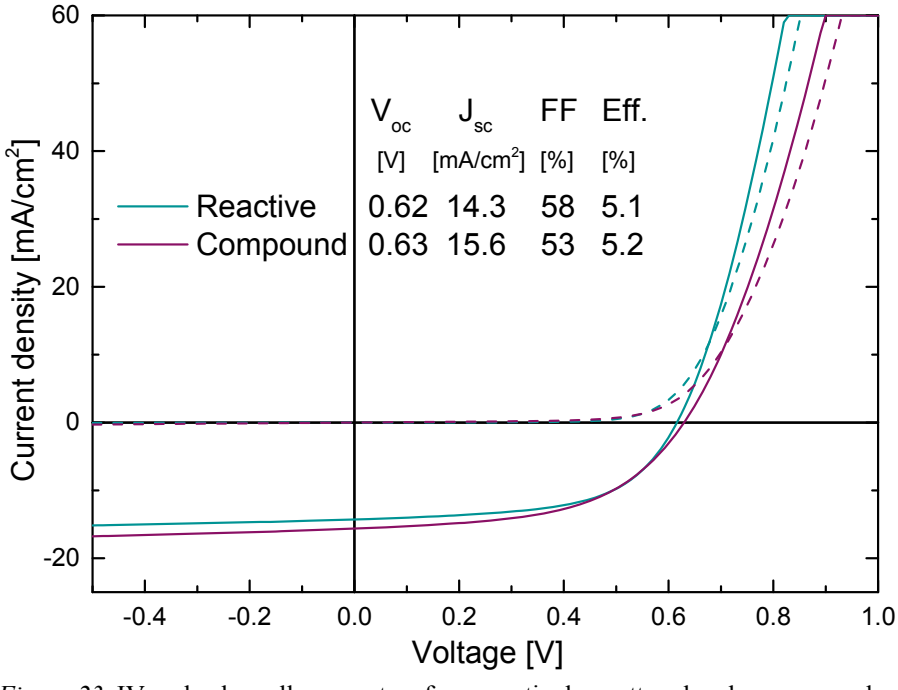

Figure 23. IV and solar cell parameters for a reactively sputtered and a compound sputtered precursor annealed in the same process run by Y. Ren. Light IV with solid lines and dark IV with dashed lines. Annealing parameters: 80 g S, large uncoated box, 35 kPa Ar, 560 °C, 10 min.

However, as also concluded in Paper II, within the range obtained for these precursors, stress does not seem to impact the final solar cell performance. Well performing solar cells can thus be made from both sputtering setups. A direct comparison between a reactively sputtered and a compound sputtered sample, annealed in the same process run, can be seen in Figure 23. The

slightly lower current for the solar cell from reactively sputtered precursor could be due to a higher Zn-content in this film (Zn/(Cu+Sn)=0.43 vs. 0.38), which could mean a slightly larger amount of ZnS secondary phase (Section 2.5). CZTS solar cells with up to 7.9 % efficiency have been made from the reactive sputter approach [20] and for the compound sputtering a 7.2 % (with CdS buffer) and a 9.0 % cell (with ZTO buffer and antireflective coating) are presented in Paper VIII.

To summarize, the reactive approach is more versatile and enable variation of all the elements in CZTS, but can be challenging to control. A compound sputter setup might more quickly give reproducible results when the desired composition is known and the sulfur content is not critical. It is possible to obtain high quality CZTS precursors from both setups.

4.2 Annealing of CZTS precursors

As discussed in Section 2.4 the two-step approaches for making CZTS absorbers include a second step with heating or sulfurization to produce high quality solar cell material. In this thesis, the precursors prepared by sputtering have a metastable, small grained phase, not suitable as an absorber, as shown by the low efficiencies achieved when processing it into a solar cell (see Paper IV). To improve grain size and absorber quality an annealing is necessary.

Annealing setup

For all the papers presented in the thesis annealing was performed in a home-built tube furnace. The furnace includes a sample loading plate which can be transferred between a loading zone, a cold zone and a hot zone, to ensure fast heating and cooling of the samples. Argon was used as the process gas and the background pressure could be adjusted. The annealing procedure was developed over time and optimized at several occasions, especially when changes were made in the precursor step, such as when shifting from reactive to compound sputtered precursors. The different annealing procedures are presented in Table 2 and discussed below.

For Paper II-IV no sulfur was added in the annealing process, instead the volume above the film was kept small by covering it with a piece of glass. Further understanding of the chemistry during annealing, such as the importance of sulfur pressure to counteract the decomposition and back contact reaction [20, 40], led to development of the process, and for Paper VI-VIII the sample was encased in a graphite box together with elemental sulfur pellets, before being loaded into the furnace. The box was designed to have a lid that fitted tightly, to limit the leakage of sulfur vapor. However, a small hole in the lid made it possible to evacuate the air before annealing. The hole

became covered as soon as the box entered the hot zone since the graphite block in this part of the furnace was designed to match the box thickness.

Table 2. *The annealing parameters used in this thesis.*

Paper no.	Added S [mg]	Ar [kPa]	Temp. [°C]	Time [min]
I	-	-	-	-
II	0	35	560	3
III	0	35	560	3 and 10
IV	0	35	560	3
V	-	-	-	-
VI	20 (small uncoated box)	35	560	10
VII	30 (large uncoated box)	35	560	10
VIII	80 (large coated box)	47	580	13

The first version of the box could hold a 25x25 mm sample and this box was used in Paper VI. To enable larger sample sets and thus better comparisons, a larger box, with room for four 25x25 mm samples was developed. This was used for Paper VII. In Table 2 it can be seen that the amount of added sulfur was increased slightly to compensate for the larger volume. However, we observed that moderate variations of the sulfur amount did not have a noticeable impact on the quality of the annealed film.

The graphite boxes were observed to give different results depending on previous processes, indicating a memory effect. To try to avoid this, boxes coated with pyrolytic carbon were introduced. The idea was to limit possible absorption and re-absorption of Sn-S in the graphite. A coated box was used in Paper VIII.

The re-optimisation of annealing for compound sputtered precursors included evaluation of time, background pressure and temperature. As can be seen in Table 2 for Paper VIII, this resulted in new parameters for annealing, with slightly longer time, higher temperature and higher background pressure.

Properties of annealed films

The film morphology is drastically changed by the annealing step, as can be seen in Paper II and IV. The grains grow substantially and no columnar structure is left. The metal composition is almost unchanged by annealing while the thickness decreases slightly. This is also part of the cause for the slightly higher densities of the annealed films. However, the densities are still lower than the bulk value for CZTS, most likely due to voids in the films.

In XRD, several additional peaks appear after annealing and the pattern fits well to CZTS. The (112)-peak is now generally found at 28.48 which is close to the reference position for CZTS, indicating that the stress has relaxed during annealing. The relative peak intensities are also closer to the

powder reference, although do not match perfectly, suggesting that some of the texture of the precursor may remain. The Raman peaks are narrower and match CZTS.

Examining the samples in SEM, many of them exhibit small, bright grains. By EDS mapping in TEM (Paper III) these were observed to be ZnS secondary phase.

Effect of precursor substrate heating and composition

In Paper II, nine samples, with three different sputtering substrate temperatures and three compositions, were annealed. The grain size after annealing seems to increase both with precursor deposition temperature and copper content. The trend in grain size with precursor deposition temperature in the annealed films could indicate that the structure of the heated precursors is more similar to CZTS, which would mean that larger grains could form during the same annealing time. Another parameter changing with the deposition temperature in this series is the sulfur content and as also discussed in Section 4.1.4 we have seen indications that this could affect the grain size. Additionally, the different temperatures during precursor deposition could mean that different amount of Na have diffused into the films and that this influences the grain size, as mentioned in Section 2.2. A later study using secondary ion mass spectroscopy on compound sputtered precursors showed however only low amounts of Na for a sample sputtered at 225 °C [105]. A larger grain size with increasing copper content is well known for CIGS [106] and has also been reported for CZTS [107].

When annealing the temperature series in Paper I and Paper II, the precursors sputtered at room temperature yielded cracked films. The room temperature precursor in Paper I had a large compressive stress, which was suspected to be a reason for the behavior. However, the room temperature samples in Paper II had a large variation in stress values but no correlation with the amount of cracking was seen. Instead it appears that what differentiate the precursors deposited at room temperature are slightly lower densities, slightly higher sulfur contents and minor differences in texture and crystallinity, judging from XRD and Raman spectroscopy. It is unclear if the low density and the higher sulfur content are connected or if the low density originates from a more porous morphology. Either could however be a plausible explanation for the annealing behavior, both the loss of excess sulfur or elimination of porosity could lead to formation of cracks during the annealing process.

Due to the cracks solar cells from precursors sputtered at room temperature were shunted. Solar cells from the films sputtered at higher temperatures in Paper II had efficiencies between 2-4.5 % without trends for composition or temperature. However, the annealing here was done without added sulfur, generally yielding lower efficiencies, and it is possible that the result would have been different for other annealing parameters.

4.3 Low temperature post-annealing of CZTS

Several research groups have reported changes in the CZTSSe material due to post-annealing. Alterations have been observed already for low temperatures and short times, down to 100-150 °C and 30 min [108, 109]. In Paper VIII the main ambition was to continue the investigation on ZTO as a buffer material for CZTS solar cells and this is the further discussed in Chapter 5. However, since the buffer layers were grown with ALD at temperatures of 105-165 °C, and due to the apparent temperature sensitivity of the CZTS material, additional experiments were carried out in an attempt to decouple the influence of the buffer variation from possible annealing effects on the CZTS absorber.

A sample series including an additional post-annealing in N_2, after the absorber formation but before buffer deposition, was evaluated (see Figure 1 and Figure 24). Four different temperatures with a holding time of 40 min were used, to mimic the temperature load the absorbers would experience during a ZTO buffer deposition. The samples were then processed with the standard CdS buffer (as described in Section 5.2).

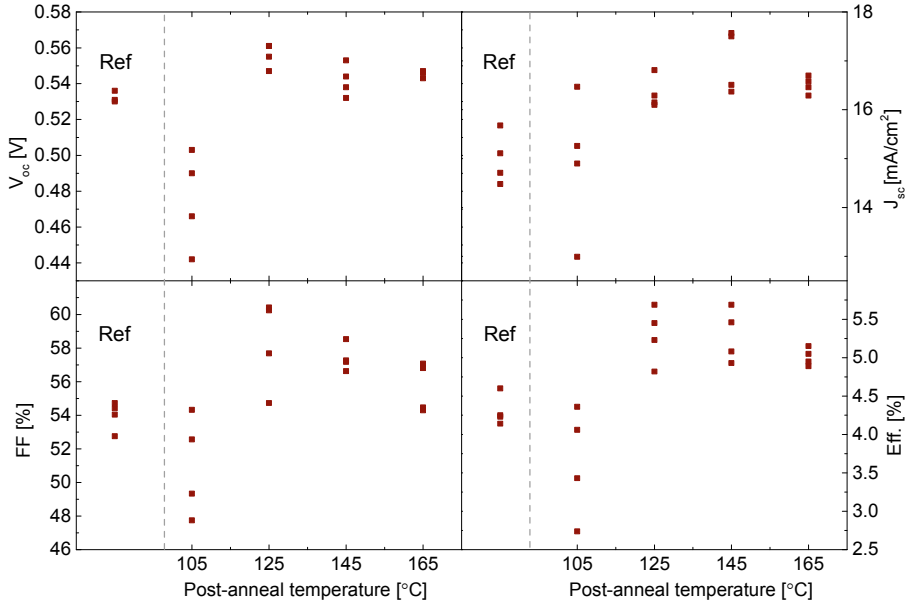

Figure 24. Device parameters for solar cells made from post-annealed absorbers. Reference without post-annealing to the left. Adapted from Paper VIII.

The device characterization showed small improvements in all parameters for 125, 145 and 165 °C while the sample heated at 105 °C had worse performance than the unheated reference. Capacitance-voltage (CV) measurements were performed on this series and indicated a slightly higher doping

density for the 105 °C sample, which could be a reason for the degraded electrical properties. However, a change in absorber doping may both be detrimental and beneficial, depending on several parameters, such as the initial absorber doping, absorber quality, doping level of the buffer and properties of the interface. Many of these properties could be affected by the heat treatment and thus influence the electrical behavior in opposite directions.

To further investigate the impact of post-annealing, another set of samples were treated in the ALD-system, usually used for producing ZTO buffers, but in this case without depositing anything. The highest process temperature, 165 °C, was chosen for this study. The samples were kept in the ALD chamber for 15 min in 2 mbar flowing N_2 atmosphere but were also heated and cooled the same way as would have been done in an ALD buffer process. One sample was only heated, but for the next sample also the gaseous ALD Zn-precursor was added into the chamber atmosphere. The last sample was instead exposed to the ALD Sn-precursor. The samples were then removed from the ALD, coated with the standard CdS buffer and finished to solar cells.

The three different treatments gave cells with similar electrical properties, judging from the IV curves. A larger V_{oc} improvement was seen compared to the previous heat treatment experiment. As before, a slight FF increase was observed, but in this series only one of the samples (the Zn-treated) showed a very small improvement in J_{sc}, when measured in IV. These results indicated that post-annealing was the main affecting parameter and that the treatment with ALD Zn/Sn-precursor did not have a significant effect on the solar cell performance. However, QE measurements on the surface treated series showed a larger J_{sc} improvement for the Zn-treated sample and a better collection for long wavelengths was observed. The difference between the results from IV and QE could depend on that the QE measurement was not performed under full illumination. Additionally, negatively biased QE (see Section 3.2.2) showed an improvement in the long wavelength region for the just-heated and the Sn-treated samples, indicating a short diffusion length or a narrow space charge region [110]. For the Zn-treated sample the unbiased QE response for the long wavelength region was higher, and the increase with bias was less, which indicates a larger space charge region or a longer diffusion length for this sample.

To summarize, the results from these series thus show that the heating is the main contributor for changes in device properties, but that there may also be an effect of a modified surface by the Zn-treatment.

Numerous papers have been published about the effect of post-annealing on CZTSSe [9, 88, 108, 109, 111, 112]. However due to the complexity of the starting material, especially the S/Se-ratio and the various kinds of impurities, caused by the many different deposition methods used, and additionally due to the many kinds of post-annealing chosen, such as different atmos-

phere type and pressure, different temperatures and performed at different stages of the solar cell fabrication, there is no general conclusion regarding the reason for the changes seen, and possibly this might also differ from case to case.

There could be several reasons for the absorber to be affected by these rather short, low temperature heat treatments. Without extensive material and electrical characterization it is hard to decipher what is the origin of the changes. Suggested explanations in literature are, for example, changes in the Cu-Zn disorder, changes in absorber surface composition, re-distribution of Na and oxidation of grain boundaries [108, 112-114].

Since the annealing in our case was done in an inert atmosphere, the risk for oxidation should be limited, however oxygen can of course never be completely avoided. For the Cu-Zn disorder our previous experiments indicate that major changes only occur for longer times or higher temperatures [113]. Additionally, the absorber band gap should be affected by the ordering process and no such shift was seen here. The changes in doping for the temperature series point towards changes in the Na-distribution, while the changes in QE for the Zn-treated sample indicate that surface composition of Zn has an influence on the device properties, however, in this case it was not seen in the IV-measurements. Most probably both effects can occur simultaneously.

For these two series it is not possible to conclude what causes the changes seen with post-annealing treatment, but the results indicate that any step after the absorber deposition that includes heating, even at a low temperature and short time, may affect the solar cell behavior. The CZTS sensitivity to low temperature annealing may both be beneficial and disadvantageous. If it can be used to consistently and permanently improve cells, it could be a valuable step in a production line. However, any steps subsequent to the absorber formation containing heat may be problematic, especially if the time and temperature optima are different for the different layers in the solar cell. At the very least, possible changes of the absorber have to be taken into account when comparing CZTSSe samples that have different thermal histories.

5. Buffer layers for Cu_2ZnSnS_4

5.1 Background

To form the pn-junction in the CZTS solar cell an n-doped layer needs to be added to the p-type CZTS absorber. In principle one could use a single layer that would work as both the n-side of the junction and a front contact. However, due to the high demand on the quality of the pn-junction to avoid interface recombination, and at the same time the need for exceptional transparency and conductivity of the front contact, there are benefits of using two different layers and optimize them separately, thus a buffer layer is often applied in-between the absorber and the transparent front contact.

As discussed in Section 2.1.3 and Section 2.6.2, one of the limiting factors for high efficiency sulfur CZTS solar cells could be a sub-optimal band alignment with the standard buffer material CdS. Accordingly, other materials are investigated for this kind of absorber. The record efficiency sulfur CZTS solar cells are actually made with modified CdS buffers, containing Zn or In to improve the cell performance, which is also shown to alter their band alignment [52, 70].

The heterojunction band alignment is sensitive to several parameters which are difficult to simultaneously control in experimental setups, such as interdiffusion, surface termination, grain orientation, impurities and charge densities. These may originate from absorber formation and temperature treatment as well as sample handling before buffer deposition and growth conditions of the buffer layer. In this thesis care has been taken to ensure as similar treatments of the samples as possible to enable comparable results. However, as the example of the low temperature annealing shows (see Section 4.3), it is difficult to completely avoid differences in sample treatment. Section 5.5 discusses different surface treatments before buffer deposition.

Besides the possible band misalignment there are also other disadvantages with CdS. The band gap of CdS is small enough to absorb part of the incoming light. Changing to a buffer material with higher band gap allows more light to be transmitted to the absorber material which in turn enables a higher maximum current from the solar cell. Additionally, since Cd is toxic it is positive to be able to omit it, both because of the risk of exposure during production and to facilitate waste handling. To find a fitting replacement for CdS, several Cd-free alternative buffers have been researched, for both

CZTS and CZTSSe, such as ZnO, Zn(O,S), (Zn,Mg)O, $Zn_{1-x}Sn_xO_y$, In_2S_3 and an "In-based" buffers [34, 52, 115-118].

In this thesis, two different Cd-free material systems were investigated, namely $ZnO_{1-x}S_x$ (Zn(O,S)) and $Zn_{1-x}Sn_xO_y$ (ZTO). For both materials the ALD deposition process was varied to create buffers with different band gaps. In Paper VI the composition of Zn(O,S) was varied in several steps from pure ZnO to pure ZnS, which is expected to give CZTS solar cells with a range of band alignments, from a large cliff to a high barrier (see also Figure 2 and Section 2.1.3). In Paper VII and Paper VIII the ALD process temperature for ZTO was varied to alter the conduction band position of the material and find the optimal band alignment with CZTS and this yielded very promising results.

However, for the majority of the solar cells produced in this thesis the standard CdS buffer layer was used. It was also used as reference in comparison to the alternative buffer materials. Additionally, a study of the effect of different thicknesses of the CdS buffer layer was performed.

5.2 CdS on CZTS

The CdS buffer was used for the solar cells in Paper II-IV and as reference to the alternative buffers in Paper VI-VIII. A study on the influence of CdS thickness was performed in Paper VI and the results are discussed below.

CdS deposition setup

The buffer layer was deposited by CBD and the recipe developed for CIGS solar cells was used. The CBD solution was kept at 60 °C and comprised of 1.1 M ammonia, 0.100 M thiourea and 0.003 M cadmium acetate. The samples were kept in the solution for 8 min and 15 s, and stirred every minute, which yielded a 50 nm thick film. For the CdS thickness study in Paper VI samples with thicker CdS was created by repeating the standard CBD procedure a second time directly after the first. This is expected to give roughly double thickness. A sample with thinner CdS was produced by shortening the deposition time to 6 min, which is predicted to give about half the thickness.

CdS results

In Paper VI half, normal and double thickness of CdS was evaluated. For one of the samples with double CdS thickness the i-ZnO layer was omitted to investigate its effect on the solar cell performance.

In QE the expected change in the low wavelength region was observed, with higher response for samples with a thinner buffer, since less of the incoming light is absorbed by the CdS layer. The long wavelength part of the QE curve was similar for the different samples, but the solar cell with thick-

est total window layer (double CdS + i-ZnO) had a generally lower QE. The FF for the sample without i-ZnO, 66.3 %, was one of the highest reported for the CZTS material in literature [3, 39].

Negatively biased QE measurements (see Section 3.2.2) showed an increased collection for long wavelengths for all samples. Such behavior is usually explained by poor collection towards the back of the absorber [110], possibly due to short diffusion lengths in combination with a narrow space charge region.

The V_{oc} was slightly reduced for the sample with thinnest CdS layer. Comparing the thick CdS sample to its own reference also showed this trend, but when comparing to the standard thickness samples in general there was no difference between normal and double thickness. In other studies, both increase and decrease of V_{oc} with CdS thickness have been observed but no clear origin was identified [45, 119, 120].

The difference in efficiency for the thickness series was at most 1 % (absolute), and the variation between the references was 0.7 % (absolute), which indicates that the solar cell performance is rather robust with respect to thickness variation in this range.

5.3 Zn(O,S) on CZTS

The Zn(O,S) system was chosen since it has been shown that the conduction band in this material can be changed by varying the ratio of oxygen to sulfur [59], and that the optimum conduction band alignment for CZTS should lie in between the ZnO and the ZnS values. Pure ZnO is expected to give a negative conduction band offset with CZTS and has been shown to give working devices [34, 121]. ZnS should according to first-principles calculations cause current blocking due to a high barrier and for CZTSSe solar cells this was also observed in experiments [117, 122]. In Paper VI different Zn(O,S) compositions were evaluated as buffer layers for CZTS and the results are described below.

Zn(O,S) deposition setup

The Zn(O,S) was deposited by ALD in a home-built system called MP3, described in [123]. The process was performed at 120 °C using diethyl zinc (DEZ) as the Zn-precursor, H_2O as the O-precursor and H_2S as the S-precursor. The buffer composition was varied by changing the number of cycles of DEZ/N_2/H_2O/N_2 versus DEZ/N_2/H_2S/N_2 in the ALD process. For the standard thickness a total of 70 cycles was completed. Additionally, one of the buffer compositions was also tried with twice the number of cycles.

Zn(O,S) results

The variation of the Zn(O,S) composition indeed had a large influence on the electrical properties of the solar cells, as can be seen in Figure 25. Pure ZnS, as expected, blocked the current, and pure ZnO gave low V_{oc} values, as is predicted for a large negative conduction band offset. The intermediate compositions had a clear trend in V_{oc}, with the highest values for the most sulfur-rich buffer. The currents also showed the same, although weaker, trend. The parameter which limited the efficiency for the most sulfur-rich buffer was FF.

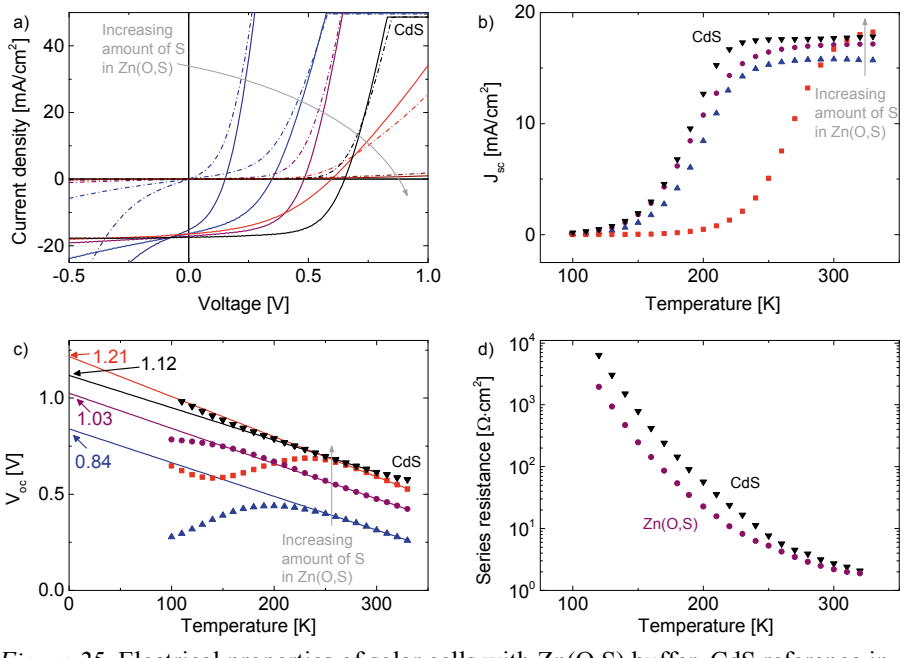

Figure 25. Electrical properties of solar cells with Zn(O,S) buffer. CdS reference in black. a) IV curves, including ZnO and ZnS buffer layers b) J_{sc} from IVT, c) V_{oc} from IVT, d) R_s from IVT. Adapted from Paper VI. ©IEEE 2014

Shunting seemed to increase with higher oxygen content in the buffer. This behavior can possibly be remedied by using a thicker buffer layer and trying this for the intermediate buffer composition indeed slightly improved the shunt conductance from 2.5 to 1.9 mS/cm^2, extracted from the dark JV curve. The V_{oc} was also increased for this sample, and this resulted in the best efficiency of the sample series.

Negatively biased QE measurement on the best Zn(O,S) sample showed an additional increase of collection towards the short wavelength side. The more sulfur rich Zn(O,S) buffer instead showed a slight increase in QE for all wavelengths at negative bias. An explanation for this could be a photo-

current barrier at the buffer-absorber interface, in agreement with the low FF for this sample.

IVT revealed that the J_{sc} of the buffer with the highest sulfur content decreased already around room temperature, while the other samples had a constant J_{sc} from 330 K to around 240 K (Figure 25b). The early decrease of J_{sc} agrees with that there is a barrier at the interface, as suggested from negatively biased QE and the low FF value.

Extrapolating the V_{oc} (T) to 0 K (as described in Section 3.2.3) showed an increase in activation energy with increasing sulfur content of the Zn(O,S) buffer (Figure 25c). However, all the values are still well below the expected band gap value of 1.5 eV. This indicates that the band alignment of Zn(O,S) buffer on CZTS absorber can be changed by the oxygen to sulfur ratio in Zn(O,S) but that interface recombination is still dominant, possibly due to a defective interface and maybe still a non-ideal band alignment.

TEM studies of the CZTS-buffer interface in the best Zn(O,S)-sample showed no obvious causes for bad electrical performance. The buffer conformally covers the CZTS grains and the crystallinity at the interface seems high. TEM-EDS across the interface also showed a sharp transition without gradients across the buffer layer or diffusion of elements between the buffer and absorber.

To obtain additional properties, the IV curves can be fitted to a one-diode model (as discussed in Section 3.2.1). However, for these solar cells it is dubious if the fitting is reasonable, due to the non-ideal behavior of the devices, especially at lower temperatures. Nevertheless, the CdS reference and the best alternative buffer gave tolerable fits and could be compared. Early investigations for CZTSSe-CdS solar cells had shown an increase in series resistance for low temperatures [124]. Our experiments showed that the increase in series resistance was similar for the Zn(O,S) buffer layer and the CdS reference, indicating that either the two different buffer layers cause a similar problem, or that the origin of the high series resistance at low temperatures is not the buffer (Figure 25d).

5.4 ZTO on CZTS

The band gap of ZTO can be altered both by changing process temperature and Sn/(Zn+Sn)-ratio. Both parameters affect the structure of the ZTO film, which is observed to be amorphous with embedded ZnO or ZnO(Sn) nanometer-sized crystallites. The small size of the crystallites causes quantum confinement effects which modifies the band gap of the material [125]. Results from ZTO buffer on CIGS indicate that the band gap change induced by the process temperature occurs mainly in the conduction band, while a change in Sn-content affects both conduction and valence band [126, 127].

In Paper VII and VIII different ZTO buffer layers were evaluated together with CZTS, yielding promising results, as described below.

ZTO deposition setup

The ZTO layers in Paper VII and VIII were deposited by ALD in a Microchemistry F-120 system. The samples were first heated for 30 min in the process chamber to equilibrate at the process temperature. The films were grown using diethyl zinc [$Zn(C_2H_5)_2$], tetrakisdimethylaminotin(IV) [$Sn(N(CH_3)_2)_4$] and deionized water as precursor gases, while N_2 was used as carrier gas. For Paper VII the growth cycle was Zn/Sn-precursor:N_2:H_2O:N_2 and the pulse lengths were 400/400:800:400:800 ms respectively. A 1:1 ratio of Zn:Sn cycles was used and the number of cycles varied between 730 and 1100. For Paper VIII the pulse lengths were 400/400:2000:400:2000 ms and the ratio of Zn:Sn cycles was 1:2. To keep the same thickness of the buffers within this sample series the number of cycles was varied from 500 to 800, since the growth rate was slightly slower for lower process temperatures. The resulting deposition times were between 40 and 65 min.

ZTO results

In Paper VII the ZTO buffer layers developed for CIGS [128] were applied to CZTS solar cells. When using an ALD process temperature that was observed to give similar conduction band offset as CdS (on CIGS) [127], the resulting V_{oc} was comparable to the CdS reference, as expected. A significantly lower ALD process temperature, which should yield a ZTO with higher conduction band level, indeed gave a low FF, indicating a barrier at the interface. An intermediate temperature yielded solar cells with clearly higher voltages and efficiencies than the CdS reference.

The activation energy of the dominant recombination path was obtained by extrapolating V_{oc} (T) to 0 K and resulted in 1.36 eV for the best ZTO sample, see Figure 26. This is one of the highest activation energies observed for a full-sulfide CZTS solar cell in current literature [129]. It is however still lower than the optical band gap of 1.5 eV. Nevertheless, it is comparable to the PL peak position of the absorber which was measured to be 1.3-1.34 eV for this sample. This can be interpreted as the bulk radiative recombination energy for the material, which indicates that the dominant recombination pathway has been moved from the interface to the CZTS bulk, most likely due to better band alignment.

The top efficiency achieved in Paper VII was 7.4 % for a sample with ZTO buffer. That an alternative buffer performed better than its CdS reference had not been observed previously for Cd-free alternative buffers and was of course very promising [81, 130]. The top efficiency solar cell in Paper VII however came from a batch with a relatively poorly performing CdS reference of 5.8 %, which is in the lower part of the expected baseline re-

sults. Additionally there was a variation of buffer thickness and absorber composition in Paper VII which could influence the results. This encouraged us to continue experiments with the ZTO buffer layer.

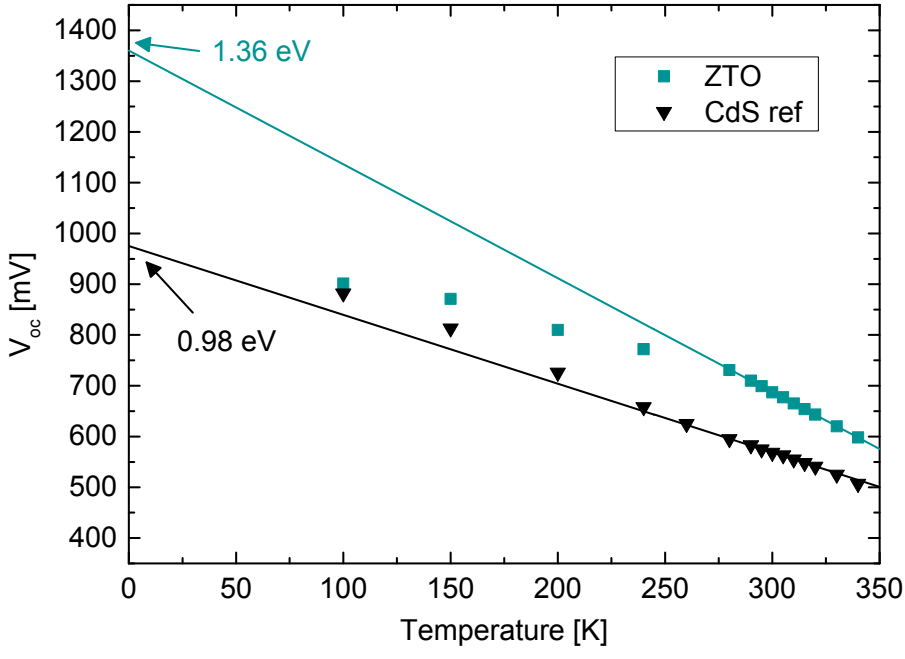

Figure 26. IVT from Paper VII comparing ZTO buffer with CdS buffer, with extrapolation to 0 K to obtain the activation energy of the dominant recombination path.

In Paper VIII a different Zn:Sn ratio was chosen, yielding films with slightly higher Sn-content. The process temperature in the ALD reactor was varied between 105 and 165 °C to find the optimum band alignment (see Figure 27). TEM investigation showed no indication of interdiffusion between buffer and absorber, but due to very thin ZTO layers (10-13 nm) more thorough characterization would have to be done to rule this out.

The V_{oc} was generally higher for the ZTO devices compared to the CdS references, and the highest value was seen for the 145 °C process temperature. However, if strictly comparing with each sample's CdS reference the buffer layers produced at 125 and 145 °C, showed comparable improvement of the voltage. The trend for J_{sc} was similar within the ZTO sample set. It is however not possible to directly compare the currents of the ZTO buffers with the CdS references due to their different thicknesses and thus difference in reflectance. Nevertheless, from the low wavelength part of the QE measurements the benefit of a higher band gap buffer was clearly visible. The FF was similar for all samples besides a decrease for the ZTO deposited at 105

°C. Noteworthy is that the FF was slightly better for the highest process temperature.

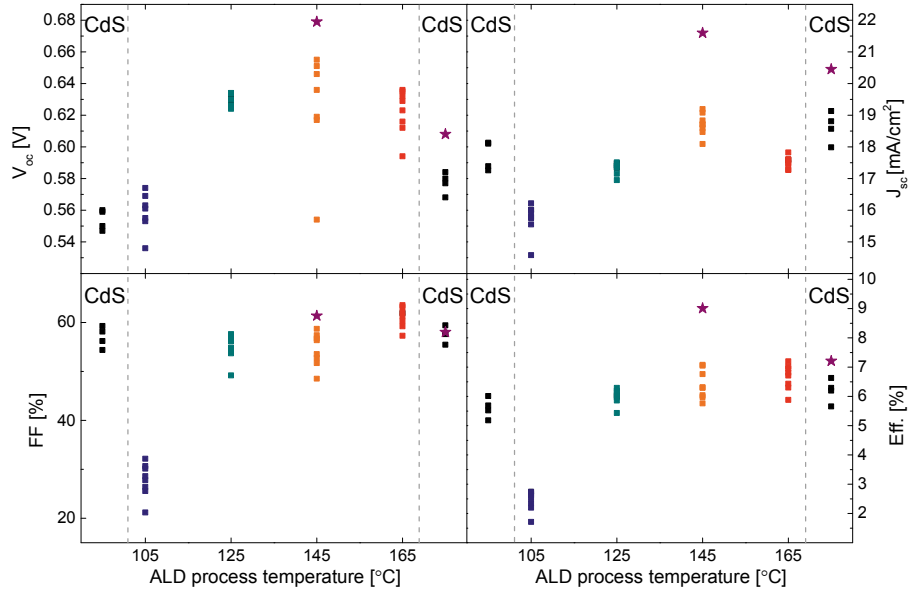

Figure 27. Device parameters for cells with ZTO buffers, deposited at different ALD process temperatures, and their CdS references. The left CdS reference belongs to the 105 and 125 °C sample and the right CdS reference to the 145 and 165 °C samples. Stars indicate the parameters for the record sample (with AR coating) and its CdS reference. Adapted from Paper VIII.

The band gaps of the buffer layers were measured with ellipsometry and, as expected, a decrease with increasing process temperature was observed. The buffer layers prepared at 125 and 145 °C showed similar band gaps, which is consistent with their equal increase in V_{oc} compared to their respective CdS reference.

The IV curve for the buffer layer deposited at 105 °C showed a blocking behavior with very low FF. This indicates that there is a too high barrier in the conduction band at the buffer-absorber interface, which agrees with the band gap measurement. V_{oc} initially increases with increasing buffer deposition temperature but the sample deposited at the highest temperature, with the lowest buffer band gap, has a tendency of lower V_{oc} again. This could indicate that the conduction band line up is getting more cliff-like for this sample. This sample also has a higher FF which could come from a lower barrier at the buffer-absorber interface. However, the higher FF could also be a direct result of the higher process temperature, causing a better interface between buffer and absorber, either by an improved growth process or by modification of the absorber surface. Additionally, the bulk absorber properties can also have been affected by heating, as was seen in the control exper-

iment, where both V_{oc} and FF were slightly improved when similar absorbers were heated and then processed with CdS buffer, as described in Section 4.3.

The activation energies of the dominant recombination path measured by IVT were observed to be higher for the well-performing ZTO buffers compared to their CdS references, indicating that the interface recombination is reduced for the ZTO samples. However, the values of 1.24 and 1.27 eV are lower than the absorber band gap obtained from the QE band edge, which was 1.49-1.51 eV for these samples, and also lower than the measured room temperature PL peak at 1.31-1.32 eV. This implies that the devices are still limited by interface recombination. Nevertheless, the increase in activation energy, the improved V_{oc}, the behavior of IV curves for the different ZTO buffers and the band gaps determined by ellipsometry, together suggest that the band alignment is improved for the optimized ZTO samples compared to the CdS references.

The activation energies measured in Paper VIII were lower than what was observed in Paper VII. The decrease may come from a more defective interface, but might also indicate that the band alignment in Paper VIII could have been further improved. The IV results in Paper VIII point to that the best band alignment was achieved for the buffer deposited at 145 °C, but also that a more optimal band alignment for this particular CZTS absorber possibly could have been obtained for an ALD process temperature in-between 145 and 165 °C.

In Paper VII the thickness of the buffer varied between the samples, but in Paper VIII the same thickness was kept for the different ZTO buffer deposition temperatures. The same trends in device parameters were seen in both papers confirming that the trends were coming from the change of buffer properties, rather than the varied thickness. These results also demonstrated that well-performing solar cells can be fabricated for a wide range of ZTO buffer layer thicknesses (10-100 nm).

Record cell

In Paper VIII a solar cell with an efficiency of 9.0 % was presented (see also Figure 28). This is to our knowledge the highest efficiency reported for Cd-free pure sulfide CZTS, as was also stated in a recent review paper [81].

The buffer layer for this solar cell was made at an ALD process temperature of 145 °C. The resulting ZTO composition was Sn/(Zn+Sn)=0.28 and the thickness 10 nm. The band gap was determined to be 3.5 eV by ellipsometry and IVT gave an activation energy of 1.29 eV. An AR-coating (MgF_2, 110 nm thick) was evaporated on the device, which resulted in the record efficiency of 9.0 %.

The high efficiency for this sample comes partly from a well performing absorber, the CdS reference had an efficiency of 7.2 % (without AR) which is higher than the references for the main series in Paper VIII. This could be

due to the slightly different Cu/Sn-ratio of the absorber (1.89 vs 1.94). Additionally, the slightly higher activation energy for recombination suggests that the interface recombination has been decreased for this sample, which could originate from better interface properties or that the band alignment is further improved. This is supported by the higher FF for the record sample compared to the 145 °C sample in the main series, especially in comparison with respective CdS reference. The band gap determined by ellipsometry for this buffer was in-between the values for the 145 and the 165 °C in the main series, which further strengthens the hypothesis that the optimal band alignment lies within this range.

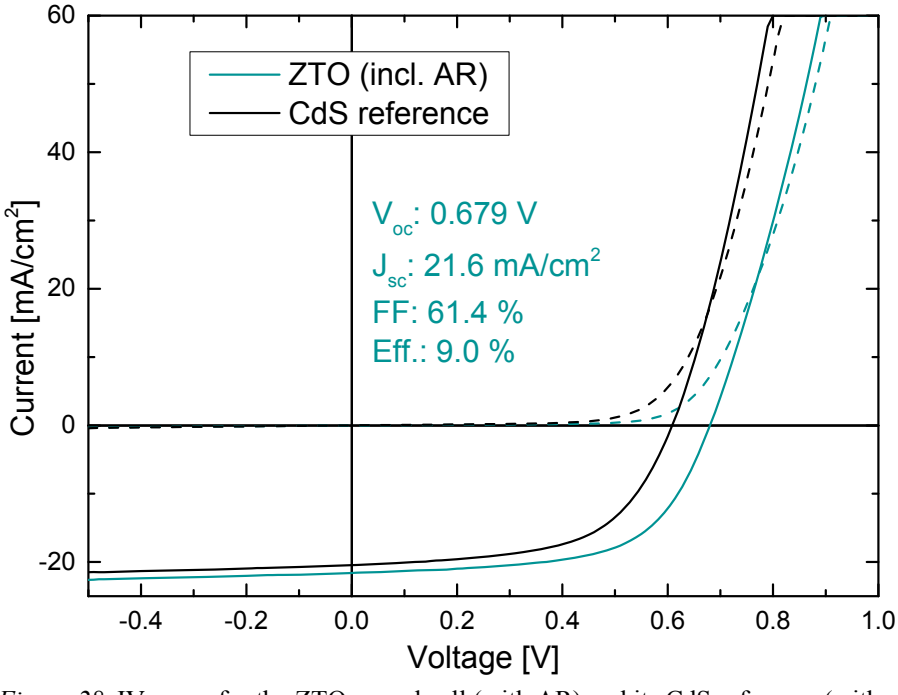

Figure 28. IV curve for the ZTO record cell (with AR) and its CdS reference (without AR). Device parameters are given for the record cell. Dashed lines show dark IV of respective sample. Adapted from Paper VIII.

Compared to the best cell from Paper VII it is mainly the current that has been increased, and looking at the J_{sc} for the CdS references (20.5 versus 17.1 mA) the improvement seems to originate mostly from a better absorber. The annealing process was slightly different for the two absorbers, as can be seen in Table 2. The absorbers were also sputtered in different setups, as discussed in Section 4.1. This is however not expected to yield large differences, as supported by Figure 23 where the small change in current is instead suspected to come from slightly different Zn-contents of the absorbers. The Zn-content is also the main compositional difference between these two ab-

sorbers (Paper VII: Zn/(Cu+Sn)=0.47 and Paper VIII: Zn/(Cu+Sn)=0.38) and this is most likely the reason for the lower current here too.

5.5 Surface treatment before buffer deposition

An excellent quality of the absorber-buffer interface is required to avoid interface recombination. The CdS and the alternative buffer layers are deposited with two different methods and this may affects the level of contaminants present at the surface before the buffer begins to grow. The CdS film is deposited by a wet method, CBD, while the alternative buffers were produced by ALD, which is a dry process. This means that surface compounds and contaminations may be rinsed off, or etched by the ammonia in the solution, in the CBD bath, but remain in the case of the ALD deposition, if no pre-treatment is done.

Figure 29 shows a comparison between an as-annealed absorber and an absorber dipped in water. A surface layer is clearly observed for the untreated sample and EDS indicated additional Na and O in this case. Later investigations in [131] showed that different Na-S-O compounds are found on the as-annealed absorbers, and that this also varies with the duration of air exposure after the annealing.

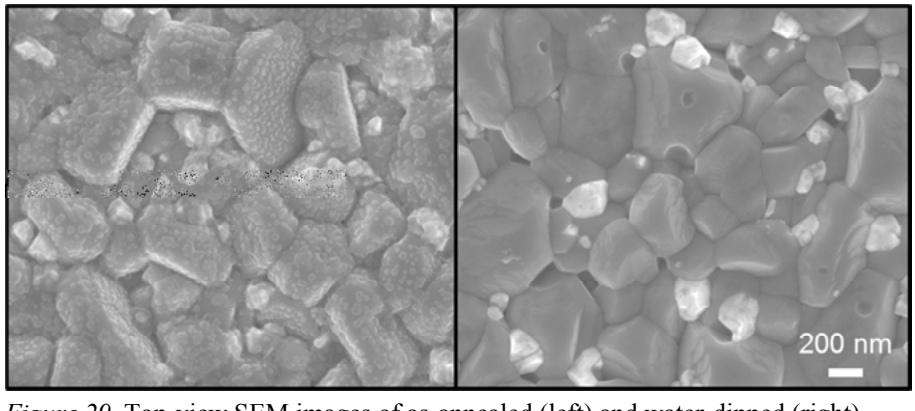

Figure 29. Top-view SEM images of as-annealed (left) and water-dipped (right) absorber.

The difference in interface contamination may affect both the growth process and the electrical properties. In Figure 30 solar cell parameters of samples with various surface treatments is presented. Similar absorbers as in Paper VI, processed with either Zn(O,S) or CdS buffer layers, were used to compare as-annealed, KCN-etched and water-dipped absorbers. As expected the untreated sample was worse for both buffer types and the dry processed Zn(O,S) buffer was clearly more affected. The Zn(O,S) buffer also exhibited

different results for KCN and water treatment, while the CdS samples for these two treatments were similar. The water-dipped sample with ALD Zn(O,S) actually yielded slightly higher efficiencies, 4.8 %, compared to the standard KCN-etch, 4.6%, in this case. In Paper VII, the same comparison was done for ZTO buffer. Here water-dipping and KCN-etching before ZTO buffer deposition yielded samples with similar efficiencies while the untreated absorber, as expected, showed much worse performance.

Generally our experiments with water dipping have yielded widely different results at different test occasions, sometimes resulting in complete peeling of the sample. The variation may depend on the absorbers sensitivity to air exposure time found in [131], which was not controlled in previous tests. To ensure a stable process all the samples in this thesis were KCN-etched, both before the CBD and the ALD process, as also described in Section 2.4. However, the fact that the water-dipped samples perform well indicate that the absorbers do not contain Cu-S secondary phases (see Section 2.5), and the investigations in [131] point to the possibility of exchanging the KCN-etch to air exposure or water-dipping and still yield well-performing solar cells.

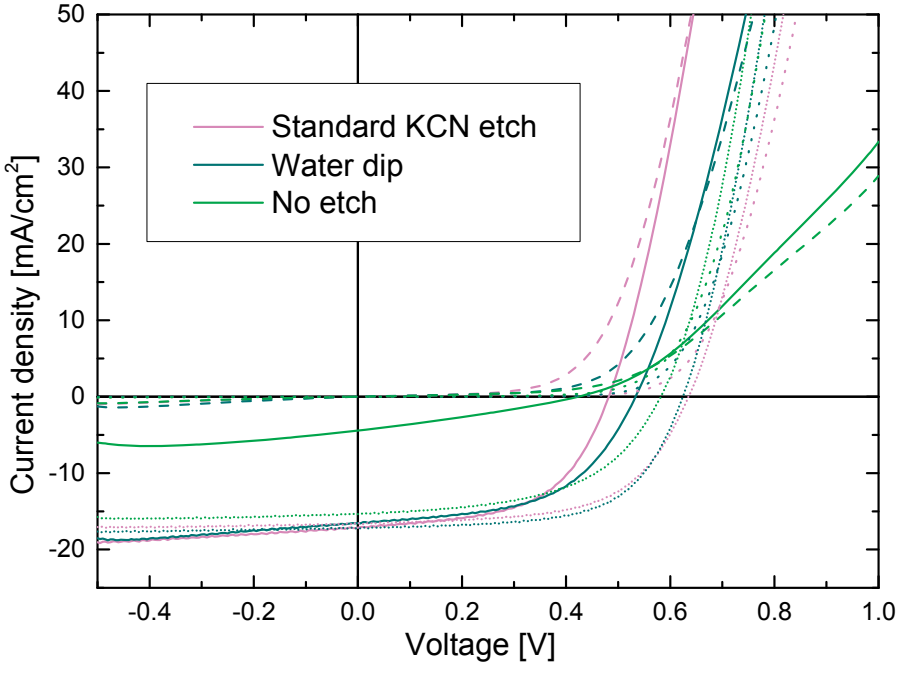

Figure 30. Comparison between different absorber treatments before buffer deposition. Dotted lines are cells with CBD CdS buffer, solid (light IV) and dashed (dark IV) lines are Zn(O,S) buffer made by ALD.

5.6 Discussion

The quality of the buffer layer and the buffer-absorber interface is crucial for high solar cell performance. It is clear that the CdS buffer is generally well-performing and robust to changes in for example thickness. However, the results from Paper VII and Paper VIII show that the ZTO buffer layer can outperform CdS, which is good news in the effort to create a solar cell with only abundant and non-toxic materials. The ZTO buffer is also observed to work well for a large range of thicknesses. The layer thickness in Paper VIII (10-13 nm) is on the limit to what one would expect to be completely covering for such a rough surface as the CZTS absorber, and there is a risk that the film would be non-continuous. However, since the trends in Paper VIII are comparable to what was observed in Paper VII, where the buffer layers were significantly thicker, it implies that also the layers in Paper VIII were continuous.

The Zn(O,S) buffer system unfortunately does not perform well for CZTS in our studies. It was possible to vary the band alignment but either the interface or buffer quality is not sufficient. In previous studies of the Zn(O,S) buffer layer on CIGS there have been indications that the film may be inhomogeneous, both laterally and in depth, and this may affect the performance also with the CZTS absorber [132]. Another hypothesis would be that it is the Sn in ZTO that makes this buffer well-performing compared to the Zn(O,S). SnO_x has been suggested to have a beneficial effect both as an intermediate layer at the CZTS/CdS and CZTS/Zn(O,S) interface, and in the grain boundaries of CZTSSe [58, 114, 133].

An effect of a low temperature treatment was discussed in Section 4.3 and this was evaluated for the samples in Paper VIII. For Paper VI and Paper VII no heated CdS reference samples were investigated and it is likely that the ALD process temperature may have affected the absorber layers also in these cases. For Paper VI the same process temperature was used for all samples and the results should therefore be comparable within the series. However, one of the samples was made with double buffer thickness, which means that it was kept at the process temperature for twice as long time, something that also may be important for the changes of the absorber. The low temperature post-annealing experiments in Paper VIII showed that V_{oc} and FF were most sensitive to the temperature treatment. The higher voltage seen for the thicker sample in Paper VI could therefore partly come from the longer time at temperature. There is also a risk that the generally poor performance of the Zn(O,S) buffer samples was caused by a degradation of the absorber at these specific anneal conditions. In Paper VII different temperatures were used in the ALD process and this may have impacted the resulting solar cell properties. However, the variation in temperature in this series was smaller than for Paper VIII. The main conclusions from Paper VI and Paper VII are therefore not suspected to have been changed by the low temperature annealing effect.

In Figure 31 electrical properties of the best cells from the two alternative buffer systems are presented, together with their respective CdS references (the notation A, for the Zn(O,S) and its CdS reference, and B, for the ZTO and its CdS reference, are added to clarify which samples that share the same absorber). The B-CdS showed in Figure 31a-b is also one of the best CdS solar cells made in this work, with an efficiency of 7.2 %. Another B-CdS sample from the ZTO series, with efficiency 6.6 %, is shown in Figure 31c-d. The A-CdS reference also had an efficiency of 6.6 %.

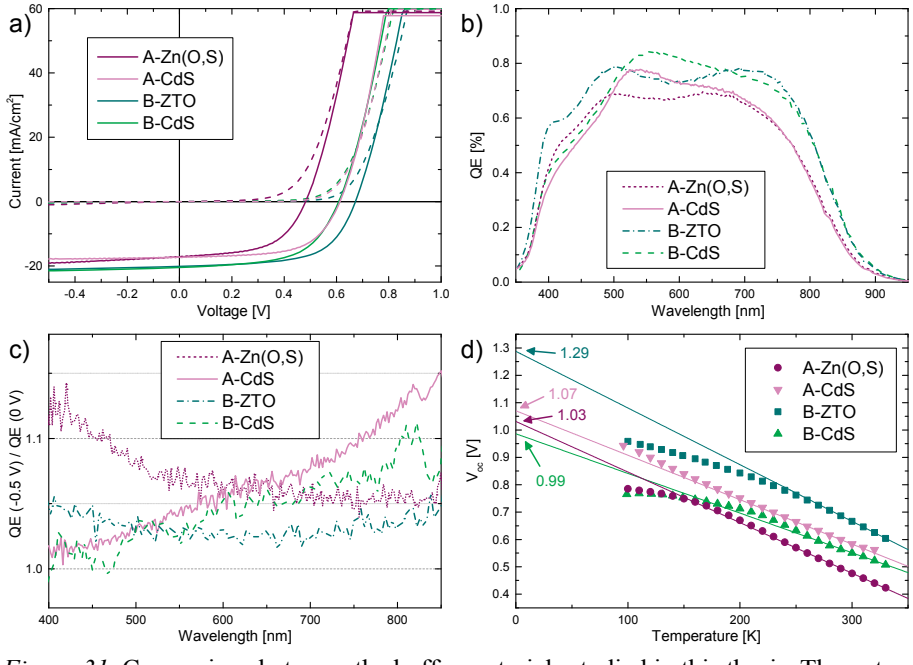

Figure 31. Comparison between the buffer materials studied in this thesis. The notation A, for the Zn(O,S) and its CdS reference, and B, for the ZTO and its CdS reference, are added to clarify which samples that share the same absorber. A-Zn(O,S) and A-CdS data originate from Paper VI while B-ZTO and B-CdS data originate from Paper VIII. a) IV curves, dashed lines show dark IV of respective sample, b) QE measurement, c) Ratio between QE measured at -0.5 V and 0 V, d) IVT showing extrapolation to 0 K for activation energies of the dominant recombination paths.

When examining the device properties of the two CdS references a clear difference between the two absorbers (A and B) is observed with significantly higher current for the B-CdS sample (Figure 31a). This is also apparent when comparing all the device results in Paper VI and Paper VIII, the currents are generally higher for the CdS references in Paper VIII. As described in Section 4.1 and Section 4.2, both the sputtering of the precursor and the annealing conditions differ between absorber A and B. Additionally there is a difference in composition and thickness of the absorbers, where the B-absorber from Paper VIII has more Sn and less Zn, both of which we have

seen indications on giving higher current. However, when examining the CdS references within the papers one can also see a large spread in-between both annealing runs and indeed also cells from the same sample. Actually, the top efficiency for the CdS references in the two papers is similar, where the lower current for the sample in Paper VI is compensated by higher V_{oc} and FF.

When comparing the IV curves for the alternative buffer samples (Figure 31a), a large difference in V_{oc} is observed and the superiority of ZTO is obvious. The Zn(O,S) sample also shows signs of low FF and shunting. The current is, as also discussed in Section 5.4, not possible to compare as readily in-between the buffer layer types due to the difference in thickness and thus the effect of reflectivity. From the QE curves (Figure 31b) it is however clear that the alternative buffers have a higher transmittance at the short wavelengths side. Here again the difference in current from the two CdS references is observed and the A-CdS sample has a generally lower QE over all wavelengths compared to the B-CdS.

The negatively biased QE for the CdS samples (Figure 31c) qualitatively show the same behavior, with increasing QE for the long wavelengths at negative bias. The two alternative buffers show other trends, where an increase for short wavelengths is seen for the Zn(O,S) sample while the ZTO sample only exhibits a smaller increase over the entire wavelengths, indicating a clear difference in sample behavior.

The $V_{oc}(T)$ data in Figure 31d again show the superiority of ZTO which clearly yields the highest activation energy when extrapolated to 0 K. The two CdS references look similar in this measurement, besides the behavior at the lowest temperatures, even though the extrapolation ends up at rather different values. This is however mostly due to the difficulty of finding a linear region for the extrapolation in these samples, which means that the resulting activation energy may have a substantial error.

The application of different buffer layers can both increase our knowledge about CZTS and enhance solar cell efficiencies. From these studies ZTO stands out as a possible new standard buffer layer for CZTS.

6. Concluding remarks and outlook

6.1 Conclusions

The aim of this thesis was to understand the influence of deposition processes and film properties on Cu_2ZnSnS_4 thin film solar cells. Two main aspects were studied, namely sputtering of precursors for CZTS with focus on sulfur incorporation, and alternative cadmium free buffer materials with better energy band alignment. Additionally, low temperature treatment of CZTS absorbers was explored since the alternative buffer materials chosen were deposited at 105-165 °C.

Reactive sputtering was used to grow dense and homogeneous precursor films containing all elements needed for CZTS absorbers. Both the sputtering process and the resulting films were characterized.

The addition of H_2S gas to the inert Ar sputter atmosphere led to an abrupt and drastic decrease of Zn deposition rate due to the sulfurization of the target surface. Surface sulfurization also led to process instabilities for targets made of Cu-Sn, Cu and Cu_2S, while sputtering with a CuS-target gave acceptable process stability.

It was found that both film morphology and composition were affected when adjusting H_2S/Ar-flow ratio and substrate temperature. Process pressure was observed to have limited effect on the film properties.

The precursors with a sulfur content close to stoichiometric CZTS had a columnar, crystalline structure. Materials analysis of these films suggests a non-equilibrium phase with a cubic structure where each S atom is randomly surrounded by 2:1:1 Cu:Zn:Sn-atoms.

Substrate heating was shown to be important to avoid cracks in the annealed films while stress in the precursor films was not observed to affect the absorber or solar cell quality. Precursors with higher copper content or sputtered at higher substrate temperatures generally yielded larger grains when annealed, although no correlation with device parameters was seen.

A comparison with sputtering from compound targets in Ar atmosphere showed similar film properties as the reactively sputtered precursors with close to stoichiometric sulfur content. Both types of precursors were shown to work well in the solar cell processing, and yielded comparable parameters when processed in the same anneal run.

Low temperature post-annealing of CZTS absorbers in inert atmosphere was shown to deteriorate device properties when performed at 105 °C. On

the other hand, for higher annealing temperatures (125-165 °C) beneficial effects were observed. This indicates that the thermal history of the CZTS absorber is important and could affect both experimental results and choice of production processes.

Alternative buffer material systems, to exchange the standard CdS, without cadmium and with expected improved band alignment with CZTS, were evaluated. $ZnO_{1-x}S_x$ was shown to be a viable buffer material system for CZTS, in which it was possible to vary the conduction band offset between the absorber and the buffer. However, the efficiencies achieved were lower than expected, possibly due to inferior interface or buffer quality.

The experiments with the $Zn_{1-x}Sn_xO_y$ buffer material showed more promising results. The buffer band gap was successfully varied and the expected effect on solar cell device properties was observed. For optimized parameters the devices with ZTO buffer layers showed clearly better performance than the CdS reference samples, which is seldom the case for the Cd-free alternatives. The activation energy for the main recombination path was increased for the optimized ZTO samples, indicating an improved interface quality or band alignment. The highest activation energy measured coincides with the energy of the PL peak of the absorber, which can be interpreted as a shift of dominant recombination path from the interface, to the CZTS bulk. This has not previously been observed for the sulfide CZTS solar cells. A well-performing CZTS-ZTO solar cell, with antireflective coating, yielded an efficiency of 9.0 %, which at the time of publication was the highest value published for a cadmium free pure sulfide CZTS solar cell.

6.2 Future work

One of the recent results in this thesis concerned the effect of low temperature post-annealing on device properties. For future progress it would be beneficial to further understand and control this behavior. There is also a need to extend the investigations to include, and separate, the effect on the different layers in the solar cell stack. A prime suspect for the sensitivity to temperature treatment is the Na-content, and its distribution within the solar cell stack. With the lessons learned from the CIGS case this may need extensive attention also for CZTS.

Due to the complexity of the reactive sputtering process there are many aspects remaining to investigate. Initial experiments were done on optical emission spectroscopy of the sputter process and this could be further pursued. More can also be done regarding limiting the detrimental effect of H_2S on the targets, and possibly decreasing the amount of negative sulfur ions, for example by moving the gas inlet to close to the substrate, instead of in the middle of the chamber as was the case for these experiments.

Regarding the influence of sulfur content in the precursors it would be interesting to retry the intended experiments in Section 4.1.4 to obtain a clearer composition variation. Preferably a better measurement of sulfur content should then be developed. Comparisons with purely metallic precursors could also be done, but the formation path during annealing is very different in this case and would require another set of annealing parameters, which could complicate the interpretation of the results.

The formation path in annealing of these non-equilibrium precursors has been initially studied but is not yet fully understood. This, together with experiments to understand formation of secondary phases and the influence of the exact composition of the CZTS phase is on-going, and necessary to uncover the defect physics of the material and improve the efficiencies.

An aspect not covered in this thesis is “light soaking”, a term commonly used to describe that device parameters of thin film solar cells can change slightly depending on their illumination history. This means that the electrical properties measured for a solar cell can have minor differences depending on if it has been kept in the dark before the measurement or if it has been exposed to light for some minutes. This effect is usually most pronounced for alternative buffers, and was also observed for the solar cells in this thesis, however not methodically studied. Generally the device performance becomes slightly better after a couple of minutes illumination and the parameter most affected is FF. The effect is largest for poorly performing solar cells and for solar cells that have been stored in dark for several days. For a more thorough understanding of the buffer material this behavior should be further investigated.

The ZTO buffer yields very promising results and could be the new standard buffer material for CZTS solar cells. To improve the understanding of the band alignment and the quality of this interface, more experiments are needed. Tuning may also be needed to find a deposition temperature that both enhances the absorber performance and creates an optimal buffer material and interface.

7. Sammanfattning på svenska

Idag kommer en stor del av den energi vi använder från icke-förnybara energikällor och det finns ett stort behov av att vidareutveckla denna sektor för att istället uppnå en hållbar energiförsörjning. I ett hållbart system behöver alla delar vara antingen förnybara eller återvinningsbara. Det gäller både energikällan och metoden som används för att utvinna den. Energiomvandlingen bör därför ske med material som finns i riklig mängd och som inte är skadliga för människa eller miljö. Detta för att förenkla möjligheten till storskalig produktion och återvinning.

För tunnfilmssolceller så innebär detta att de sällsynta och giftiga ämnen som finns i många av dagens solcellsmoduler bör bytas ut, såsom indium i $Cu(In,Ga)Se_2$ (CIGS) eller kadmium i CdTe. Man undersöker därför nya material som kan vara möjliga ersättare. Bland dem har $Cu_2ZnSn(Se,S)_4$ (CZTSSe) fått stor uppmärksamhet de senaste tio åren, både p g a dess lämpliga solcellsegenskaper och dess likhet med det kommersiellt tillgängliga CIGS-materialet. I CZTSSe kan Se/S-halten varieras för att ändra materialets elektriska bandgap, men en ren sulfid kan vara att föredra eftersom svavel finns i större mängd än selen. Denna avhandling är därför begränsad till Cu_2ZnSnS_4 (CZTS).

En tunnfilmssolcell kännetecknas av att det aktiva materialet har en hög ljusabsorberande förmåga och därför behövs endast ett mycket tunt lager, ca 0.001 mm. Det innebär att det finns potential för låga material- och produktionskostnader och möjlighet att använda olika underlag (substrat) för solcellen, inklusive böjliga filmer av plast eller metall. På substratet läggs oftast först en metallisk bakkontakt, ovanpå denna läggs det aktiva lagret och för att färdigställa solcellen behövs ett komplementlager, ofta kallat buffert. Överst läggs en genomskinlig framkontakt och eventuellt ett metallmönster för att förbättra ledningsförmågan.

Målet med denna avhandling har varit att undersöka och förstå solceller av CZTS-typ för att kunna öka verkningsgraden och ersätta giftiga ämnen. Två forskningsområden valdes ut som särskilt intressanta, nämligen att inkludera alla nödvändiga grundämnen tidigt i produktionsprocessen för att få ett homogent CZTS-material med bra morfologi och därmed potential för hög verkningsgrad, samt att byta ut den CdS som ofta används som komplementlager till CZTS och CIGS solceller. Att byta ut tungmetallen Cd är positivt utifrån ett hälso- och miljöperspektiv men har också, vid val av rätt

ersättningsmaterial, möjligheten att öka solcellens verkningsgrad p g a högre ljusgenomsläpplighet och bättre matchning med CZTS.

Solcellerna i avhandlingen tillverkades på glassubstrat genom att först belägga detta med en bakkontakt av molybden. Sedan användes sputtring, även kallat katodförstoftning på svenska, för att skapa en tunn, homogen film av Cu, Zn, Sn och S. Här studerades både processen och det resulterande materialet. Det andra steget i tillverkningen av CZTS var en uppvärmning vid hög temperatur (560-580 °C), med eller utan tillsatt svavel. För buffertmaterialen med och utan kadmium användes olika processmetoder. Standardbufferten av CdS belades med en våtkemisk process medan en vakuumbaserad kemisk beläggningsmetod (Atomic Layer Deposition (ALD)) användes för de kadmiumfria buffertarna $ZnO_{1-x}S_x$ (Zn(O,S)) och $Zn_{1-x}Sn_xO_y$ (ZTO). Avslutningsvis användes sputtring för att skapa en genomskinlig framkontakt av aluminiumdopad ZnO och förångning för ett komplementerande Ni-Al-Ni-metallmönster.

Sputtring är en fysikalisk vakuumytbeläggningsmetod där atomer slås loss (sputtras) ut från ett fast material med hjälp av högenergetiska joner. Processen utförs i en vakuumkammare men med ett kontrollerat tryck av antingen en inert gas, såsom Ar, eller en reaktiv gas, såsom H_2S, det senare kallat reaktiv sputtring. Det material man vill använda i beläggningen placeras som katod och kopplas till en hög negativ spänning vilket gör att gasen i kammaren joniseras och bildar ett plasma. De positiva gasjonerna dras till beläggningsmaterialet och när de krockar in i ytan slås delar av materialet ut i form av atomer och molekyler. Dessa färdas genom vakuumkammaren och bildar när de landar en tunn film av beläggningsmaterialet. Flera faktorer påverkar processen och den resulterande filmen, såsom processtryck, temperatur på substratet och mängden reaktiv gas.

Två olika metoder att inkludera svavel i sputterprocessen undersöktes, först testades metalliska katodmaterial i kombination med en sputteratmosfär innehållandes H_2S, sen användes metall-svavelföreningar som katodmaterial i en inert Ar-atmosfär.

När H_2S-gas introduceras så kan metalliska katodmaterial sulfuriseras och detta påverkar sputterprocessen. Cu-Sn, Cu och Cu_2S var alla problematiska att använda som beläggningsmaterial i svavelatmosfär eftersom sulfuriseringen av katodytan gjorde processen instabil. CuS visade sig vara ett bättre val som kopparkälla. Sulfuriseringen gav också en snabb och drastisk minskning av deponeringshastigheten från Zn-katoden, vilket kan förväntas eftersom Zn är relativt reaktivt. Om man använder en H_2S-halt som är mer än tillräcklig för att hålla Zn-katoden sulfuriserad så är detta oftast oproblematiskt, men om man vill använda lägre flödesmängder, nära omställningspunkten mellan en metallisk och en sulfuriserad katodyta, så kan processen bli svårkontrollerad.

Att ändra på H_2S/Ar-förhållandet i sputteratmosfären gav, som förväntat, filmer med varierande mängd svavel och därför olika morfologi. Även tem-

peraturen på substratet kan påverka filmmorfologin eftersom en högre temperatur innebär större möjlighet för de utsputtrade atomerna att hitta fördelaktiga platser i den tillväxande filmen. Det gynnar en högre densitet och en mer orienterad film, något som också observerades i experimenten. Det var också tydligt att mängden Zn, Sn och S minskade för filmer belagda vid högre substrattemperaturer. Detta beror förmodligen på höga ångtryck hos Zn, SnS och S. De olika totalprocesstryck som undersöktes hade dock begränsad inverkan på filmegenskaperna.

När svavelinnehållet i de sputtrade filmerna var tillräckligt nära det hos CZTS bildades en kristallin och kolumnär film. Materialanalys på dessa filmer tyder på en metastabil kubisk fas där varje svavelatom omges av slumpmässigt ordnade Cu:Zn:Sn-atomer i proportionerna 2:1:1.

Att värma beläggningssubstratet under sputtringen visade sig vara viktigt för att undvika att filmerna krackelerade när de upphettades i CZTS-tillverkningens andra steg. Ingen koppling mellan stress hos de sputtrade filmerna och materialegenskaper hos de värmda filmerna observerades.

Eftersom beläggningstemperaturen för de alternativa buffertmaterialen var 80-165 °C så gjordes en extra experimentserie för att studera effekten av en sådan värmning på CZTS-materialet. En 40 min värmning av CZTS vid 105 °C gav en försämring av de elektriska egenskaperna, medan 125, 145 och 165 °C istället gav något bättre solceller än referensen. Detta påvisar att CZTS-materialet kan påverkas av oväntat låga temperaturer, vilket kan vara viktigt att ha i åtanke när man väljer jämförelser i experimentserier eller ordning på produktionsprocesser.

För de båda valda alternativa buffertmaterialen så kan det elektriska bandgapet varieras genom att ändra sammansättningen eller beläggningstemperaturen. Det gör att man kan optimera matchningen mellan bandgapen hos CZTS och buffertmaterialet och på så sätt få förbättrade elektriska egenskaper hos solcellen.

Solceller med Zn(O,S) på CZTS visade att det var möjligt att variera bandmatchningen, men att verkningsgraden var lägre än förväntat, förmodligen p g a dålig kvalitet på gränsytan eller sammansättningsvariationer i buffertlagret.

ZTO som buffertmaterial gav generellt bättre resultat och optimering av materialet gav solceller med högre verkningsgrad än CdS-referenserna, något som sällan ses för kadmiumfria alternativ. Mätningar på dessa solceller pekar också på att gränsytan och bandmatchningen förbättrats så pass mycket att det istället är CZTS-materialet som är den begränsande faktorn för att öka verkningsgraden.

En ZTO-CZTS solcell med en verkningsgrad på 9.0 % presenteras i avhandlingen och detta var vid publikationen det dittills högsta värdet för en kadmiumfri solcell av Cu_2ZnSnS_4.

8. Acknowledgements

I have really appreciated this chance to do research and study, and I would like to thank my supervisors a lot for giving me this opportunity! I also want to thank them so much for all the explanations and encouragement over the years. **Lotten**, thanks for all the help, inspiration, corrections and nice chats. **Tomáš**, thanks for all discussions, clean room assistance and new ways of seeing things. **Marika**, thanks for all the inspiration, positive attitude and apples!

Thanks also to **Shili** for running the division and providing suggestions for improvement of the thesis. And to **Tomas** for encouraging comments on the thesis and co-sputtering!

Thanks to the **solar cell group** for all the lab work, discussions and nice fikas! **Jonathan**, for many enjoyable lunches and excellent research. **Tobias**, for a lot of help in the labs and ice cream inspiration. **Uwe**, for getting everything to work and the German chocolate. **Jes**, for countless experiments and new records. **Adam**, for endless lab help and fun debates. **Bart**, for novel ideas and GT. **Pedro**, for solid knowledge and enjoyable chats. **Nils**, for hours of sputtering and entertaining stories. **Sebastian**, for trustworthy scripts and nice chats both on- and offline. **Carl**, for imagination and inspiration. **Volodymyr**, for careful measurements and fun stories. **Viktor**, for clever solutions both on and off work. **Alexandra**, for interesting research and for being so nice! **Shuyi**, for skillful measurements and fun food. **Jan**, for new ideas and cheerful communication. **Filippo**, for fun experiments and good times. **Nina**, for co-operative lab work and nice discussions. **Sethu**, for new insights and inspiration. **Oleksandr**, for easy collaboration and nice chats.

Thanks to all fellow **PhD students** who are working hard but still have time to help out, and thanks for being such nice people! **Ray**, for all good chats and incredible amount of experiments. **Johan**, for all the support and your knowledge about the real solar world. **Christopher**, for countless explanations and sincere chats. **Erik**, for co-sputtering and fun clean room hours. **Fredrik**, for skillful experiments and easy communication, despite the wall. **Sven**, for interesting discussion topics and thorough research. **Timo**, for fun chats and co-lab teaching. **Katharina**, for energetic involvement and methodical research. **Olivier**, for doctoral support and encouragement. **Dorothea**, for clean room co-work and inspiration. **Piotr**, for tech support and games. **Patrice**, for cool sputtering and interesting discussions.

Jonas, for solid research and inspiration. **Nishant** and **Faraz**, for keeping up the good work and being such nice new neighbors. **Milena**, for good muffins and good discussions. **Lina**, for sincere chats and advice. **Malkolm**, **Patrik**, **Lukas** and many more for fun and unexpected lunch discussions. **Balazs**, **Per-Oskar**, **Sara**, **Shabnam**, **Li** for entertaining stories and nice chats!

Thanks to the rest of **FTE** for interesting Friday seminars and enjoyable corridor chats! Special thanks to **Marianne**, **Ramy**, **Lars**, **Pia**, **Hans-Olof** and **Jörgen**.

Thanks to others at **Ångström laboratory** for help and making life at work easier! **Daniel**, **Anders**, **Jens** and the others at **ITC,** for excellent measurements and knowledge. **Mikael**, for enabling such nice x-ray measurements. **Jonatan**, for smooth computer support and enjoyable discussions. **Ingrid** and **Maria** for help with the endless administration and many nice chats.

Thanks to the **kesterite network** for a lot of interesting collaborations, measurements and results. And thanks for great conferences, as well as fun evenings! Special thanks to **Justus**, for enjoyable trips and caring about composition. And **Caro**, for skiing and inspirational spirit both on and off work!

Thanks to **Jessica** for making the first half year of this thesis full of fun!

Thanks to the **Solibro**-employees, **Uwe**, **Daniel**, **Erik** and others, for many fun lab hours and lunches!

Thanks to the **MSL**-employees, **Torvald**, **Jan-Åke**, **Björn**, **Victoria**, **Amit**, **Farhad**, **Örjan**, **Leif**, **Rimantas**, **Fredrik**, **Fredric** and others, for help with both stupid and complicated problems and many enjoyable chats!

Thanks to **Liv**, **Jan** and the **Midsummer**-employees for nice collaboration on the master thesis work!

Thanks to various **Ångström and clean room people** that made my days more enjoyable! Especially to **Juan**, **Stefano**, **Sofia**, **Peter** and **Peter**.

And so many thanks to **relatives** and **friends** that have made sure that life is more than work! **Erik**, for being the one I love. My children, **Malte** and **Isa**, for always lightning up my days. My parents, **Curry** and **Lars**, for long lasting support and knowledge. My in-laws, **Ann** and **Peo**, for taking care of the kids and for many nice dinners. My brother, **Petter**, for always being there. **Frida**, for putting things in perspective. **Friends**, for wonderful games and dinners.

And thanks to J. K. Rowling, Stephen Fry and Randall Munroe for making possibly boring moments more enjoyable.

And since I have been doing this for quite some time and my memory is not the best, extra many thanks to **all I have forgotten to mention**!

9. References

[1] C. S. Tao, J. C. Jiang, and M. Tao, "Natural resource limitations to terawatt-scale solar cells", *Solar Energy Materials and Solar Cells,* vol. 95, pp. 3176-3180, 2011.

[2] P. Viebahn, O. Soukup, S. Samadi, J. Teubler, K. Wiesen, and M. Ritthoff, "Assessing the need for critical minerals to shift the German energy system towards a high proportion of renewables", *Renewable & Sustainable Energy Reviews,* vol. 49, pp. 655-671, 2015.

[3] S. Zhuk, A. Kushwaha, T. K. S. Wong, S. Masudy-Panah, A. Smirnov, and G. K. Dalapati, "Critical review on sputter-deposited Cu2ZnSnS4 (CZTS) based thin film photovoltaic technology focusing on device architecture and absorber quality on the solar cells performance", *Solar Energy Materials and Solar Cells,* vol. 171, pp. 239-252, 2017.

[4] R. Roesch, T. Faber, E. von Hauff, T. M. Brown, M. Lira-Cantu, and H. Hoppe, "Procedures and Practices for Evaluating Thin-Film Solar Cell Stability", *Advanced Energy Materials,* vol. 5, 2015.

[5] M. A. Green, *Solar cells - Operating Principles, Technology and System Applications*. Englewood Cliffs, N.J.: Prentice-Hall, Inc., 1982.

[6] M. Bär, B. A. Schubert, B. Marsen, R. G. Wilks, S. Pookpanratana, M. Blum, S. Krause, T. Unold, W. Yang, L. Weinhardt, C. Heske, and H. W. Schock, "Cliff-like conduction band offset and KCN-induced recombination barrier enhancement at the CdS/Cu_2ZnSnS_4 thin-film solar cell heterojunction", *Applied Physics Letters,* vol. 99, pp. 222105-3, 2011.

[7] T. Minemoto, T. Matsui, H. Takakura, Y. Hamakawa, T. Negami, Y. Hashimoto, T. Uenoyama, and M. Kitagawa, "Theoretical analysis of the effect of conduction band offset of window/CIS layers on performance of CIS solar cells using device simulation", *Solar Energy Materials and Solar Cells,* vol. 67, pp. 83-88, 2001.

[8] M. Bodegård, L. Stolt, and J. Hedström, "The influence of sodium on the grain structure of CuInSe2 films for photovoltaic applications", in *12th European Photovoltaic Solar Energy Conference (EU PVSEC 12)*, Amsterdam, Netherlands, 1994, pp. 1743-1746.

[9] K.-J. Yang, J.-H. Sim, D.-H. Son, D.-H. Kim, and J.-K. Kang, "Two different effects of Na on Cu2ZnSnS4 thin-film solar cells", *Current Applied Physics,* vol. 15, pp. 1512-1515, 2015.

[10] W. M. H. Oo, J. L. Johnson, A. Bhatia, E. A. Lund, M. M. Nowell, and M. A. Scarpulla, "Grain Size and Texture of Cu2ZnSnS4 Thin Films Synthesized by Cosputtering Binary Sulfides and Annealing: Effects of Processing Conditions and Sodium", *Journal of Electronic Materials,* vol. 40, pp. 2214-2221, 2011.

[11] T. Gershon, C. Hamann, M. Hopstaken, Y. S. Lee, B. Shin, and R. Haight, "Chemical Consequences of Alkali Inhomogeneity in Cu2ZnSnS4 Thin-Film Solar Cells", *Advanced Energy Materials,* vol. 5, 2015.

[12] C. Y. Peng, T. P. Dhakal, S. Garner, P. Cimo, S. Lu, and C. R. Westgate, "Fabrication of Cu2ZnSnS4 solar cell on a flexible glass substrate", *Thin Solid Films,* vol. 562, pp. 574-577, 2014.
[13] P. Bras, J. Sterner, and C. Platzer-Björkman, "Influence of hydrogen sulfide annealing on copper-zinc-tin-sulfide solar cells sputtered from a quaternary compound target", *Thin Solid Films,* vol. 582, pp. 233-238, 2015.
[14] Y. Z. Zhang, Q. Y. Ye, J. Liu, H. Chen, X. L. He, C. Liao, J. F. Han, H. Wang, J. Mei, and W. M. Lau, "Earth-abundant and low-cost CZTS solar cell on flexible molybdenum foil", *Rsc Advances,* vol. 4, pp. 23666-23669, 2014.
[15] Q. W. Tian, X. F. Xu, L. B. Han, M. H. Tang, R. J. Zou, Z. G. Chen, M. H. Yu, J. M. Yang, and J. Q. Hu, "Hydrophilic Cu2ZnSnS4 nanocrystals for printing flexible, low-cost and environmentally friendly solar cells", *Crystengcomm,* vol. 14, pp. 3847-3850, 2012.
[16] T. Wada, N. Kohara, T. Negami, and M. Nishitani, "Chemical and structural characterization of Cu(In,Ga)Se-2/Mo interface in Cu(In,Ga)Se-2 solar cells", *Japanese Journal of Applied Physics Part 2-Letters & Express Letters,* vol. 35, pp. L1253-L1256, 1996.
[17] K. Wang, O. Gunawan, T. Todorov, B. Shin, S. J. Chey, N. A. Bojarczuk, D. Mitzi, and S. Guha, "Thermally evaporated Cu2ZnSnS4 solar cells", *Appl. Phys. Lett,* vol. 97, p. 143508, 2010.
[18] K. J. Yang, J. H. Sim, B. Jeon, D. H. Son, D. H. Kim, S. J. Sung, D. K. Hwang, S. Song, D. B. Khadka, J. Kim, and J. K. Kang, "Effects of Na and MoS2 on Cu2ZnSnS4 thin-film solar cell", *Progress in Photovoltaics,* vol. 23, pp. 862-873, 2015.
[19] J. J. Scragg, J. T. Wätjen, M. Edoff, T. Ericson, T. Kubart, and C. Platzer-Björkman, "A Detrimental Reaction at the Molybdenum Back Contact in Cu2ZnSn(S,Se)(4) Thin-Film Solar Cells", *Journal of the American Chemical Society,* vol. 134, pp. 19330-19333, 2012.
[20] J. J. Scragg, T. Kubart, J. T. Wätjen, T. Ericson, M. K. Linnarsson, and C. Platzer-Björkman, "Effects of Back Contact Instability on Cu2ZnSnS4 Devices and Processes", *Chemistry of Materials,* vol. 25, pp. 3162-3171, 2013.
[21] F. Y. Liu, K. W. Sun, W. Li, C. Yan, H. T. Cui, L. X. Jiang, X. J. Hao, and M. A. Green, "Enhancing the Cu2ZnSnS4 solar cell efficiency by back contact modification: Inserting a thin TiB2 intermediate layer at Cu2ZnSnS4/Mo interface", *Applied Physics Letters,* vol. 104, 2014.
[22] W. Li, J. Chen, H. T. Cui, F. Y. Liu, and X. J. Hao, "Inhibiting MoS2 formation by introducing a ZnO intermediate layer for Cu2ZnSnS4 solar cells", *Materials Letters,* vol. 130, pp. 87-90, 2014.
[23] B. Vermang, Y. Ren, O. Donzel-Gargand, C. Frisk, J. Joel, P. Salome, J. Borme, S. Sadewasser, C. Platzer-Björkman, and M. Edoff, "Rear Surface Optimization of CZTS Solar Cells by Use of a Passivation Layer With Nanosized Point Openings", *IEEE Journal of Photovoltaics,* vol. 6, pp. 332-336, 2016.
[24] S. Y. Chen, A. Walsh, X. G. Gong, and S. H. Wei, "Classification of Lattice Defects in the Kesterite Cu2ZnSnS4 and Cu2ZnSnSe4 Earth-Abundant Solar Cell Absorbers", *Advanced Materials,* vol. 25, pp. 1522-1539, 2013.
[25] T. Gershon, D. Bishop, P. Antunez, S. Singh, K. W. Brew, Y. S. Lee, O. Gunawan, T. Gokmen, T. Todorov, and R. Haight, "Unconventional kesterites: The quest to reduce band tailing in CZTSSe", *Current Opinion in Green and Sustainable Chemistry,* vol. 4, pp. 29-36, 2017.

[26] S. Y. Chen, X. G. Gong, A. Walsh, and S. H. Wei, "Crystal and electronic band structure of Cu2ZnSnX4 (X=S and Se) photovoltaic absorbers: First-principles insights", *Applied Physics Letters,* vol. 94, 2009.
[27] S. Schorr, "The crystal structure of kesterite type compounds: A neutron and X-ray diffraction study", *Solar Energy Materials and Solar Cells,* vol. 95, pp. 1482-1488, 2011.
[28] J. J. S. Scragg, J. K. Larsen, M. Kumar, C. Persson, J. Sendler, S. Siebentritt, and C. Platzer-Björkman, "Cu-Zn disorder and band gap fluctuations in Cu2ZnSn(S,Se)(4): Theoretical and experimental investigations", *Physica Status Solidi B-Basic Solid State Physics,* vol. 253, pp. 247-254, 2016.
[29] A. Ritscher, A. Franz, S. Schorr, and M. Lerch, "Off-stoichiometric CZTS: Neutron scattering investigations on mechanochemically synthesized powders", *Journal of Alloys and Compounds,* vol. 689, pp. 271-277, 2016.
[30] B. G. Mendis, M. D. Shannon, M. C. Goodman, J. D. Major, R. Claridge, D. P. Halliday, and K. Durose, "Direct observation of Cu, Zn cation disorder in Cu2ZnSnS4 solar cell absorber material using aberration corrected scanning transmission electron microscopy", *Progress in Photovoltaics,* vol. 22, pp. 24-34, 2014.
[31] H. Katagiri, K. Saitoh, T. Washio, H. Shinohara, T. Kurumadani, and S. Miyajima, "Development of thin film solar cell based on Cu2ZnSnS4 thin films", *Solar Energy Materials and Solar Cells,* vol. 65, pp. 141-148, 2001.
[32] I. D. Olekseyuk, I. V. Dudchak, and L. V. Piskach, "Phase equilibria in the Cu2S-ZnS-SnS2 system", *Journal of Alloys and Compounds,* vol. 368, pp. 135-143, 2004.
[33] D. M. Berg, M. Arasimowicz, R. Djemour, L. Gutay, S. Siebentritt, S. Schorr, X. Fontane, V. Izquierdo-Roca, A. Perez-Rodriguez, and P. J. Dale, "Discrimination and detection limits of secondary phases in Cu2ZnSnS4 using X-ray diffraction and Raman spectroscopy", *Thin Solid Films,* vol. 569, pp. 113-123, 2014.
[34] H. Katagiri, K. Jimbo, M. Tahara, H. Araki, and K. Oishi, "The Influence of the Composition Ratio on CZTS-based Thin Film Solar Cells", *MRS Online Proceedings Library,* vol. 1165, 2009.
[35] J. K. Larsen, J. J. S. Scragg, C. Frisk, Y. Ren, and C. Platzer-Björkman, "Potential of CuS cap to prevent decomposition of Cu2ZnSnS4 during annealing", *Physica Status Solidi a-Applications and Materials Science,* vol. 212, pp. 2843-2849, 2015.
[36] A. Davydova, K. Rudisch, and J. J. S. Scragg, "The Single Phase Region in Cu2ZnSnS4 Thin Films from Theory and Combinatorial Experiments", *Chemistry of Materials,* vol. 30, pp. 4624-4638, 2018.
[37] K. Rudisch, A. Davydova, C. Platzer-Björkman, and J. J. S. Scragg, "The effect of stoichiometry on Cu-Zn ordering kinetics in Cu2ZnSnS4 thin films", *Journal of Applied Physics,* vol. 123, 2018.
[38] S. Y. Chen, L. W. Wang, A. Walsh, X. G. Gong, and S. H. Wei, "Abundance of Cu-Zn + Sn-Zn and 2Cu(Zn) + Sn-Zn defect clusters in kesterite solar cells", *Applied Physics Letters,* vol. 101, 2012.
[39] G. Altamura and J. Vidal, "Impact of Minor Phases on the Performances of CZTSSe Thin-Film Solar Cells", *Chemistry of Materials,* vol. 28, pp. 3540-3563, 2016.
[40] J. J. Scragg, T. Ericson, T. Kubart, M. Edoff, and C. Platzer-Björkman, "Chemical Insights into the Instability of Cu(2)ZnSnS(4) Films during Annealing", *Chemistry of Materials,* vol. 23, pp. 4625-4633, 2011.

[41] S. Siebentritt and S. Schorr, "Kesterites - a challenging material for solar cells", *Progress in Photovoltaics,* vol. 20, pp. 512-519, 2012.
[42] C. Platzer-Björkman, "Kesterite compound semiconductors for thin film solar cells", *Current Opinion in Green and Sustainable Chemistry,* vol. 4, pp. 84-90, 2017.
[43] I. Repins, C. Beall, N. Vora, C. DeHart, D. Kuciauskas, P. Dippo, B. To, J. Mann, W.-C. Hsu, A. Goodrich, and R. Noufi, "Co-evaporated Cu2ZnSnSe4 films and devices", *Solar Energy Materials and Solar Cells,* 2012.
[44] B. A. Schubert, B. Marsen, S. Cinque, T. Unold, R. Klenk, S. Schorr, and H. W. Schock, "Cu2ZnSnS4 thin film solar cells by fast coevaporation", *Progress in Photovoltaics,* vol. 19, pp. 93-96, 2011.
[45] H. Sugimoto, H. Hiroi, N. Sakai, S. Muraoka, and T. Katou, "Over 8% Efficiency Cu2ZnSnS4 Submodules with Ultra-Thin Absorber", *2012 38th IEEE Photovoltaic Specialists Conference (PVSC),* pp. 2997-3000, 2012.
[46] B. Shin, O. Gunawan, Y. Zhu, N. A. Bojarczuk, S. J. Chey, and S. Guha, "Thin film solar cell with 8.4% power conversion efficiency using an earth-abundant Cu2ZnSnS4 absorber", *Progress in Photovoltaics: Research and Applications,* vol. 21, pp. 72-76, 2011.
[47] S. M. Pawar, A. I. Inamdar, B. S. Pawar, K. V. Gurav, S. W. Shin, X. Yanjun, S. S. Kolekar, J. H. Lee, J. H. Kim, and H. Im, "Synthesis of Cu2ZnSnS4 (CZTS) absorber by rapid thermal processing (RTP) sulfurization of stacked metallic precursor films for solar cell applications", *Materials Letters,* vol. 118, pp. 76-79, 2014.
[48] F. Y. Liu, C. Yan, J. L. Huang, K. W. Sun, F. Z. Zhou, J. A. Stride, M. A. Green, and X. J. Hao, "Nanoscale Microstructure and Chemistry of Cu2ZnSnS4/CdS Interface in Kesterite Cu2ZnSnS4 Solar Cells", *Advanced Energy Materials,* vol. 6, 2016.
[49] J. B. Li, V. Chawla, and B. M. Clemens, "Investigating the Role of Grain Boundaries in CZTS and CZTSSe Thin Film Solar Cells with Scanning Probe Microscopy", *Advanced Materials,* vol. 24, pp. 720–723, 2012.
[50] B. T. Jheng, P. T. Liu, and M. C. Wu, "A promising sputtering route for dense Cu2ZnSnS4 absorber films and their photovoltaic performance", *Solar Energy Materials and Solar Cells,* vol. 128, pp. 275-282, 2014.
[51] T. Kato, H. Hiroi, N. Sakai, S. Muraoka, and H. Sugimoto, "CHARACTERIZATION OF FRONT AND BACK INTERFACES ON Cu2ZnSnS4 THIN-FILM SOLAR CELLS", *27th European Photovoltaic Solar Energy Conference and Exhibition,* pp. 2236-2239, 2012.
[52] K. Sun, C. Yan, F. Liu, J. Huang, F. Zhou, J. A. Stride, M. Green, and X. Hao, "Over 9% Efficient Kesterite Cu2ZnSnS4 Solar Cell Fabricated by Using Zn1–xCdxS Buffer Layer", *Advanced Energy Materials,* vol. 6, 2016.
[53] K. J. Yang, D. H. Son, S. J. Sung, J. H. Sim, Y. I. Kim, S. N. Park, D. H. Jeon, J. Kim, D. K. Hwang, C. W. Jeon, D. Nam, H. Cheong, J. K. Kang, and D. H. Kim, "A band-gap-graded CZTSSe solar cell with 12.3% efficiency", *Journal of Materials Chemistry A,* vol. 4, pp. 10151-10158, 2016.
[54] W. Wang, M. T. Winkler, O. Gunawan, T. Gokmen, T. K. Todorov, Y. Zhu, and D. B. Mitzi, "Device Characteristics of CZTSSe Thin-Film Solar Cells with 12.6% Efficiency", *Advanced Energy Materials,* vol. 4, 2014.
[55] J. Kim, H. Hiroi, T. K. Todorov, O. Gunawan, M. Kuwahara, T. Gokmen, D. Nair, M. Hopstaken, B. Shin, Y. S. Lee, W. Wang, H. Sugimoto, and D. B. Mitzi, "High Efficiency Cu2ZnSn(S,Se)(4) Solar Cells by Applying a Double In2S3/CdS Emitter", *Advanced Materials,* vol. 26, pp. 7427-7431, 2014.

[56] F. Jiang, S. Ikeda, T. Harada, and M. Matsumura, "Pure Sulfide Cu2ZnSnS4 Thin Film Solar Cells Fabricated by Preheating an Electrodeposited Metallic Stack", *Advanced Energy Materials,* vol. 4, 2014.

[57] K. Timmo, M. Kauk-Kuusik, M. Pilvet, T. Raadik, M. Altosaar, M. Danilson, M. Grossberg, J. Raudoja, and K. Emits, "Influence of order-disorder in Cu2ZnSnS4 powders on the performance of monograin layer solar cells", *Thin Solid Films,* vol. 633, pp. 122-126, 2017.

[58] K. Ernits, C. Neubauer, X. L. Li, L. H. Wong, D. Meissner, and A. Neisser, "Improvement of V-OC in Cu2ZnSnS4 Monograin Layer Solar Cells with Tin Oxide Inter-Layer", *2015 Ieee 42nd Photovoltaic Specialist Conference (Pvsc),* 2015.

[59] C. Platzer-Björkman, T. Törndahl, D. Abou-Ras, J. Malmström, J. Kessler, and L. Stolt, "Zn(O,S) buffer layers by atomic layer deposition in $Cu(In,Ga)Se_2$ based thin film solar cells: Band alignment and sulfur gradient", *Journal of Applied Physics,* vol. 100, p. 044506, 2006.

[60] J. Just, D. Luzenkirchen-Hecht, R. Frahm, S. Schorr, and T. Unold, "Determination of secondary phases in kesterite Cu2ZnSnS4 thin films by x-ray absorption near edge structure analysis", *Applied Physics Letters,* vol. 99, 2011.

[61] I. Grozdanov and M. Najdoski, "Optical and Electrical-Properties of Copper Sulfide Films of Variable Composition", *Journal of Solid State Chemistry,* vol. 114, pp. 469-475, 1995.

[62] S. Siebentritt, "Why are kesterite solar cells not 20% efficient?", *Thin Solid Films,* vol. 535, pp. 1-4, 2013.

[63] D. M. Berg, R. Djemour, L. Gutay, G. Zoppi, S. Siebentritt, and P. J. Dale, "Thin film solar cells based on the ternary compound Cu2SnS3", *Thin Solid Films,* vol. 520, pp. 6291-6294, 2012.

[64] B. G. Mendis, M. C. J. Goodman, J. D. Major, A. A. Taylor, K. Durose, and D. P. Halliday, "The role of secondary phase precipitation on grain boundary electrical activity in Cu2ZnSnS4 (CZTS) photovoltaic absorber layer material", *Journal of Applied Physics,* vol. 112, 2012.

[65] Y. Ren, N. Ross, J. K. Larsen, K. Rudisch, J. J. S. Scragg, and C. Platzer-Björkman, "Evolution of Cu2ZnSnS4 during Non-Equilibrium Annealing with Quasi-in Situ Monitoring of Sulfur Partial Pressure", *Chemistry of Materials,* vol. 29, pp. 3713-3722, 2017.

[66] Y. Ren, M. Richter, J. Keller, A. Redinger, T. Unold, O. Donzel-Gargand, J. J. S. Scragg, and C. Platzer-Björkman, "Investigation of the SnS/Cu2ZnSnS4 Interfaces in Kesterite Thin-Film Solar Cells", *Acs Energy Letters,* vol. 2, pp. 976-981, 2017.

[67] C. Yan, J. Huang, K. Sun, S. Johnston, Y. Zhang, H. Sun, A. Pu, M. He, F. Liu, K. Eder, L. Yang, J. M. Cairney, N. J. Ekins-Daukes, Z. Hameiri, J. A. Stride, S. Chen, M. A. Green, and X. Hao, "Cu2ZnSnS4 solar cells with over 10% power conversion efficiency enabled by heterojunction heat treatment", *Nature Energy,* 2018.

[68] H. Katagiri, K. Jimbo, W. S. Maw, K. Oishi, M. Yamazaki, H. Araki, and A. Takeuchi, "Development of CZTS-based thin film solar cells", *Thin Solid Films,* vol. 517, pp. 2455-2460, 2009.

[69] B. Shin, Y. Zhu, N. A. Bojarczuk, S. J. Chey, and S. Guha, "High efficiency Cu2ZnSnSe4 solar cells with a TiN diffusion barrier on the molybdenum bottom contact", *2012 38th Ieee Photovoltaic Specialists Conference (Pvsc),* 2012.

[70] H. Hiroi, N. Sakai, T. Kato, and H. Sugimoto, "High voltage Cu<inf>2</inf>ZnSnS<inf>4</inf> submodules by hybrid buffer layer", in *IEEE 39th Photovoltaic Specialists Conference (PVSC)*, 2013, pp. 0863-0866.
[71] T. K. Todorov, K. B. Reuter, and D. B. Mitzi, "High-Efficiency Solar Cell with Earth-Abundant Liquid-Processed Absorber", *Advanced Materials,* vol. 22, p. E156, 2010.
[72] D. A. Barkhouse, O. Gunawan, T. Gokmen, T. Todorov, and D. Mitzi, "Device characteristics of a 10.1 % hydrazine-processed $Cu_2ZnSn(Se,S)_4$ solar cell", *Progress in Photovoltaics,* vol. 20, pp. 6-11, 2012.
[73] T. K. Todorov, J. Tang, S. Bag, O. Gunawan, T. Gokmen, Y. Zhu, and D. B. Mitzi, "Beyond 11% Efficiency: Characteristics of State-of-the-Art Cu2ZnSn(S,Se)4 Solar Cells", *Advanced Energy Materials,* vol. 3, pp. 34-38, 2013.
[74] C. Platzer-Björkman, J. Scragg, H. Flammersberger, T. Kubart, and M. Edoff, "Influence of precursor sulfur content on film formation and compositional changes in Cu2ZnSnS4 films and solar cells", *Solar Energy Materials and Solar Cells,* vol. 98, pp. 110-117, 2012.
[75] J. K. Larsen, Y. Ren, N. Ross, E. Särhammar, S. Y. Li, and C. Platzer-Björkman, "Surface modification through air annealing Cu2ZnSn(S,Se)4 absorbers", *Thin Solid Films*.
[76] C. Y. Chou and S. W. Chen, "Phase equilibria of the Sn-Zn-Cu ternary system", *Acta Materialia,* vol. 54, pp. 2393-2400, 2006.
[77] T. Gokmen, O. Gunawan, T. K. Todorov, and D. B. Mitzi, "Band tailing and efficiency limitation in kesterite solar cells", *Applied Physics Letters,* vol. 103, 2013.
[78] J. H. Werner, J. Mattheis, and U. Rau, "Efficiency limitations of polycrystalline thin film solar cells: case of Cu(In,Ga)Se-2", *Thin Solid Films,* vol. 480, pp. 399-409, 2005.
[79] G. Rey, G. Larramona, S. Bourdais, C. Chone, B. Delatouche, A. Jacob, G. Dennler, and S. Siebentritt, "On the origin of band-tails in kesterite", *Solar Energy Materials and Solar Cells,* vol. 179, pp. 142-151, 2018.
[80] L. Yin, G. M. Cheng, Y. Feng, Z. H. Li, C. L. Yang, and X. D. Xiao, "Limitation factors for the performance of kesterite Cu2ZnSnS4 thin film solar cells studied by defect characterization", *Rsc Advances,* vol. 5, pp. 40369-40374, 2015.
[81] L. Grenet, M. A. A. Suzon, F. Emieux, and F. Roux, "Analysis of Failure Modes in Kesterite Solar Cells", *ACS Applied Energy Materials,* vol. 1, pp. 2103-2113, 2018.
[82] V. Kosyak, A. V. Postnikov, J. Scragg, M. A. Scarpulla, and C. Platzer-Björkman, "Calculation of point defect concentration in Cu2ZnSnS4: Insights into the high-temperature equilibrium and quenching", *Journal of Applied Physics,* vol. 122, 2017.
[83] T. Ericson, "Reactive sputtering and composition measurements of precursors for Cu_2ZnSnS_4 thin film solar cells", Licentiate dissertation, Uppsala, Available from: http://urn.kb.se/resolve?urn=urn:nbn:se:uu:diva-208543, 2013.
[84] M. Mayer, "SIMNRA User's guide Report IPP 9/113 Max-Planck-Institut für Plasmaphysik, Garching ", 1997.

[85] J. H. Hubbell and S. M. Seltzer, "Tables of X-Ray Mass Attenuation Coefficients and Mass Energy-Absorption Coefficients (version 1.4)", *[Online] Available: http://physics.nist.gov/xaamdi [2013-04-13]. National Institute of Standards and Technology, Gaithersburg, MD.,* 2004.
[86] P. A. Fernandes, P. M. P. Salome, and A. F. da Cunha, "Study of polycrystalline Cu(2)ZnSnS(4) films by Raman scattering", *Journal of Alloys and Compounds,* vol. 509, pp. 7600-7606, 2011.
[87] M. Dimitrievska, A. Fairbrother, A. Perez-Rodriguez, E. Saucedo, and V. Izquierdo-Roca, "Raman scattering crystalline assessment of polycrystalline Cu2ZnSnS4 thin films for sustainable photovoltaic technologies: Phonon confinement model", *Acta Materialia,* vol. 70, pp. 272-280, 2014.
[88] M. Dimitrievska, S. Giraldo, P. Pistor, E. Saucedo, A. Pérez-Rodríguez, and V. Izquierdo-Roca, "Raman scattering analysis of the surface chemistry of kesterites: Impact of post-deposition annealing and Cu/Zn reordering on solar cell performance", *Solar Energy Materials and Solar Cells,* vol. 157, pp. 462-467, 2016.
[89] Y. Ren, J. J. Scragg, T. Ericson, T. Kubart, and C. Platzer-Björkman, "Reactively sputtered films in the CuxS-ZnS-SnSy system: From metastability to equilibrium", *Thin Solid Films,* vol. 582, pp. 208-214, 2015.
[90] X. Fontane, L. Calvo-Barrio, V. Izquierdo-Roca, E. Saucedo, A. Perez-Rodriguez, J. R. Morante, D. M. Berg, P. J. Dale, and S. Siebentritt, "In-depth resolved Raman scattering analysis for the identification of secondary phases: Characterization of Cu(2)ZnSnS(4) layers for solar cell applications", *Applied Physics Letters,* vol. 98, p. 181905, 2011.
[91] S. van Duren, Y. Ren, J. Scragg, J. Just, and T. Unold, "In Situ Monitoring of Cu2ZnSnS4 Absorber Formation With Raman Spectroscopy During Mo/Cu2SnS3/ZnS Thin-Film Stack Annealing", *IEEE Journal of Photovoltaics,* vol. 7, pp. 906-912, 2017.
[92] P. A. Flinn, D. S. Gardner, and W. D. Nix, "MEASUREMENT AND INTERPRETATION OF STRESS IN ALUMINUM-BASED METALLIZATION AS A FUNCTION OF THERMAL HISTORY", *Ieee Transactions on Electron Devices,* vol. 34, pp. 689-699, 1987.
[93] S. S. Hegedus and W. N. Shafarman, "Thin-film solar cells: Device measurements and analysis", *Progress in Photovoltaics,* vol. 12, pp. 155-176, 2004.
[94] S.-Y. Li, "Some optical issues", ed. Uppsala University: Ångström Solar Center, 2015.
[95] C. J. Hages, N. J. Carter, and R. Agrawal, "Generalized quantum efficiency analysis for non-ideal solar cells: Case of Cu2ZnSnSe4", *Journal of Applied Physics,* vol. 119, 2016.
[96] J. A. Thornton and D. W. Hoffman, "Stress-Related Effects in Thin-Films", *Thin Solid Films,* vol. 171, pp. 5-31, 1989.
[97] T. Welzel and K. Ellmer, "Negative oxygen ion formation in reactive magnetron sputtering processes for transparent conductive oxides", *Journal of Vacuum Science & Technology A,* vol. 30, 2012.
[98] A. Weber, R. Mainz, and H. W. Schock, "On the Sn loss from thin films of the material system Cu-Zn-Sn-S in high vacuum", *Journal of Applied Physics,* vol. 107, p. 013516, 2010.
[99] E. N. Selivanov, R. I. Gulyaeva, and A. D. Vershinin, "Thermal expansion and phase transformations of copper Sulfides", *Inorganic Materials,* vol. 43, pp. 573-578, 2007.

[100] Y. Ren, J. J. S. Scragg, C. Frisk, J. K. Larsen, S. Y. Li, and C. Platzer-Björkman, "Influence of the Cu2ZnSnS4 absorber thickness on thin film solar cells", *Physica Status Solidi a-Applications and Materials Science,* vol. 212, pp. 2889-2896, 2015.
[101] P. M. Fabis, R. A. Cooke, and S. Mcdonough, "Stress State of Chromium Nitride Films Deposited by Reactive Direct-Current Planar Magnetron Sputtering", *Journal of Vacuum Science & Technology a-Vacuum Surfaces and Films,* vol. 8, pp. 3809-3818, 1990.
[102] G. F. Iriarte, J. G. Rodriguez, and F. Calle, "Effect of substrate-target distance and sputtering pressure in the synthesis of AlN thin films", *Microsystem Technologies-Micro-and Nanosystems-Information Storage and Processing Systems,* vol. 17, pp. 381-386, 2011.
[103] S. Seeger, K. Harbauer, and K. Ellmer, "Ion-energy distributions at a substrate in reactive magnetron sputtering discharges in Ar/H(2)S from copper, indium, and tungsten targets", *Journal of Applied Physics,* vol. 105, p. 053305, 2009.
[104] P. F. Carcia, R. S. McLean, M. H. Reilly, Z. G. Li, L. J. Pillione, and R. F. Messier, "Influence of energetic bombardment on stress, resistivity, and microstructure of indium tin oxide films grown by radio frequency magnetron sputtering on flexible polyester substrates", *Journal of Vacuum Science & Technology A,* vol. 21, pp. 745-751, 2003.
[105] N. Ross, J. Larsen, S. Grini, L. Vines, and C. Platzer-Björkman, "Practical limitations to selenium annealing of compound co-sputtered Cu2ZnSnS4 as a route to achieving sulfur-selenium graded solar cell absorbers", *Thin Solid Films,* vol. 623, pp. 110-115, 2017.
[106] R. A. Mickelsen, W. S. Chen, Y. R. Hsiao, and V. E. Lowe, "POLYCRYSTALLINE THIN-FILM CUINSE2/CDZNS SOLAR-CELLS", *Ieee Transactions on Electron Devices,* vol. 31, pp. 542-546, 1984.
[107] T. Tanaka, A. Yoshida, D. Saiki, K. Saito, Q. Guo, M. Nishio, and T. Yamaguchi, "Influence of composition ratio on properties of Cu2ZnSnS4 thin films fabricated by co-evaporation", *Thin Solid Films,* vol. 518, pp. 29-33, 2010.
[108] D. Hironiwa, N. Sakai, T. Kato, H. Sugimoto, Z. Tang, J. Chantana, and T. Minemoto, "Impact of annealing treatment before buffer layer deposition on Cu2ZnSn(S,Se)4 solar cells", *Thin Solid Films,* vol. 582, pp. 151-153, 2015.
[109] H. Xie, S. López-Marino, T. Olar, Y. Sánchez, M. Neuschitzer, F. Oliva, S. Giraldo, V. Izquierdo-Roca, I. Lauermann, A. Pérez-Rodríguez, and E. Saucedo, "Impact of Na Dynamics at the Cu2ZnSn(S,Se)4/CdS Interface During Post Low Temperature Treatment of Absorbers", *ACS Applied Materials & Interfaces,* vol. 8, pp. 5017-5024, 2016.
[110] R. Scheer and H. W. Schock, *Chalcogenide Photovoltaics*. Weinheim: WILEY-VCH Verlag & Co, 2011.
[111] J. K. Larsen, Y. Ren, N. Ross, E. Särhammar, S. Y. Li, and C. Platzer-Björkman, "Surface modification through air annealing Cu2ZnSn(S,Se)(4) absorbers", *Thin Solid Films,* vol. 633, pp. 118-121, 2017.
[112] S. Tajima, R. Asahi, D. Isheim, D. N. Seidman, T. Itoh, M. Hasegawa, and K. Ohishi, "Atom-probe tomographic study of interfaces of Cu2ZnSnS4 photovoltaic cells", *Applied Physics Letters,* vol. 105, p. 093901, 2014.
[113] J. J. S. Scragg, L. Choubrac, A. Lafond, T. Ericson, and C. Platzer-Björkman, "A low-temperature order-disorder transition in Cu2ZnSnS4 thin films", *Applied Physics Letters,* vol. 104, p. 041911, 2014.

[114] K. Sardashti, R. Haight, T. Gokmen, W. Wang, L. Y. Chang, D. B. Mitzi, and A. C. Kummel, "Impact of Nanoscale Elemental Distribution in High-Performance Kesterite Solar Cells", *Advanced Energy Materials,* vol. 5, 2015.
[115] M. Neuschitzer, K. Lienau, M. Guc, L. C. Barrio, S. Haass, J. M. Prieto, Y. Sanchez, M. Espindola-Rodriguez, Y. Romanyuk, A. Perez-Rodriguez, V. Izquierdo-Roca, and E. Saucedo, "Towards high performance Cd-free CZTSe solar cells with a ZnS(O,OH) buffer layer: the influence of thiourea concentration on chemical bath deposition", *Journal of Physics D: Applied Physics,* vol. 49, p. 125602, 2016.
[116] H. Daisuke, M. Nobuki, S. Noriyuki, K. Takuya, S. Hiroki, C. Jakapan, T. Zeguo, and M. Takashi, "Sputtered (Zn,Mg)O buffer layer for band offset control in Cu 2 ZnSn(S,Se) 4 solar cells", *Japanese Journal of Applied Physics,* vol. 53, p. 106502, 2014.
[117] D. A. R. Barkhouse, R. Haight, N. Sakai, H. Hiroi, H. Sugimoto, and D. B. Mitzi, "Cd-free buffer layer materials on $Cu_2ZnSn(S_xSe_{1-x})_4$: Band alignments with ZnO, ZnS, and In_2S_3", *Applied Physics Letters,* vol. 100, p. 193904, 2012.
[118] H. Hiroi, N. Sakai, S. Muraoka, T. Katou, and H. Sugimoto, "Development of high efficiency Cu<inf>2</inf>ZnSnS<inf>4</inf> submodule with Cd-free buffer layer", in *38th IEEE Photovoltaic Specialists Conference (PVSC)*, 2012, pp. 001811-001814.
[119] K. Ernits, R. Hall, K. Muska, and T. Holopainen, "Multiple CdS deposition on Cu2ZnSn(S,Se)4 monograins", *Presented at Second Kesterite workshop, Barcelona,* 2011.
[120] H. Katagiri, "Sulfurization of Physical Vapor-Deposited Precursor Layers", in *Copper Zinc Tin Sulfide-Based Thin Film Solar Cells*, K. Ito, Ed., ed: Wiley, 2015.
[121] M. T. Htay, Y. Hashimoto, N. Momose, K. Sasaki, H. Ishiguchi, S. Igarashi, K. Sakurai, and K. Ito, "A Cadmium-Free Cu2ZnSnS4/ZnO Hetrojunction Solar Cell Prepared by Practicable Processes", *Japanese Journal of Applied Physics,* vol. 50, 2011.
[122] A. Nagoya, R. Asahi, and G. Kresse, "First-principles study of Cu2ZnSnS4 and the related band offsets for photovoltaic applications", *Journal of Physics-Condensed Matter,* vol. 23, p. 404203, 2011.
[123] U. Zimmermann, M. Ruth, and M. Edoff, "Cadmium-free CIGS mini-modules with ALD-grown Zn(O, S)-based buffer layers", presented at the 21st European Photovoltaic Solar Energy Conference, Dresden, 2006.
[124] O. Gunawan, T. Todorov, and D. Mitzi, "Loss mechanisms in hydrazine-processed Cu2ZnSn(Se,S)4 solar cells", *Applied Physics Letters,* vol. 97, p. 233506, 2010.
[125] J. Lindahl, C. Hägglund, J. T. Wätjen, M. Edoff, and T. Törndahl, "The effect of substrate temperature on atomic layer deposited zinc tin oxide", *Thin Solid Films,* vol. 586, pp. 82-87, 2015.
[126] J. Lindahl, J. Keller, O. Donzel-Gargand, P. Szaniawski, M. Edoff, and T. Törndahl, "Deposition temperature induced conduction band changes in zinc tin oxide buffer layers for Cu(In,Ga)Se2 solar cells", *Solar Energy Materials and Solar Cells,* vol. 144, pp. 684-690, 2016.

[127] M. Kapilashrami, C. X. Kronawitter, T. Törndahl, J. Lindahl, A. Hultqvist, W. C. Wang, C. L. Chang, S. S. Mao, and J. Guo, "Soft X-ray characterization of Zn(1-x)Sn(x)O(y) electronic structure for thin film photovoltaics", *Physical Chemistry Chemical Physics,* vol. 14, pp. 10154-9, 2012.
[128] A. Hultqvist, M. Edoff, and T. Törndahl, "Evaluation of Zn-Sn-O buffer layers for CuIn0.5Ga0.5Se2 solar cells", *Progress in Photovoltaics,* vol. 19, pp. 478-481, 2011.
[129] A. Crovetto, M. L. N. Palsgaard, T. Gunst, T. Markussen, K. Stokbro, M. Brandbyge, and O. Hansen, "Interface band gap narrowing behind open circuit voltage losses in Cu2ZnSnS4 solar cells", *Applied Physics Letters,* vol. 110, 2017.
[130] G. Shoushuai, J. Zhenwu, W. Li, A. Jianping, Z. Yu, S. Yun, and Z. Yi, "Interfaces of high-efficiency kesterite Cu 2 ZnSnS(e) 4 thin film solar cells", *Chinese Physics B,* vol. 27, p. 018803, 2018.
[131] Y. Ren, J. J. Scragg, M. Edoff, J. K. Larsen, and C. Platzer-Björkman, "Evolution of Na-S(-O) Compounds on the Cu2ZnSnS4 Absorber Surface and Their Effects on CdS Thin Film Growth", *ACS Appl Mater Interfaces,* vol. 8, pp. 18600-7, 2016.
[132] A. Hultqvist, C. Platzer-Björkman, E. Coronel, and M. Edoff, "Experimental investigation of $Cu(In_{1-x},Ga_x)Se_2/Zn(O_{1-z},S_z)$ solar cell performance", *Solar Energy Materials and Solar Cells,* vol. 95, pp. 497-503, 2011.
[133] H. Sun, K. Sun, J. Huang, C. Yan, F. Liu, J. Park, A. Pu, J. A. Stride, M. A. Green, and X. Hao, "Efficiency Enhancement of Kesterite Cu2ZnSnS4 Solar Cells via Solution-Processed Ultrathin Tin Oxide Intermediate Layer at Absorber/Buffer Interface", *ACS Applied Energy Materials,* vol. 1, pp. 154-160, 2018.

Acta Universitatis Upsaliensis

Digital Comprehensive Summaries of Uppsala Dissertations from the Faculty of Science and Technology 1707

Editor: The Dean of the Faculty of Science and Technology

A doctoral dissertation from the Faculty of Science and Technology, Uppsala University, is usually a summary of a number of papers. A few copies of the complete dissertation are kept at major Swedish research libraries, while the summary alone is distributed internationally through the series Digital Comprehensive Summaries of Uppsala Dissertations from the Faculty of Science and Technology. (Prior to January, 2005, the series was published under the title "Comprehensive Summaries of Uppsala Dissertations from the Faculty of Science and Technology".)

Distribution: publications.uu.se
urn:nbn:se:uu:diva-357354

ACTA
UNIVERSITATIS
UPSALIENSIS
UPPSALA
2018